To the Graduate Council:

I am submitting herewith a dissertation written by Thada Somphone entitled "Micromechanics of Smart Electrostrictive Materials." I have examined the final copy of this dissertation for form and content and recommend that it be accepted in partial fulfillment of the requirements for the degree of Doctor of Philosophy, with a major in Engineering Science.

Niann-i Yu, Major Professor

We have read this dissertation
and recommend its acceptance:

Accepted for the Council:

Interim Vice Provost
and Dean of the Graduate School

MICROMECHANICS OF SMART ELECTROSTRICTIVE MATERIALS

A Dissertation

Presented for the

Doctor of Philosophy

Degree

The University of Tennessee, Knoxville

Thada Somphone

December, 2000

DEDICATION

This dissertation is dedicated to my parents

and

all Somphone's families

ACKNOWLEDGMENT

I would like to take this opportunity to express my sincere appreciation to my advisor, Dr. N. Yu, for his insightful guidance, constant support, encouragement, and invaluable help throughout my research.

I would also like to thank Dr. J. A. M. Boulet, Dr. G. Kawiecki, and Dr. X. Feng for serving as the members of my dissertation committee.

Finally, I would like to thank my parents, my family, and all my good friends for their constant support and encouragement.

This work was supported by the Office of Naval Research (ONR) Historically Black Engineering Colleges (HBEC) Future Faculty Fellowship Program (Sub-grant No. N000014-92-J-1252-TENN-001 with North Carolina A&T State University, ONR Prime Grant No. N000014-92-J-1252 P00005) and monitored by Dr. Harold L. Martin and Dr. John C. Kelly, North Carolina A&T State University.

ABSTRACT

Two micromechanics models have been developed to estimate the local fields, the effective properties, and the electro-mechanical coupling in smart electrostrictive materials.

The first model is based on the laminated plate theory. The nonlinear relations between the polarization and the electric field are considered in the model and an iterative formulation has been developed. Closed-form solutions are also obtained by ignoring the nonlinear terms in the constitutive relations between the polarization and the electric field. The effects of material properties, and the thickness and the number of plies on the mechanical and electrical response of the electrostrictive composite are studied. The model focuses on laminated composites and considers not only applied mechanical loads but also prescribed electric fields. However, it is not able to predict the deformation in the thickness direction of the composites.

The second model considers electrostrictive materials containing periodically distributed inhomogeneities. The local fields and the effective properties of three-dimensional electrostrictive composites are predicted using the equivalent inclusion method (Esheby, 1957) and the Fourier series (Nemat-Nasser *et al.*, 1993). Linear constitutive relations between the polarization and the electric field are employed in the model, which involves very few assumptions and can be applied

to a broad class of electrostrictive composites. Furthermore, the effective properties of electrostrictive materials containing periodically distributed, aligned two dimensional (2-D) line cracks are studied. A 2-D line crack can be considered as a limiting case of a flat elliptical cylindrical void with its thickness approaching zero. Thus, a limiting process is employed to estimate the effective properties of an electrostrictive solid with periodically distributed, aligned 2-D line cracks.

Contents

List of Tables

List of Figures

Chapter 1

Introduction

1.1 Background

Piezoelectric and electrostrictive materials can be regarded as smart materials since they show electrical as well as mechanical response under mechanical loading and mechanical as well as electrical response under electric excitation, and are capable of acting as both sensors and actuators.

In response to the requirements for high precision positioning, quick response, low driving power, and miniaturization of devices, new transducers are in demand (Uchino, 1986). Smart piezoelectric and electrostrictive materials are promising candidates for meeting these challenges and thus receive extensive attention (Chopra, 1996; Crowe, 1996).

The deformation of structural materials usually results from thermo-mechanical loads. That is, structural materials traditionally transform mechanical inputs into mechanical outputs only. Unlike traditional structural materials, piezoelectric materials show considerable deformations in response to electric fields. They also produce polarizations in response to mechanical loads. At a low electric field, the relationship between electric fields and strains in piezoelectric materials is linear. But, the coupling becomes nonlinear at a high electric field and there exists a significant hysteresis, which can be unfavorable (Uchino 1986). A widely used piezoelectric ceramic is lead zirconate titannate (PZT).

In order to generate large strains due to electric fields with no hysteresis, the electrostrictive materials have been developed. Electrostrictive materials can also transform mechanical inputs into electrical as well as mechanical outputs, or transform electric inputs into mechanical as well as electrical outputs. The newly developed electrostrictive materials, such as lead magnesium niobate (PMN) and PMN-based ceramics like PMN-$PbTiO_3$, exhibit strains up to 0.1% without hysteresis (Uchino, 1986). The resulting electrostrictive strains are comparable with those of the best piezoelectric materials (Damjanovic and Newnham, 1992; Newnham, 1991). Since the relationship between strains and electric fields of electrostrictive materials is nonlinear, the electromechanical coupling can be tuned under suitable bias fields (Newnham, 1991).

When a ceramic is placed between two capacitor plates, shown in Figure 1.1, the voltage, V, and the charge, Q, can be measured independently. The electric field, E, the electric displacement, D, and the polarization, P, can thus be determined by

$$E = V/d, \tag{1.1}$$

$$D = Q/A, \tag{1.2}$$

$$P = D - \kappa_o E, \tag{1.3}$$

where d is the distance between the two electrodes (i.e., the thickness of the ceramic specimen), A is the area of the electrode, and κ_o is the permittivity of free space. The relationship between the electric field (or the voltage) and the electric displacement (or the charge) characterizes the dielectric property of ceramics.

For a *dielectric*, the relationship between the electric field and the electric displacement is linear and can be expressed by

$$D = \kappa E, \tag{1.4}$$

where κ is the permittivity of the dielectric; see Figure 1.2(a).

An electric field can polarize a *ferroelectric* material until saturation is reached. If the electric field, E, is reduced to zero, a permanent electric displacement remains

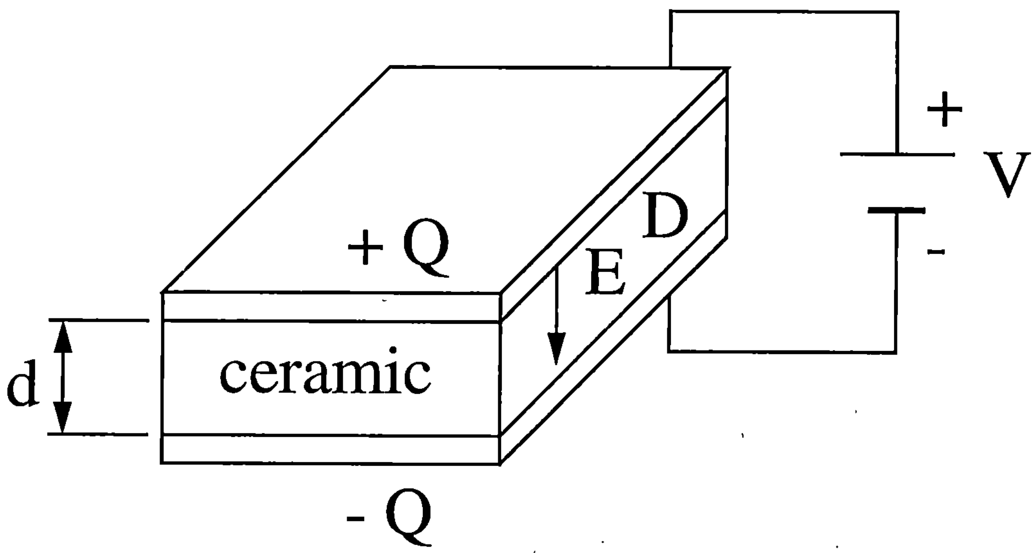

Figure 1.1: Ceramic subjected to a voltage.

in ferroelectric materials. An idealized hysteresis loop may be expressed by

$$D = \pm P_s + \kappa E, \tag{1.5}$$

where P_s is the spontaneous polarization; see Figure 1.2(b). Both piezoelectric as well as electrostrictive materials are ferroelectric materials.

The relationship between the electric field and the electric displacement in relaxors is also nonlinear; see Figure 1.2(c). Hence, relaxors can be regarded as a special class of ferroelectrics. However, the hysteresis is insignificant for relaxors. Electrostrictive materials, such as PMN, are presently the most popular relaxors.

The crystal structure of piezoelectric materials is unsymmetrical, but the crystal structure of electrostrictive materials is symmetrical. Moreover, piezoelectric materials have a spontaneous polarization, whereas electrostrictive materials do not. However, they also have a lot in common. For example, the deformation of both piezoelectric and electrostrictive materials can be induced by an electric field. Generally, electrostriction occurs in all dielectric materials, but the strains due to electrostriction in those materiasls are usually too small and are negligible (Uchino, 1986). However, the strain generated in relaxor ferroelectrics is large and can be up to 0.1%.

PZT has been used as an actuator element in adaptive optical components and the active element in a deformable mirror. The aging and hysteresis are the main problems associated with PZT actuator: As the PZT actuator requires poling, it will age. That is, it loses sensitivity over a period of time. The multilayer PMN actuators require no poling and exhibit negligible hysteresis and negligible thermal growth with very low power dissipation. Therefore, they can be used as stable devices and athermalized components with no aging or creep. Also, the PMN actuators can survive severe environments and operate at high temperature cycles. Thus, the PMN actuator has replaced the PZT actuator for adaptive optical components and has been used as the active element in an athermalized stable deformable mirror structure.

To provide a standardized actuator configuration and to improve large scale production of PMN actuators, the Standardized Electrodisplacive Transducer (SELECT) actuator concept has been developed (Mark and Paul, 1990). The technique improves sensitivity, uniformity, large displacement and yield rates of PMN actuators. Also the cost of the actuator can be reduced by eliminating recurring costs associated with custom design and tooling fixtures. To develop SELECT designs, finite element models of rectangular and cylindrical actuators were constructed by ALGOR and NASTRAN. The laminate multilayer actuator stacks were simulated by solid and composite elements. As a result, the cylindrical geometry was structurally superior to the rectangular configuration. The cylindrical geometry can produce improved electrical and structural responses for the transducer. The SELECT also considers the standard design that provides a basic unit of stroke form, a segment structure, from which multiple designs can be created. Then, the multilayer PMN actuator design is reduced to a selection of the number of segments required to produce the specified stroke response. The production rate is greatly increased because the segment can be made using batch processing.

In summary, the SELECT design allows the manufacturing of standard designs of actuators, and improves actuator sensitivity, uniformity, and large displacement with negligible hysteresis, low thermal expansion, low operating voltage, low dissipation and no aging.

Electrostrictive materials have been used in a number of applications, such as deformable mirrors, impact dot-matrix printer (Uchino, 1986), underwater transducers (Rittenmyer, 1994), and medical ultrasonic probes (Takeuchi, *et al.*, 1989).

A deformable mirror composed of three thin layers of PMN stacking on an elastic glass mirror is reported by Uchino (1986). The contour of the mirror surface can be controlled by the applied electric field and the electrode patterns. The deformable mirror can be used to control the phase of light wave and to correct the telescope image distortion caused by air disturbance. Particularly, three Articulating Ford mirrors (Fanson, 1995), each of which uses six PMN multilayer actuators, are installed in the Hubble Telescope's primary mirror to control the precise position of the mirror in order to correct the refocusing aberration .

An impact dot-matrix printer head using a multilayered, PMN-based ceramic with internal electrodes is developed (Uchino, 1986). The PMN actuator is installed in a specially-designed displacement magnification unit to produce sufficient dot-pin strokes. The printer offers a higher printing speed, lower energy consumption, and lower noise than the conventional electromagnetic type printer.

To utilize its large displacement and to avoid a significant hysteresis, a PMN-based multimorph actuator is used to fabricate the flapper of oil-pressure servo values (Ohuchi, *et al.*, 1986). The force generated and the response speed of servo valves are increased by using PMN multimorph actuators. Similar nozzle-flapper mechanisms are employed in air-pressure servo values (Yamamoto, *et al.*, 1982).

A PMN-PT fiber-reinforced polyurethane composite is considered as a medical ultrasonic probe (Takeuchi, *et al.*, 1989). The sensitivity of the probe is controlled by a direct-current (DC) bias field. Because that the electrostrictive composite has a large electromechanical coupling factor under a bias field and no residual electromechanical coupling after the bias field being removed, the echo amplitude of the probe increases with the aid of a bias field.

Presently, The main use of electrostrictive ceramics is in producing fine displacements. The electrostrictive ceramics are also used in deformable mirrors for adaptive systems, which provide displacements to correct the reflecting surfaces. Unlike piezoelectric ceramic, when the voltage is removed, there is no residual deformation in electrostrictive materials. Multilayer electrostrictive mirrors with each layer being designed to correct one particular optical distortion or to provide refocusing are used in adaptive optics. Furthermore, bimorphic and multilayer electrostrictive elements are used in valves and switches for microangular adjustment and in oil valves. Devices which consist of eletrotrictive ceramic may exhibit low electromechanical hysteresis, no aging, high frequency response, and low cost (Smolenskii, *et al.*, 1987).

Basically, the piezoelectric and electrostrictive actuators can offer (Uchino, 1986): (1) high precision positioning, (2) quick response time ($\sim 10\,\mu$s), (3) high generative force ($\sim 400\,\mathrm{kgf/cm^2}$), and (4) less driving power. In fact, piezoelectric and electrostrictive actuators have been applied to ultrasonic motors, servo displacement transducers, pulse-driven motors, deformable mirrors, cutting error correction mechanisms, and impact dot-matrix printers. Based on the resulting strains, the piezoelectric and electrostrictive actuators are divided into two categories: (1) a unidirectional displacement is produced by an electric field, which includes servo displacement transducers controlled by a feedback system and pulse-driven motors operated in an on/off manner, and (2) a resonating strain is excited by an ac field.

Systems that combine television cameras and graphic processing devices have been used as sensors to inspect the automatic manufacturing processes. To obtain high-quality graphics, an autofocusing system consisting of an optical microscope with high magnification (x100) of the objective lens is developed (Suyama *et al.*, 1990). Since the hysterisis of electrostrictive actuators is very small, the precise positioning table of the autofocusing system using electrostrictive actuators moves smoothly and the resolving power of positioning is high. The autofocusing system using a precise positioning table can improve the high precision of a repeated positioning from 1 μm to 0.035 μm.

Many new robots, manipulators, and unmanned vehicles require a high degree of mobility or dexterity. An actuator with muscle-like performance, including high energy density, fast speed of response, and large stroke, would be well suited to the aforementioned applications. The electrostriction of polymer dielectric with compliant electrodes can be used in electrically controllable, muscle-like actuators, specifically, electrostrictive polymer artificial muscle (EPAM), which can produce strain up to 30% and pressure up to 1.9 MPa. A rotary motor using EPAM actuator elements produces a torque of 19 mNm/g and a specific power of 0.1 W/g (Kornbluh *et al.*, 1998).

Electrostrictive ceramics are brittle and stiff, and therefore are prone to fracture. Based on the experience in developing piezoelectric transducers (Smith, 1986), electrostrictive ceramics may be combined with other ductile materials, such as metals or polymers to make the transducers more compliant and effective. For example, a moonie actuator - layers of PMN sandwiched between layers of specially designed metal cap has been recently developed (Sugawara *et al.*, 1992; Newnham *et al.*, 1994). The displacement of each metal cap due to an electric field is ten times larger than that of the electrostrictive ceramic alone.

1.2 Literature Review

One of the earliest mechanics modeling works on electrostrictive materials is reported by Knops (1963), who considers two-dimensional isotropic electrostriction. The stress, σ, is assumed to be linearly proportional to the strain, ε, and is proportional to the square of the electric field, E, and the electric displacement, D, is assumed to be linearly proportional to the electric field. That is,

$$\sigma_{ij} = \lambda\varepsilon_{kk}\delta_{ij} + 2\mu\varepsilon_{ij} + aE_iE_j + bE_kE_k\delta_{ij}, \quad (i,j = 1,2) \tag{1.6}$$

$$\sigma_z = \lambda\varepsilon_{kk} + bE_kE_k, \tag{1.7}$$

$$D_i = \kappa_{ij}E_j, \tag{1.8}$$

where δ_{ij} is the Kronecker delta, λ is the Lamé constant, μ is the shear modulus, κ_{ij} are the dielectric constants, and a and b are constants descriptive of the dielectric properties. A more general constitutive relation for electrostrictive materials is given by Ikeda (1990)

$$\varepsilon_{ij} = s_{ijkl}\sigma_{kl} + Q_{ijmn}P_mP_n, \tag{1.9}$$

$$E_n = \beta_{nm}P_m - 2Q_{klmn}\sigma_{kl}P_m, \tag{1.10}$$

where s is the compliance tensor, β $(= \kappa^{-1})$ is the permittivity tensor, and Q_{klmn} are electrostrictive constants. It is noted that the electrically induced strain is proportional to the square of the polarization, P, rather than electric displacements, D, for electrostrictive materials under high electric fields (Newnham, 1991). Furthermore, when the electric field increases, the polarization decreases and approaches asymptotic values, the so-called saturation of polarization. Thus, Suo (1991) suggests that the electric field in electrostrictive materials may be expressed as an odd-power polynominal function. Specifically, for one-dimensional problems,

$$\varepsilon = s\sigma + QD^2, \tag{1.11}$$

$$E = -2Q\sigma D + f(D), \tag{1.12}$$

where

$$f(D) = \beta D + \beta' D^3 + ... \tag{1.13}$$

with β and β' being constants. This constitutive relation is used to predict the mechanical behavior of relaxor-ferroelectrics containing defects subjected to a constant electric field and its electric behavior due to a constant stress. The Griffith's energy release rate has been derived for conducting and non-conducting cracks. It is reported that the energy release rates are positive for the conducting crack but negative for the non-conducting crack. A similar constitutive relation for electrostrictive materials is proposed by Hom and Shankar (1994):

$$\varepsilon_{ij} = s_{ijkl}\sigma_{kl} + Q_{ijmn}P_mP_n, \tag{1.14}$$

$$E_i = -2Q_{klij}\sigma_{kl}P_j + \frac{1}{\kappa^*}\text{arctanh}\left(\frac{|P|}{P_s}\right)\frac{P_i}{|P|}, \tag{1.15}$$

where $|P|$ is magnitude of polarization, P_s is the spontaneous polarization, and κ^* is a new material constant. Both, P_s and κ^*, are functions of temperature. Another similar constitutive relation for electrostrictive materials is suggested by Winzer *et al.* (1989)

$$\sigma_{ij} = C_{ijkl}\varepsilon_{kl} - B_{ijkl}E_kE_l, \tag{1.16}$$

$$D_i = \kappa_o K_{ij}E_j + M_{ijkl}E_j\sigma_{kl}, \tag{1.17}$$

where $B_{ijkl} = M_{ijmn}C_{mnkl}$, M_{klpq} is the electrostriction coefficient, K_{ij} are components of the relative dielectric permittivity, and κ_o is the permittivity of free space. The second term in Eq. (1.17) is an order of magnitude smaller than the first term even under a load of 15 MPa. Thus, Winzer *et al.* (1989) suggest that the second term on the right of Eq. (1.17) can be neglected, i.e.,

$$D_i = \kappa_o K_{ij}E_j. \tag{1.18}$$

Based on the above constitutive relations, a finite element analysis is conducted to compute the stresses and strains in multilayer electrostrictive actuators. The displacements on the surface of the actuator with a tab electrode are computed and are also measured at the center, edges, and corners of the actuator. The results show that the maximum tensile stress is near the tab interface. The model prediction agrees quite well with the experimental data.

A crack emanating from an internal electrode in a multilayer actuator is studied by Yang and Suo (1994). To estimate the stress at the edge of the conducting sheet under an electric field, and to estimate whether the stress will cause cracking, two models are employed. In the first model, the relation between the electric field, E, and the electric displacement, D, is assumed to be linear, $D = \kappa E$, and the strain is quadratic in the electric field. The stress at the edge of the conducting sheet and the stress intensity factor under the electric field are estimated. It is shown that the stress intensity factor, K_I, is quadratic in the electric intensity, K_E, and is inversely proportional to the square-root of the crack length. When the crack grows, K_I declines, and the crack arrests when the fracture toughness K_{Ic} is reached. The prediction agrees well with the experimental data. Since the model disregards the nonlinearity of the electric displacement at a high electric field, the model overestimates the electrostriction effect on cracking ahead of the electrode edge. The second model assumes that the electric field induces a step-like strain in the field direction

$$\varepsilon = \begin{cases} \varepsilon_s & \text{when } |E| > E_c, \\ 0 & \text{when } |E| < E_c, \end{cases} \tag{1.19}$$

where E_c is a coercive electric field and ε_s is the saturation strain. The stress and stress intensity factor at the edge of the conducting sheet under the electric field are estimated.

A possible failure mode in multilayered PMN-PT-BT actuators is the cracking in the tab region near the internal electrode tips (Hom and Shankar, 1995). The stress state near an internal electrode of the actuator is computed. Using a fully-coupled constitutive relation for electrostrictive materials, a plane strain finite element analysis is performed to model a multilayered PMN-PT-BT actuator at various levels of compressive stress. The results show that a significant stress concentration exists at the tips of the internal electrodes.

The interfacial cracking due to an electric field in multilayer electrostrictive actuators is studied for two cases: (i) an interface crack with one tip at the embedded electrode-edge; and (ii) an interface crack lying between an electrode layer and a ceramic matrix (Ru *et al.*, 1998). A direct method is used to compute the electric field-induced stress intensity factors without calculating the stress field. It is reported that the maximum mode-I stress intensity factor induced at the electrode-tip interface is considerably greater than that is associated with the matrix cracks directly ahead of the electric tip. The result agrees with the experimental observation that the interfacial cracking is the dominant failure mechanism in electrostrictive multilayer devices.

Experiments on the crack propagation in an electrostrictive PMN-PT ceramic subjected simultaneous mechanical and electrical loads are conducted by Wang and Singh (1995) using the Vickers indentation technique. The indenter is positioned so that the cracks emanating from the four corners of the indentation are either parallel or perpendicular to the electric field. It is observed that the lengths of the cracks perpendicular to the electric field increases when the electric field is increased. However, the lengths of the cracks parallel to the electric field are decreased, as the electric field is increased.

A two-dimensional electrostrictive finite element based on Eq. (1.9) and (1.10) is developed in the ATILA code (Debus and Debus, 1996). An iterative procedure is used to solve the nonlinear problem. To validate the development of the finite element, a long electrostrictive bar with electrodes at both ends is made. A static force is applied at both ends and a quasi-static (10 Hz) electric voltage is prescribed between the electrodes. It is assumed that the width and the thickness of the bar are small in comparison with its length, and only the electric field and mechanical load on lateral faces are prescribed. The bar is assumed to be axisymmetrical. Four finite elements are used for one half of the bar. The relationship between the electric displacement and the applied electric field and that between the strain and the applied electric field for various prestresses are obtained. A simple analytical model is also developed. The difference between model and experimental data is possibly due to non-linearity of the dielectric permittivity. Furthermore, a finite element based on Eq. (1.14) and (1.15) has also been developed for nonlinear static and transient analysis (Coutte *et al.*, 1998). A direct iterative procedure is used to solve the nonlinear static and transient problems. A long electrostrictive bar with electrodes located at both ends is again used. An electric field parallel to the longitudinal axis of bar is prescribed, and mechanical forces are applied to both ends. The finite element mesh for the bar consists of two axisymmetric electrostrictive elements, and eight-node isoparametric quadrilaterals are employed. The FEA predictions agree well with experimental data.

The mechanical coupling coefficients are important parameters for determining the power consumption of an actuator in a system design. They are a measure of the material's efficiency as an electrostrictive actuator. These coupling coefficients are related to the ratio of mechanical work available to electrical energy stored. For a linear piezoelectric materials, the coupling coefficients are well known and are functions of material properties. But for relaxor materials, the calculation of mechanical coupling coefficients based on three-dimensional constitutive relations, Eq. (1.14) and (1.15), shows that the coupling factors are functions of the polarization as well as material properties (Hom *et al.*, 1994). Lead magnesium niobate based relaxor ferroelectrics, PMN-PT-BT, are used as an example to compute the longitudinal and transverse coupling coefficients, k_{13} and k_{33}. The results show that the k_{13} asymptotically approaches 0.248 and k_{33} asymptotically approaches

0.544 at high electric fields (>1.5 MV/m).

The lead magnesium niobate (PMN) and its solid solution system with lead titanate (PT) show promise for sensor and actuator. The maximum dielectric of PMN occurs at low temperatures (close to 0^0 C), and PT-based relaxors can offer the improvement in high dielectric constants and electromechanical coupling of PMN-based relaxors. Therefore, Brown *et al.* (1998) study the dielectric properties and electromechanical coupling of (1-x)PMN-xPT, ($0 \leq x \leq 0.5$). The results show that the transition range as well as the maximum dielectric constant of PMN-PT increases and shifts to high temperatures with increasing the composition of PT. But as the frequency increases, the maximum dielectric constant of PMN-PT decreases. The dielectric properties of PMN-PT are functions of temperature and frequency, and the maximum dielectric constant occurs at room temperature. The transition temperature of the 0.95PMN-0.05PT is close to room temperature (approximate 20^oC), which means the maximum dielectric constant of 0.95PMN-0.05PT occurs at room temperature. The maximum dielectric constant of 0.9PMN-0.1PT occurs at 40^oC. Moreover, the electromechanical coupling factor of the 0.95PMN-0.05PT is a function of a DC bias. The electromechanical coupling factor is 0 for a DC bias field of 0 kV/cm, and is maximum at a value of 0.52 for a DC bias field of 15 kV/cm. The dielectric and electromechanical properties of the PMN-PT materials near their transition temperature can be tuned by the DC bias. Then, the PMN-PT transducer can be turned ON and OFF by applying and removing the DC bias field.

Ultrasonic transducers built by using PMN-PT based electrostrictive materials are investigated by Chen *et al.* (1996), who report that the dielectric constants of PMN-PT are functions of temperature with or without DC bias. The maximum dielectric constant is obtained at the temperature, T_{max}, of 60^o. The thickness coupling constant k_t of PMN-PT is a fuction of temperature at 0 kV/cm and 5 kV/cm DC bias. The large thickness coupling constant was obtained in this material near room temperature at low DC bias ($k_t = 0.43 \sim 0.50$ at 5kV/cm). When the DC bias is removed, the thickness coupling becomes zero at $T > 15^oC$ (T_d). PMN-PT loses its field-induced polarization property and exhibits zero remanent polarization above T_d. Therefore, when the DC bias is applied, the field-induced polarization can be used as an ON switch, and when the DC bias is removed, the zero remanent polarization can be used as an OFF switch. Thus, the electrostrictive transducer with aperture groups of different elevation can be turned ON and OFF by simply applying or removing the DC bias. Since near above T_{max}, the thickness coupling decreases with increasing temperature, the optimal operating temperature range for electrostrictive transducers is from T_d to T_{max}. Also the sensitivity of electrostrictive traducer is relatively stable at this range of temperature. For PZT transducers, when the DC bias is removed, the remanent polarization still remains. This is a disadvantage of the PZT materials for medical ultrasonic application.

The response of a soft PZT, a hard PZT, and a 0.9PMN-0.1PT due to uniaxial compressive stresses is measured by Zhao and Zhang (1996). The piezoelectric coefficient of the soft PZT drops quite rapidly. It is clear that the soft PZT is not suitable for high stress application. On the other hand, the piezoelectric coefficient of the hard PZT increases as the uniaxial compressive stresses increase. The piezoelectric coefficient of the 0.9PMN-0.1PT depends on the DC bias field level. The lower the DC field bias, the more the piezoelectric coefficient drops.

The electrostrictive strain due to electric field is also measured for pure PMN and PMN-PT (Jang *et al.*, 1980). It is shown that large strains without hysteresis can be induced at room temperature. The content of PT in PMN-PT ranging from 0.1 to 0.13 offers large strain without hysteresis, but when the content of PT is over 0.13, the hysteresis will exist. The hysteresis increases as the content of PT increases beyond 0.13.

Wang *et al.* (1996) investigate the dielectric ageing behavior of lead-based relaxor ferroelectric ceramic multilayer capacitors. They claim that dopants are found to play an important role in ageing induction. Moreover, the ageing behavior of PMN-0.9PT ceramics doped with different ions, such as Fe, Co, and Ni ions, are studied, and the results show that the dielectric of the PMN-0.9PT doped with Fe ion is larger than that of PMN-0.9PT doped with Co or Ni ions. In addition, the annealing atmosphere such as air and N_2-H_2 has effect on the ageing behavior of the sample.

High dielectric constants of relaxor feroelectrics occur near the temperature of the dielectric phase transition (T_{max}); therefore, different modifications of PMN-PT with Ba, Sr, and La have been made to control T_{max} and other properties. One finds that the 90/10 PMN/PT solid solution with 3% lanthanum dopant (90/10/3 PMN/PT/La) has a nominal T_{max} of 25°C and behaves as a relaxor. One of most important criteria for electromechanical materials is a coupling coefficient, k, which is used to determine the efficiency of energy conversion between the electrical and mechanical domains. To predict the coupling coefficient of 90/10/3 PMN/PT/La, the model proposed by Hom *et al.* (1994) is used. The remanent polarization, polarization at bias field, compliance, dielectric constant, and electrostrictive coefficient need to be measured to calculate the transverse coupling. The result shows that the transverse coupling for 90/10/3 PMN/PT/La is function of the applied electric field (Mangin *et al.*, 1996).

Multilayer ceramics consist of alternating layers of ferroelectric ceramic and conductive layers have been used as actuators and capacitors. To improve the performance of PMN-PT ceramics, the 0.9PMN-0.1PT ceramics modified with different amounts of ZnO prepared by molten salt synthesis (MSS) are studied by Yoon, *et al.* (1996). Also, the dielectric and electrostrictive properties are investigated in terms of ZnO content and the number of active layers. It is shown that the addition of the proper amount of ZnO and MSS method can improve the dielectric properties, phase stability, and sinterbility of the PMN-PT ceramics. It is also indicated that the temperature dependence of capacitance for the PMN-PT is a function of ZnO content and the number of active layers. The capacitance of the specimen with four active layers increases with increasing ZnO content up to 2 mol%, and then decreases with further increasing the additions of ZnO; however, a maximum dielectric is obtained with an addition of 2 mol% ZnO to the specimens with 4 active layers. But, the dielectric constant of PMN-PT decreases with further addition of ZnO. Moreover, increasing the number of active layers in the 2 mol% ZnO added PMN-PT results in an increase in the capacitance. The magnitude of induced strain increases with an increases in ZnO content up to 2 mol% and then decreases with further addition of ZnO.

The properties of actuators based on $0.55Pb(Mg_{1/3}Nb_{2/3})O_3$-$0.45Pb(Sc_{1/2}Nb_{1/2})O_3$ (0.55PMN-0.45PSN) electrostrictive ceramic are studied by Isopov *et al.* (1994). The displacement of 0.55PMN-0.45PSN is linear within the driving force range of 200 V to 800 V, and there exists a negligible hysteresis. The displacement obtained for 0.55PMN-0.45PSN is stable in the temperature region of 10^oC to 30^oC, which meet the majority of applications.

The existence of defects in multilayer PMN ceramic actuators may affect the performance of the actuator. Defects may include internal delamination at the interface between the PMN and electrode or microcracking which can be induced by electromechanical cycling of the devices. To determine the lifet of the device, research using three ultrasonic techniques, Contact ultrasound, acoustic emission, and ultrasonic second harmonic generation, to detect defects in multilayer PMN ceramic actuators before and after electromechanical cycling have been conducted (Bernstein *et al.*, 1996). The results indicate that the contact ultrasound is a good method to detect the delamination. The acoustic emission and ultrasonic second harmonic generation methods have potential for evaluating the changes in actuator condition since they can indicate whether the actuators were damaged during cycling.

PMN and PZT bimorph actuators and sensors for smart microsystem have been studied by Gaucher (1996). The PMN/PZT actuators and sensors are used in a cantilever laminated structure for active vibration control. It is reported that the displacement can be reduced by the active damping control of using PMN/PZT actuators and sensors. It also shows that the cantilever laminated structure can be a self-regulated structure using PMN/PZT actuators. The technology is later applied to microsystems. The device made of silicon and is actuated and sensed by a PZT thin film can be made ten times smaller than current one.

The electrostrictive polymer can offer fast and large response to excitations, and therefore, they are promising in a lot of applications such as acoustic transducer and artificial muscles. The electrostrictive response of a polyurethane elastomer consisting of alternating polyurethane and polyol segments is studied by Zhenyi *et al.* (1994). The thickness coefficient, d_t, and the strain of the polyurethane film (PU) are measured. The thickness coefficient for electrostrictive materials is defined as the ratio of the change in strain to the change in applied electric field. It is reported that the thickness coefficient and the strain of PU are both nonlinear functions of the applied DC bias electric field. The value of d_t is linearly increased with increasing electric field. When the electric field reaches 15 MV/m, the d_t tends to approch a constant value of 6.2 Å/V, which is about 20 times larger that the largest d_t coefficient of any piezoelectric polymer known. The applied DC bias field could be increased to 40 MV/m for the polyurethane film without causing dielectric breakdown.

1.3 Problem Statement

To provide guidelines for designing advanced transducers, accurate mechanics models involving the microstructure of transducer materials need to be developed, so that the interactions among processing, microstructure, and macroscopic properties can be delineated. The objective of the present work is to study the electro-mechanical coupling in electrostrictive materials from a microstructural point of view.

Piezoelectric materials exhibiting linear coupling between mechanical and electrical fields have received extensive attention in recent years. Electrostrictive materials involving nonlinear electro-mechanical coupling in principle can be tuned under a bias field, and therefore, may be promising in light of smart sensors and actuators development. A systematic, comprehensive study of electro-mechanical coupling in electrostrictive materials is not available. The present work is extended to bridge that gap.

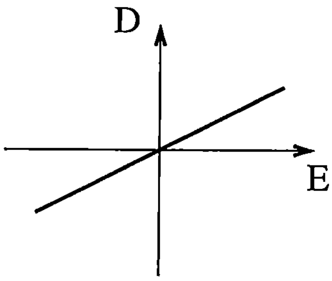

(a)

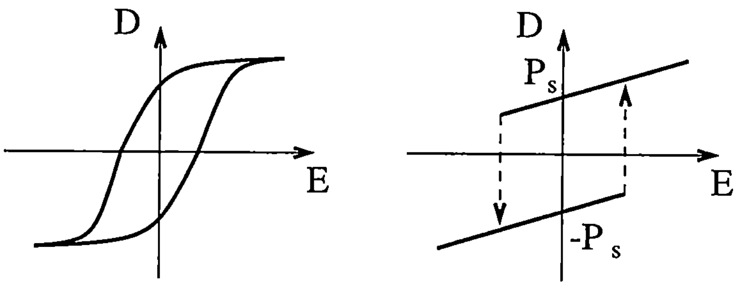

(b)

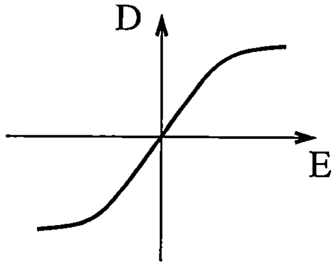

(c)

Figure 1.2: D-E relation for (a) dielectrics, (b) ferroelectrics, and (c) relaxors.

Chapter 2

Application of Laminated Plate Theory to Smart Electrostrictive Composites

2.1 Lamina Analysis

The constitutive relations for three-dimensional electrostrictive materials can be expressed by (Ikeda, 1990)

$$\varepsilon_{ij} = s_{ijkl}\sigma_{kl} + Q_{ijkl}P_kP_l, \tag{2.1}$$

$$E_i = \beta_{ij}P_j - 2Q_{jkli}\sigma_{jk}P_l, \tag{2.2}$$

where $i, j, k,$ and $l = 1, 2, 3$, ε is the strain tensor, s is the compliance tensor, σ is the stress tensor, Q are the electrostrictive constants, P is the polarization vector, E are the electric fields, and β is the permittivity tensor. The summation convention is used throughout the dissertation. Conversely, Eq. (2.1) can be written by

$$\sigma_{ij} = C_{ijkl}\varepsilon_{kl} - H_{ijkl}P_kP_l, \tag{2.3}$$

where C $(= s^{-1})$ is the stiffness tensor, and H is given by

$$H_{ijkl} = C_{ijmn}Q_{mnkl}; \tag{2.4}$$

Eq. (2.2) and (2.3) for orthotropic materials can be rewritten in matrix form by

$$\begin{Bmatrix} E_1 \\ E_2 \\ E_3 \end{Bmatrix} = \begin{bmatrix} \beta_{11} & 0 & 0 \\ 0 & \beta_{22} & 0 \\ 0 & 0 & \beta_{33} \end{bmatrix} \begin{Bmatrix} P_1 \\ P_2 \\ P_3 \end{Bmatrix} - 2 \begin{bmatrix} q_{11} & q_{12} & q_{13} \\ q_{12} & q_{22} & q_{23} \\ q_{13} & q_{23} & q_{33} \end{bmatrix} \begin{Bmatrix} P_1 \\ P_2 \\ P_3 \end{Bmatrix}, \tag{2.5}$$

$$\begin{Bmatrix} \sigma_{11} \\ \sigma_{22} \\ \sigma_{33} \\ \sigma_{23} \\ \sigma_{31} \\ \sigma_{12} \end{Bmatrix} = \begin{bmatrix} C_{1111} & C_{1122} & C_{1133} & 0 & 0 & 0 \\ C_{1122} & C_{2222} & C_{2233} & 0 & 0 & 0 \\ C_{1133} & C_{2233} & C_{3333} & 0 & 0 & 0 \\ 0 & 0 & 0 & C_{2323} & 0 & 0 \\ 0 & 0 & 0 & 0 & C_{3131} & 0 \\ 0 & 0 & 0 & 0 & 0 & C_{1212} \end{bmatrix} \begin{Bmatrix} \varepsilon_{11} \\ \varepsilon_{22} \\ \varepsilon_{33} \\ 2\varepsilon_{23} \\ 2\varepsilon_{31} \\ 2\varepsilon_{12} \end{Bmatrix}$$

$$
-\begin{bmatrix} H_{1111} & H_{1122} & H_{1133} & 0 & 0 & 0 \\ H_{2211} & H_{2222} & H_{2233} & 0 & 0 & 0 \\ H_{3311} & H_{3322} & H_{3333} & 0 & 0 & 0 \\ 0 & 0 & 0 & 2H_{2323} & 0 & 0 \\ 0 & 0 & 0 & 0 & 2H_{3131} & 0 \\ 0 & 0 & 0 & 0 & 0 & 2H_{1212} \end{bmatrix} \begin{Bmatrix} P_1^2 \\ P_2^2 \\ P_3^2 \\ P_2 P_3 \\ P_3 P_1 \\ P_1 P_2 \end{Bmatrix}, \tag{2.6}
$$

where

$$q_{11} = Q_{1111}\sigma_{11} + Q_{2211}\sigma_{22} + Q_{3311}\sigma_{33}, \tag{2.7}$$

$$q_{12} = 2Q_{1212}\sigma_{12}, \tag{2.8}$$

$$q_{13} = 2Q_{3131}\sigma_{31}, \tag{2.9}$$

$$q_{22} = Q_{1122}\sigma_{11} + Q_{2222}\sigma_{22} + Q_{3322}\sigma_{33}, \tag{2.10}$$

$$q_{23} = 2Q_{2323}\sigma_{23}, \tag{2.11}$$

$$q_{33} = Q_{1133}\sigma_{11} + Q_{2233}\sigma_{22} + Q_{3333}\sigma_{33}, \tag{2.12}$$

$$H_{1111} = C_{1111}Q_{1111} + C_{1122}Q_{2211} + C_{1133}Q_{3311},$$

$$H_{1122} = C_{1111}Q_{1122} + C_{1122}Q_{2222} + C_{1133}Q_{3322},$$

$$H_{1133} = C_{1111}Q_{1133} + C_{1122}Q_{2233} + C_{1133}Q_{3333},$$

$$H_{2211} = C_{1122}Q_{1111} + C_{2222}Q_{2211} + C_{2233}Q_{3311},$$

$$H_{2222} = C_{1122}Q_{1122} + C_{2222}Q_{2222} + C_{2233}Q_{3322}, \tag{2.13}$$

$$H_{2233} = C_{1122}Q_{1133} + C_{2222}Q_{2233} + C_{2233}Q_{3333},$$

$$H_{3311} = C_{1133}Q_{1111} + C_{2233}Q_{2211} + C_{3333}Q_{3311},$$

$$H_{3322} = C_{1133}Q_{1122} + C_{2233}Q_{2222} + C_{3333}Q_{3322},$$

$$H_{3333} = C_{1133}Q_{1133} + C_{2233}Q_{2233} + C_{3333}Q_{3333},$$

$$H_{2323} = 2C_{2323}Q_{2323},$$

$$H_{3131} = 2C_{3131}Q_{3131},$$

$$H_{1212} = 2C_{1212}Q_{1212}.$$

It is noted that the electrostrictive constants of orthotropic electrostrictive materials can be expressed in matrix form by

$$[Q] = \begin{bmatrix} Q_{1111} & Q_{1122} & Q_{1133} & 0 & 0 & 0 \\ Q_{2211} & Q_{2222} & Q_{2233} & 0 & 0 & 0 \\ Q_{3311} & Q_{3322} & Q_{3333} & 0 & 0 & 0 \\ 0 & 0 & 0 & 4Q_{2323} & 0 & 0 \\ 0 & 0 & 0 & 0 & 4Q_{3131} & 0 \\ 0 & 0 & 0 & 0 & 0 & 4Q_{1212} \end{bmatrix}. \tag{2.14}$$

A plane stress state is assumed in a thin electrostrictive lamina; see Figure 2.1(a). That is,

$$\sigma_{33} = \sigma_{23} = \sigma_{31} = 0, \tag{2.15}$$

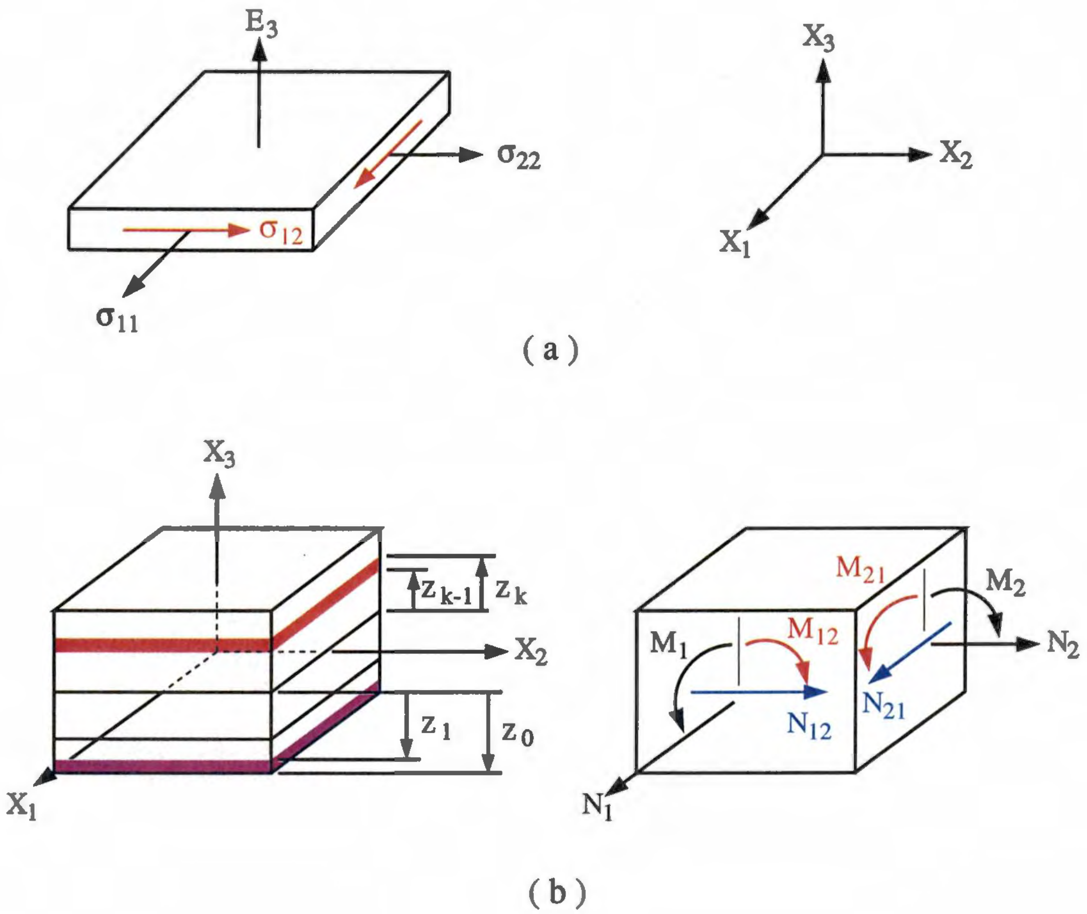

Figure 2.1: A schematic of : (a) a lamina, and (b) a laminate.

$$E_1 = E_2 = 0, \tag{2.16}$$

which implies that $P_1 = P_2 = 0$ in view of Eq. (2.5). Eq. (2.5) and (2.6) are thus reduced to

$$E_3 = \beta_{33} P_3 - 2(Q_{1133}\sigma_{11} + Q_{2233}\sigma_{22})P_3, \tag{2.17}$$

or

$$P_3 = \frac{E_3}{\beta_{33} - 2(Q_{1133}\sigma_{11} + Q_{2233}\sigma_{22})}, \tag{2.18}$$

and

$$\begin{Bmatrix} \sigma_{11} \\ \sigma_{22} \\ \sigma_{12} \end{Bmatrix} = \begin{bmatrix} C^*_{1111} & C^*_{1122} & 0 \\ C^*_{1122} & C^*_{2222} & 0 \\ 0 & 0 & C^*_{1212} \end{bmatrix} \begin{Bmatrix} \varepsilon_{11} \\ \varepsilon_{22} \\ 2\varepsilon_{12} \end{Bmatrix} - \begin{Bmatrix} H^*_{1133} \\ H^*_{2233} \\ 0 \end{Bmatrix} P_3^2, \tag{2.19}$$

where

$$C^*_{1111} = C_{1111} - \frac{C^2_{1133}}{C_{3333}}, \tag{2.20}$$

$$C^*_{2222} = C_{2222} - \frac{C^2_{2233}}{C_{3333}}, \tag{2.21}$$

$$C^*_{1122} = C_{1122} - \frac{C_{1133}C_{2233}}{C_{3333}}, \tag{2.22}$$

$$C^*_{1212} = C_{1212}, \tag{2.23}$$

$$H^*_{1133} = H_{1133} - \frac{C_{1133}H_{3333}}{C_{3333}}, \tag{2.24}$$

$$H^*_{2233} = H_{2233} - \frac{C_{2233}H_{3333}}{C_{3333}}. \tag{2.25}$$

2.2 Laminate Analysis

Based on the classical laminated plate theory (see Appendix A for a brief review), the laminate strains, $\{\varepsilon\} = \{\varepsilon_{11}, \varepsilon_{22}, 2\varepsilon_{12}\}^T$, are related to the midplane strains, $\{\varepsilon^o\} = \{\varepsilon^o_{11}, \varepsilon^o_{22}, 2\varepsilon^o_{12}\}^T$, and curvatures, $\{\rho\} = \{\rho_{11}, \rho_{22}, 2\rho_{12}\}^T$, by

$$\{\varepsilon\} = \{\varepsilon^o\} + z\{\rho\}, \tag{2.26}$$

where z $(= x_3)$ is the coordinate in the laminate thickness direction.

The resultant forces per unit length, $\{N\} = \{N_1, N_2, N_{12}\}^T$, and moments per unit length, $\{M\} = \{M_1, M_2, M_{12}\}^T$, acting on a laminate are related to the ply stresses by

$$\{N\} = \int_{-t/2}^{t/2} \{\sigma\} dz = \sum_{k=1}^{n} \int_{z_{k-1}}^{z_k} \{\sigma\}_k dz, \tag{2.27}$$

$$\{M\} = \int_{-t/2}^{t/2} \{\sigma\} z dz = \sum_{k=1}^{n} \int_{z_{k-1}}^{z_k} \{\sigma\}_k z dz, \tag{2.28}$$

where $\{\sigma\} = \{\sigma_{11}, \sigma_{22}, \sigma_{12}\}^T$, and t is the laminate thickness. The subscript k designates the ply number, n is the total number of laminae, z_k and z_{k-1} are the z-coordinates of the top and bottom surfaces of the k^{th} lamina, respectively; see Figure 2.1(b).

Substituting Eq. (2.19) into Eq. (2.27) and (2.28), with the help of Eq. (2.26), gives

$$[A]\{\varepsilon^o\} + [B]\{\rho\} = \{N\} + \{N^e\}, \tag{2.29}$$

$$[B]\{\varepsilon^o\} + [D]\{\rho\} = \{M\} + \{M^e\}, \tag{2.30}$$

where the three-by-three extensional stiffness, coupling stiffness, and bending stiffness are given by

$$[A] = \sum_{k=1}^{n} [C^*]_k (z_k - z_{k-1}), \tag{2.31}$$

$$[B] = \frac{1}{2} \sum_{k=1}^{n} [C^*]_k (z_k^2 - z_{k-1}^2), \tag{2.32}$$

$$[D] = \frac{1}{3} \sum_{k=1}^{n} [C^*]_k (z_k^3 - z_{k-1}^3), \tag{2.33}$$

respectively, where the subscript k again designates the ply number and the reduced stiffness matrix, $[C^*]$, is given in Eq. (2.19) - (2.23). The forces and moments due to the electrical fields, $\{N^e\} = \{N_1^e, N_2^e, N_{12}^e\}^T$ and $\{M^e\} = \{M_1^e, M_2^e, M_{12}^e\}^T$, are given by

$$\{N^e\} = \sum_{k=1}^{n} \int_{z_{k-1}}^{z_k} \{H^*\}_k P_3^2 dz, \tag{2.34}$$

$$\{M^e\} = \sum_{k=1}^{n} \int_{z_{k-1}}^{z_k} \{H^*\}_k P_3^2 z dz, \tag{2.35}$$

where $\{H^*\}$ is given in Eq. (2.19), (2.24), and (2.25). Substituting Eq. (2.18) into Eq. (2.34) and (2.35), one finds

$$\{N^e\} = \sum_{k=1}^{n} \int_{z_{k-1}}^{z_k} \{H^*\}_k \left(\frac{E_3}{\beta_{33} - 2(Q_{1133}\sigma_{11} + Q_{2233}\sigma_{22})}\right)^2 dz, \tag{2.36}$$

$$\{M^e\} = \sum_{k=1}^{n} \int_{z_{k-1}}^{z_k} \{H^*\}_k \left(\frac{E_3}{\beta_{33} - 2(Q_{1133}\sigma_{11} + Q_{2233}\sigma_{22})}\right)^2 z dz. \tag{2.37}$$

It is noted that σ_{11} and σ_{22} involved in Eq. (2.36) and (2.37) are unknowns. Therefore, closed-form solutions to the nonlinear, coupled Eq. (2.29) and (2.30) may not be obtained and an iterative solution strategy is to be developed. To this end, one assumes that the normal stresses, σ_{11} and σ_{22}, within each ply are linear functions of the z coordinate and can be expressed by

$$\sigma_{11}(z) = (\sigma_{11})_{k-1} + \frac{(\sigma_{11})_k - (\sigma_{11})_{k-1}}{z_k - z_{k-1}}(z - z_{k-1}), \tag{2.38}$$

$$\sigma_{22}(z) = (\sigma_{22})_{k-1} + \frac{(\sigma_{22})_k - (\sigma_{22})_{k-1}}{z_k - z_{k-1}}(z - z_{k-1}). \tag{2.39}$$

where $(\sigma_{11})_k$ and $(\sigma_{22})_k$ are the stresses on the top of the k^{th} ply, and $(\sigma_{11})_{k-1}$ and $(\sigma_{22})_{k-1}$ are the stresses on the bottom of the k^{th} ply. Substituting Eq. (2.38) and (2.39) into (2.36) and (2.37), gives

$$\{N^e\} = \sum_{k=1}^{n} \frac{E_3^2}{b}(\frac{1}{a} - \frac{1}{c})\{H^*\}, \tag{2.40}$$

$$\{M^e\} = \sum_{k=1}^{n} \frac{E_3^2}{b^2}[\ln(\frac{c}{a}) - (a - bz_{k-1})(\frac{1}{a} - \frac{1}{c})]\{H^*\}, \tag{2.41}$$

where

$$a = \beta_{33} - 2[Q_{1133}(\sigma_{11})_{k-1} + Q_{2233}(\sigma_{22})_{k-1}], \tag{2.42}$$

$$b = \frac{-2[Q_{1133}((\sigma_{11})_k - (\sigma_{11})_{k-1}) + Q_{2233}((\sigma_{22})_k - (\sigma_{22})_{k-1})]}{z_k - z_{k-1}}, \tag{2.43}$$

$$c = a + b(z_k - z_{k-1}). \tag{2.44}$$

Given material properties, $[C]$, $[Q]$, and $[\beta]$, composite geometry, z_k, and loading conditions, $\{N\}$, $\{M\}$ and $\{E\}$, one can compute $[A]$, $[B]$, and $[D]$ matrices using Eq. (2.31) - (2.33). By assuming trial stresses $\{\sigma\}^i$ at the top and bottom of each ply (see next section), one can compute the forces and moments due to electric fields, $\{N^e\}$ and $\{M^e\}$, using Eq. (2.40) and (2.41). Eq. (2.29) and (2.30) can therefore be readily solved for the midplane strains $\{\varepsilon^o\}$ and curvatures $\{\rho\}$. Finally, the ply strains $\{\varepsilon\}$ and the new ply stresses $\{\sigma\}^{i+1}$ can be obtained from Eq. (2.26) and (2.19), respectively. The relative errors between the new ply stresses $\{\sigma\}^{i+1}$ and the old ply stresses $\{\sigma\}^i$ are computed and compared with a specified tolerance:

$$\frac{\{\sigma\}^{i+1} - \{\sigma\}^i}{\{\sigma\}^{i+1}} \leq \text{tolerance.} \tag{2.45}$$

If the above convergence criterion is satisfied, the latest stresses and strains are the final results. Otherwise, the new stresses are used in computing $\{N^e\}$ and $\{M^e\}$, and the aforementioned procedures are repeated until the convergence condition is satisfied; see Figure 2.2. To generate a good initial guess of the ply stress for the iterative solution, a closed form solution is developed in the next section.

2.3 Closed-Form Solution

To develop a closed-form estimate of the ply stresses in electrostrictive composite laminates, and to generate an initial trial solution to the iterative method derived in the previous section, one assumes that the second term on the right side of Eq. (2.2), $2Q_{jkli}\sigma_{jk}P_l$, is negligible in comparison with the first term, $\beta_{ij}P_j$. Thus,

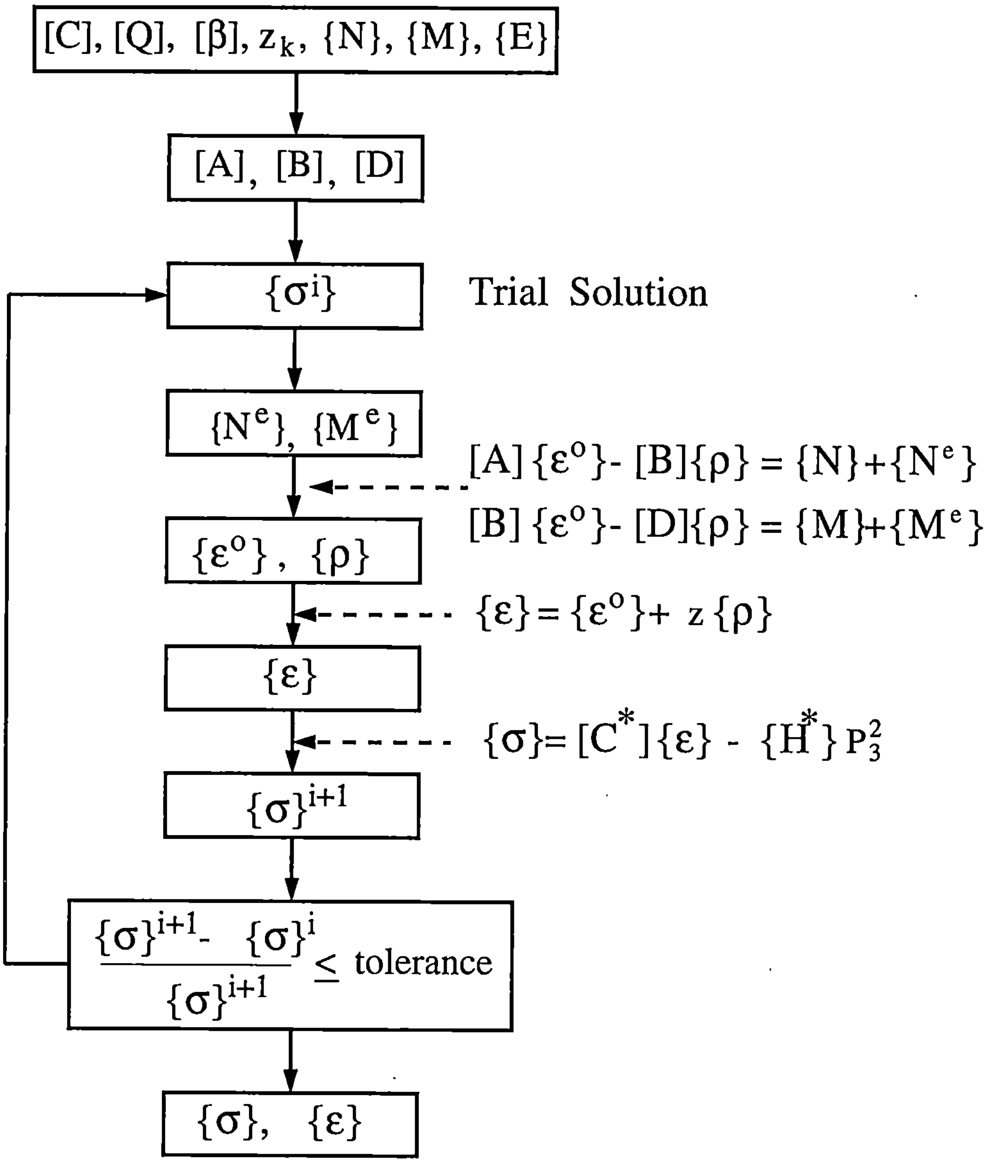

Figure 2.2: Solution strategy.

Eq. (2.2) becomes

$$E_i = \beta_{ij} P_j. \tag{2.46}$$

Consequently, Eq. (2.36) and (2.37) reduce to

$$\{N^e\} = \sum_{k=1}^{n} \int_{z_{k-1}}^{z_k} (\frac{E_3}{\beta_{33}})^2 \{H^*\}_k dz, \tag{2.47}$$

$$\{M^e\} = \sum_{k=1}^{n} \int_{z_{k-1}}^{z_k} (\frac{E_3}{\beta_{33}})^2 z \{H^*\}_k dz. \tag{2.48}$$

Eq. (2.29) and (2.30) can then be solved analytically for the midplane strains and curvatures

$$\left\{ \begin{array}{c} \varepsilon^o \\ \\ \rho \end{array} \right\} = \left[\begin{array}{cc} A & B \\ \\ B & D \end{array} \right]^{-1} \left\{ \begin{array}{c} N + N^e \\ \\ M + M^e \end{array} \right\}. \tag{2.49}$$

Specifically,

$$\begin{aligned} \{\varepsilon^o\} &= ([A]^{-1} + [A]^{-1}[B]([D] - [B][A]^{-1}[B])^{-1}[B][A]^{-1})\{N + N^e\} \\ &\quad -[A]^{-1}[B]([D] - [B][A]^{-1}[B])^{-1}\{M + M^e\}, \end{aligned} \tag{2.50}$$

$$\begin{aligned} \{\rho\} &= -([D] - [B][A]^{-1}[B])^{-1}[B][A]^{-1})\{N + N^e\} \\ &\quad +([D] - [B][A]^{-1}[B])^{-1}\{M + M^e\}. \end{aligned} \tag{2.51}$$

The ply strains and stresses can be readily obtained from Eq. (2.26) and (2.19), respectively.

2.4 Results and Discussions

Three types of electrostrictive materials are studied in the present work using the iterative and closed-form formulations: (1) a PMN ceramic, (2) an unsymmetric two-layered composite of brass/PMN, aluminum/PMN, or epoxy/PMN, and (3) a symmetric three-layered composite with a layer of PMN being sandwiched between two layers of brass. The material properties of isotropic PMN, brass, aluminum (Al), and epoxy are given in Table 2.1.

To check the validity of the constitutive relations, Eq. (2.1) and (2.2), one considers a PMN ceramic with a thickness of 0.1 mm subjected to an electric field, E_3, in the x_3 direction. The predicted compressive strains, $\varepsilon_{11} = \varepsilon_{22}$, in the x_1 and x_2 directions in response to an electric field in the x_3-direction are shown in Figure 2.3. The iterative solution shows a nonlinear relationship between resulting strains and applied electric fields and agrees very well with the experimental data (Jang *et al.*, 1980).

Consider a two-layered brass/PMN composite with the thickness of each layer being 1 mm. The brass/PMN is subjected to an electric field, $E_3 = 1$ kV/mm. The compressive strains of the top PMN layer and the tensile strains of the bottom brass layer, ε_{11} $(= \varepsilon_{22})$, obtained from the iterative and closed-form formulations, as a function of the vertical position, z, of the composite are shown in Figure 2.4. Both the iterative and closed-form formulations give almost the same linear

Table 2.1: Material properties of PMN, brass, aluminum, and epoxy

Material	E (GPa)	ν	$\beta_{11} = \beta_{22} = \beta_{33}$ (m/F)	Q_{11} (m^4/C^2)	Q_{12} (m^4/C^2)
PMN	112	0.26	1.5066×10^7	0.026	-0.0096
Brass	110	0.37			
Aluminum	69	0.33			
Epoxy	2.5	0.40			

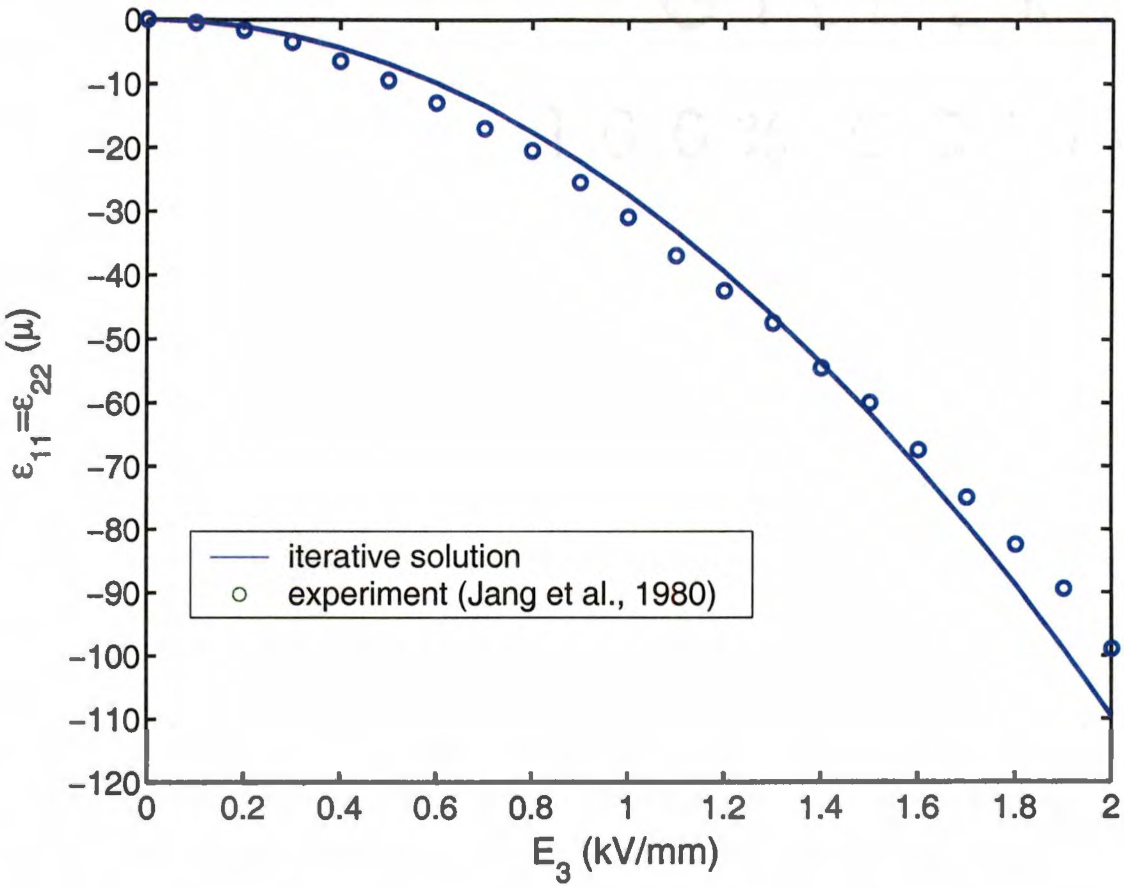

Figure 2.3: Strain ε_{11} ($= \varepsilon_{22}$) of PMN as a function of E_3.

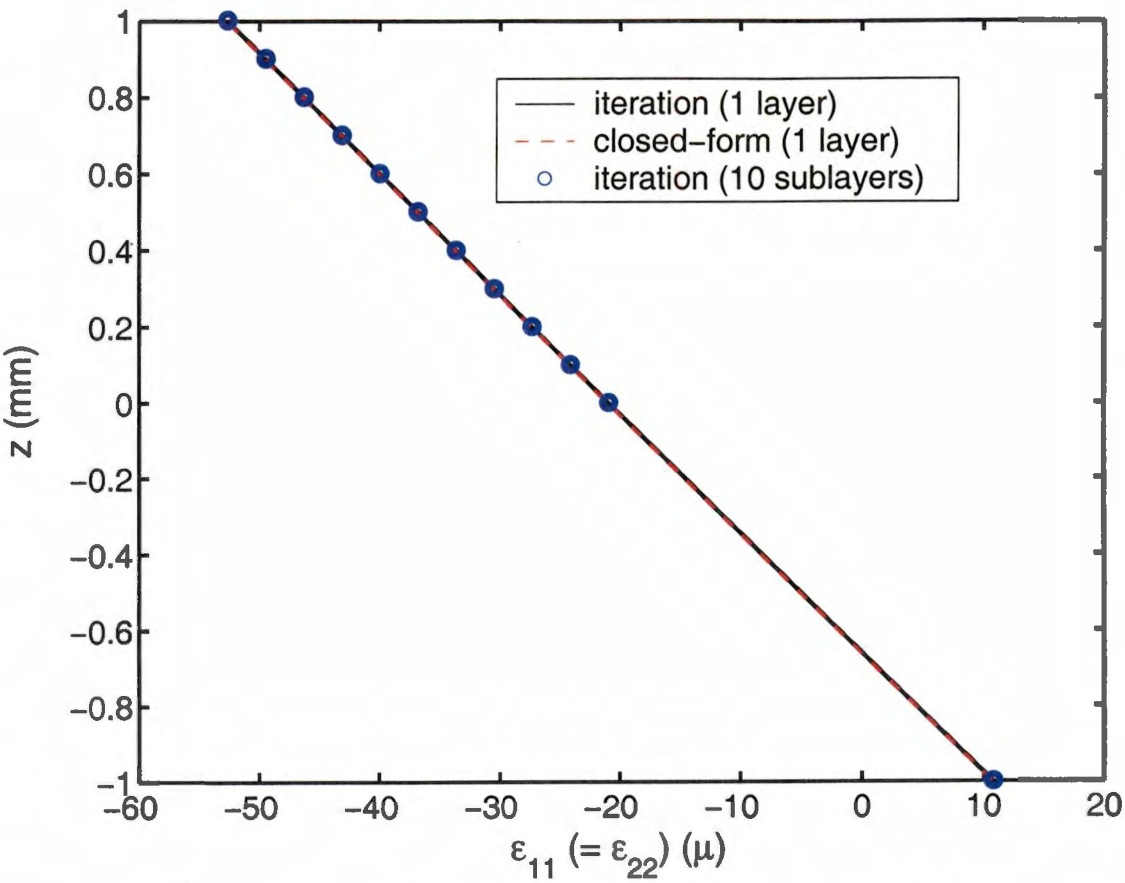

Figure 2.4: Strain ε_{11} ($= \varepsilon_{22}$) as a function of vertical position, z, for a brass/PMN subjected to $E_3 = 1$ kV/mm.

distribution of strains; see Eq. (2.26). The stress σ_{11} (= σ_{22}) as a function of z is shown in Figure 2.5. To check the validity of the assumption of linear stress distribution within each ply, the top PMN layer is divided into ten sub-layers of equal thickness of 0.1 mm. Within each sub-layer, Eq. (2.38) and (2.39) are used. It is shown in Figure 2.4 and Figure 2.5 that the assumption of linear stress distribution within the entire PMN layer is acceptable. The nonlinear relationship between the applied electric field and the resulting strains is shown in Figure 2.6. When the electric field increases, the magnitude of the compressive strains of the top PMN, those of the interface, and the tensile strains of the bottom brass all increase.

The effect of the thickness of brass is studied in Figure 2.7 while the thickness of PMN remains 1 mm. When the thickness of brass is less than 0.5 mm, the compressive strains of the top of PMN ply increases, while the compressive strains of the bottom of brass ply decreases. On the other hand, when the thickness of brass is greater than 0.5 mm, the compressive strains of the top PMN ply decreases, whereas the tensile strains of the bottom brass ply increases and these approaches as asymptotic value.

The relationship between the polarization P_3 and the electric field E_3 in brass/PMN is shown in Figure 2.8. For iterative solutions, Eq. (2.17) is used and thus P_3 is a nonlinear function of E_3. On the other hand, Eq. (2.46) is

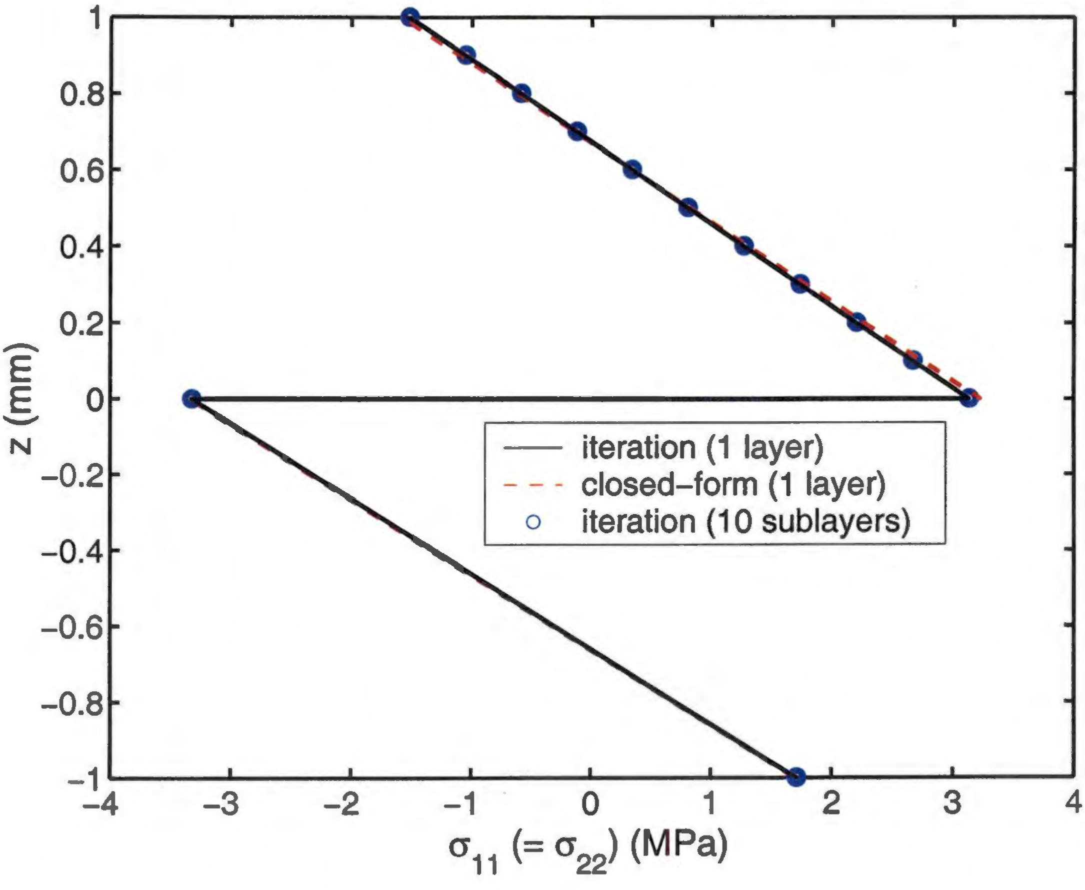

Figure 2.5: Stress σ_{11} $(= \sigma_{22})$ as a function of vertical position, z, for a brass/PMN subjected to $E_3 = 1$ kV/mm.

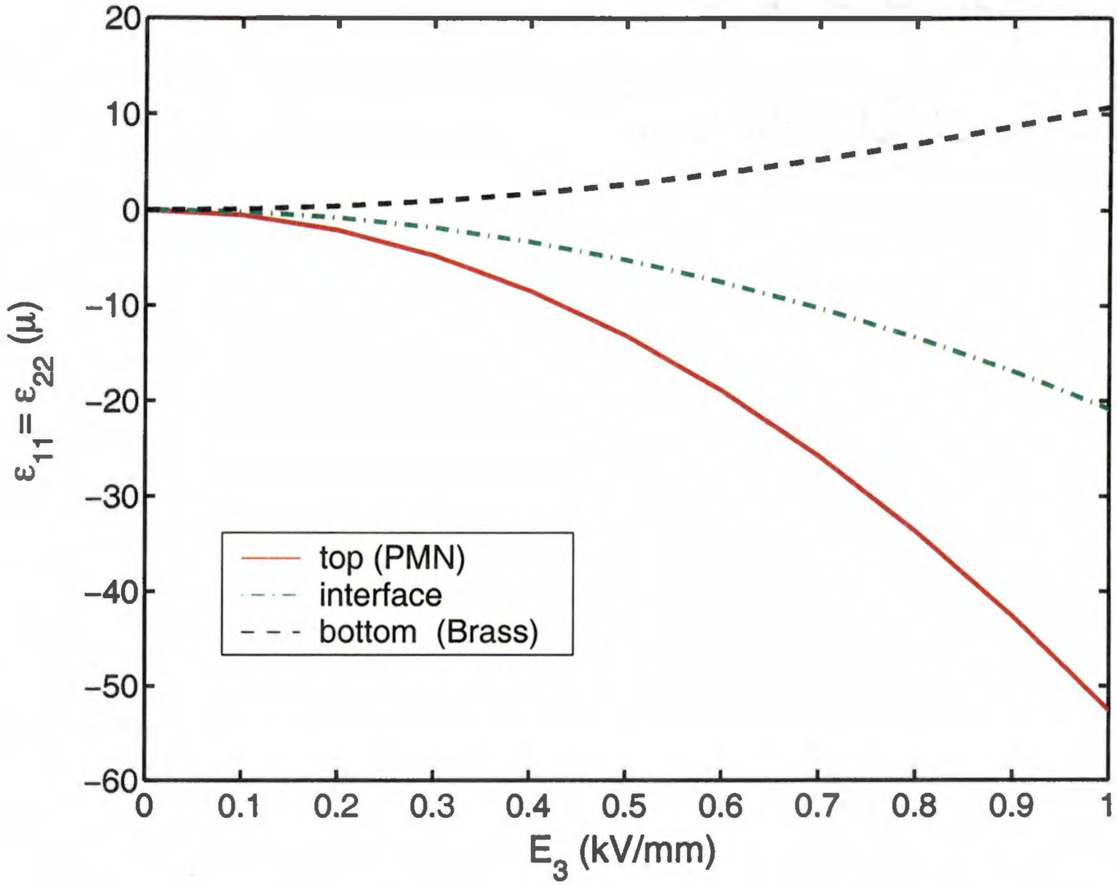

Figure 2.6: Strain ε_{11} ($= \varepsilon_{22}$) at the bottom, interface, and top of brass/PMN as a function of E_3.

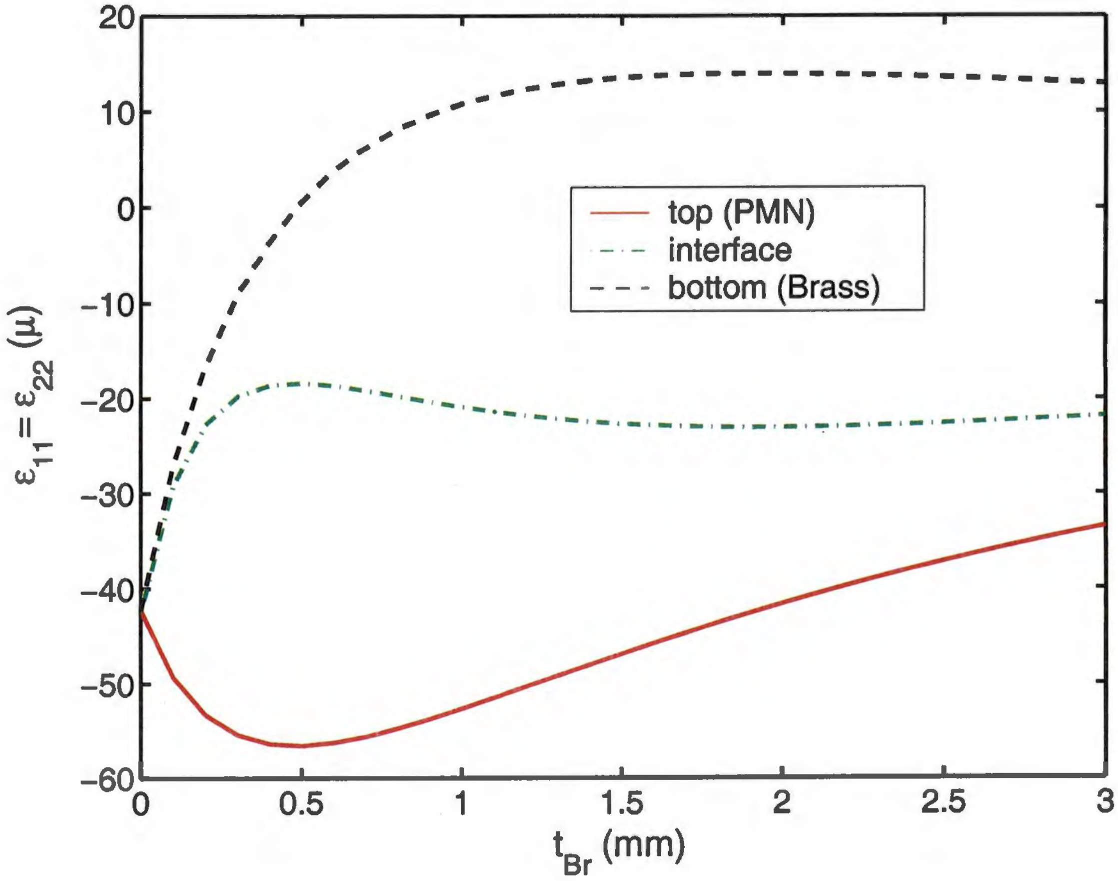

Figure 2.7: Strain ε_{11} ($= \varepsilon_{22}$) at the bottom, interface, and top of brass/PMN, subjected to $E_3 = 1$ kV/mm, as a function of the thickness of brass.

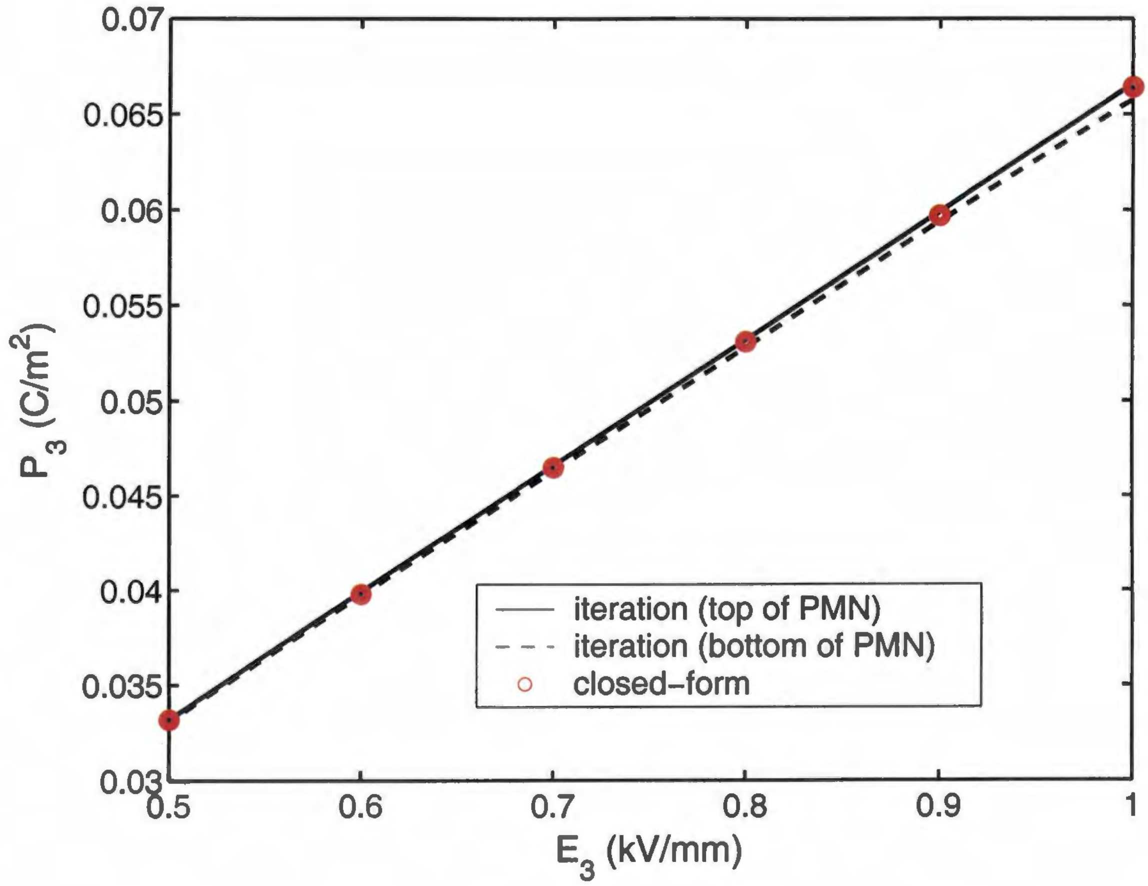

Figure 2.8: Polarization P_3 as a function of electric field E_3 in brass/PMN.

employed in the closed-form solutions and thus P_3 is a linear function of E_3 . However, the closed-form solution again agrees quite well with the iterative solution, which again indicates that the second term on the right-hand side of Eq. (2.2), $2Q_{jkli}\sigma_{jk}P_l$, is negligible.

When an electric field is applied to (brass/PMN)$_2$ in the x_3 direction, the four-layered composite with each ply thickness of 1mm exhibits compressive strains. For the two-layered composite brass/PMN, compressive strains are developed in the top PMN ply whereas tensile strains are developed in the bottom brass ply; see Figure 2.9.

In order to study the effects of material properties on the electromechanical coupling in electrostrictive composites, the brass layer is replaced by an aluminum (Al) or an epoxy ply. When an electric field, E_3, is applied to a brass/PMN and an Al/PMN, the top PMN ply contracts, whereas the bottom brass or Al undergoes elongation. For the epoxy/PMN composite, however, the top PMN ply, PMN/epoxy interface, and the bottom epoxy ply all contract; see Figure 2.10. However, it is noted that more compressive strains are developed in the PMN ply in the brass-based and Al-based composites than those of the epoxy-based composite. But the compressive strains at the interface of brass/PMN and Al/PMN are lower than that of PMN/epoxy.

When an electric field E_3 is applied to a two-layered brass/PMN composite,

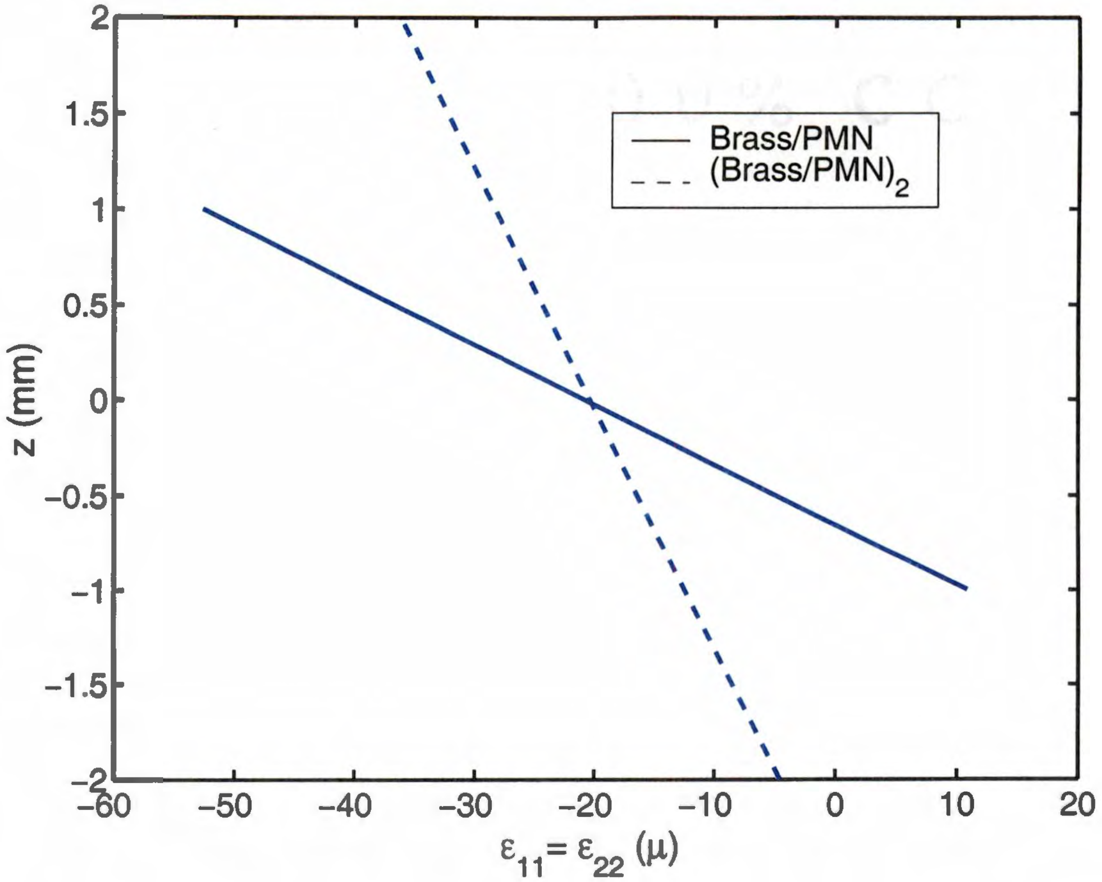

Figure 2.9: In-plane strain ε_{11} ($= \varepsilon_{22}$) as a function of vertical position, z, for brass/PMN and brass/PMN/brass/PMN composites subjected to $E_3 = 1$ kV/mm.

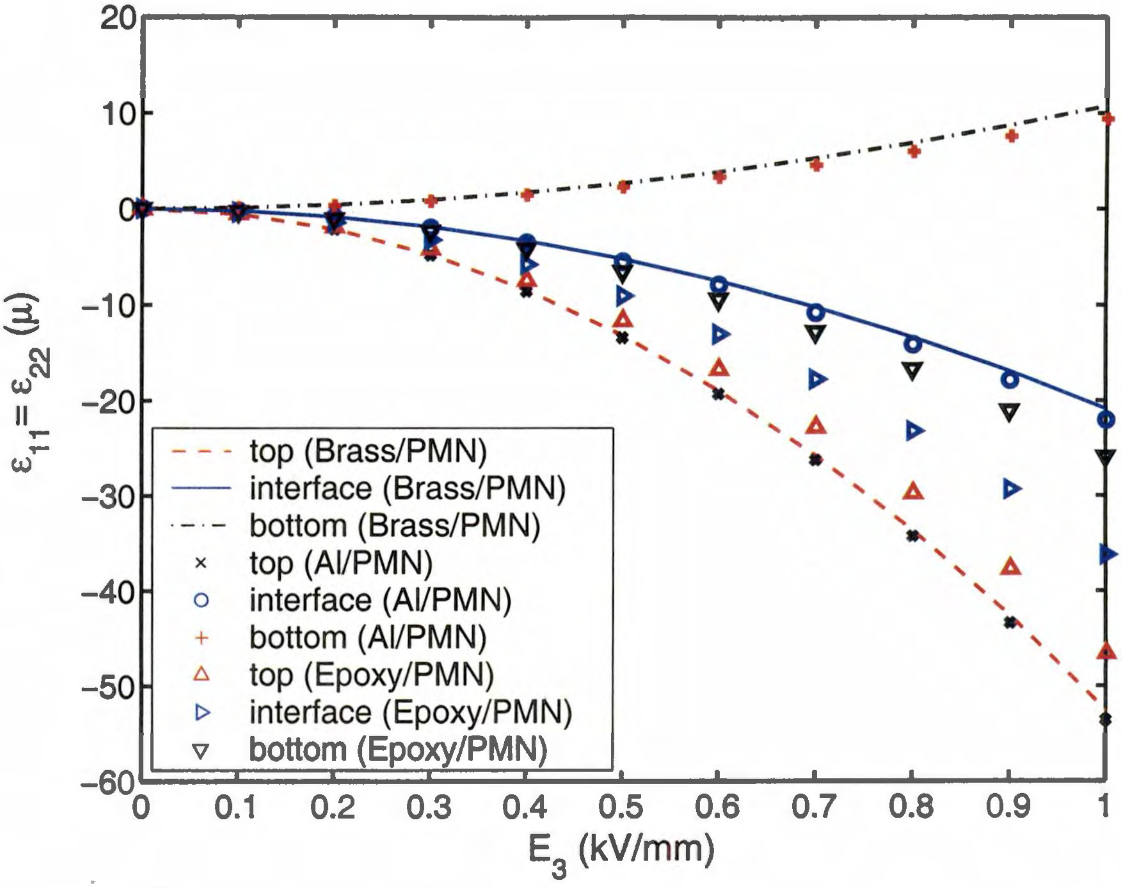

Figure 2.10: Strain ε_{11} ($= \varepsilon_{22}$) in brass/PMN, aluminum/PMN, and epoxy/PMN as a function of E_3.

a curvature, ρ_{11} $(= \rho_{22})$, will be developed because the composite is unsymmetric. To ensure no wrappage of the composite, one can apply a moment M_1 $(= M_2)$ to eliminate the curvature. On the other hand, if the curvature is caused by moment M_1 $(= M_2)$, one also can apply an electric field E_3 to the composite to eliminate the curvature. Figure 2.11 shows the relation between the resultant moments per unit length and the electric field for zero curvatures of brass/PMN.

Consider a symmetric brass/PMN/brass composite subjected to $E_3 = 1$ kV/mm. Each layer has a thickness of 1 mm. Both the iterative and the closed-form solution predict the same strain, $\varepsilon_{11} = -133\text{x}10^{-6}$. The in-plane stress, σ_{11} $(= \sigma_{22})$ as a function of vertical position, z, is shown in Figure 2.12. Again, the closed-form solution gives accurate estimates in comparison with the iterative solution, where the relative error is 2.2%. Moreover, the comparison between the compressive strains, which is equal to the compressive strain of the mid-surface, of the PMN ceramic with those of the brass/PMN/brass is shown in Figure 2.13. For brass/PMN/brass, the contraction of the PMN ply is constrained by the brass layers. Therefore, the compressive strain ε_{11} $(= \varepsilon_{22})$ of the three-layered brass/PMN/brass is less than that of PMN ceramics. When an electric field, $E_3 = 1$ kV/mm, is applied to a brass/PMN/brass, an increase in thickness of brass results in a decrease in the compressive strains ε_{11} $(= \varepsilon_{22})$ in the composite; see Figure 2.14.

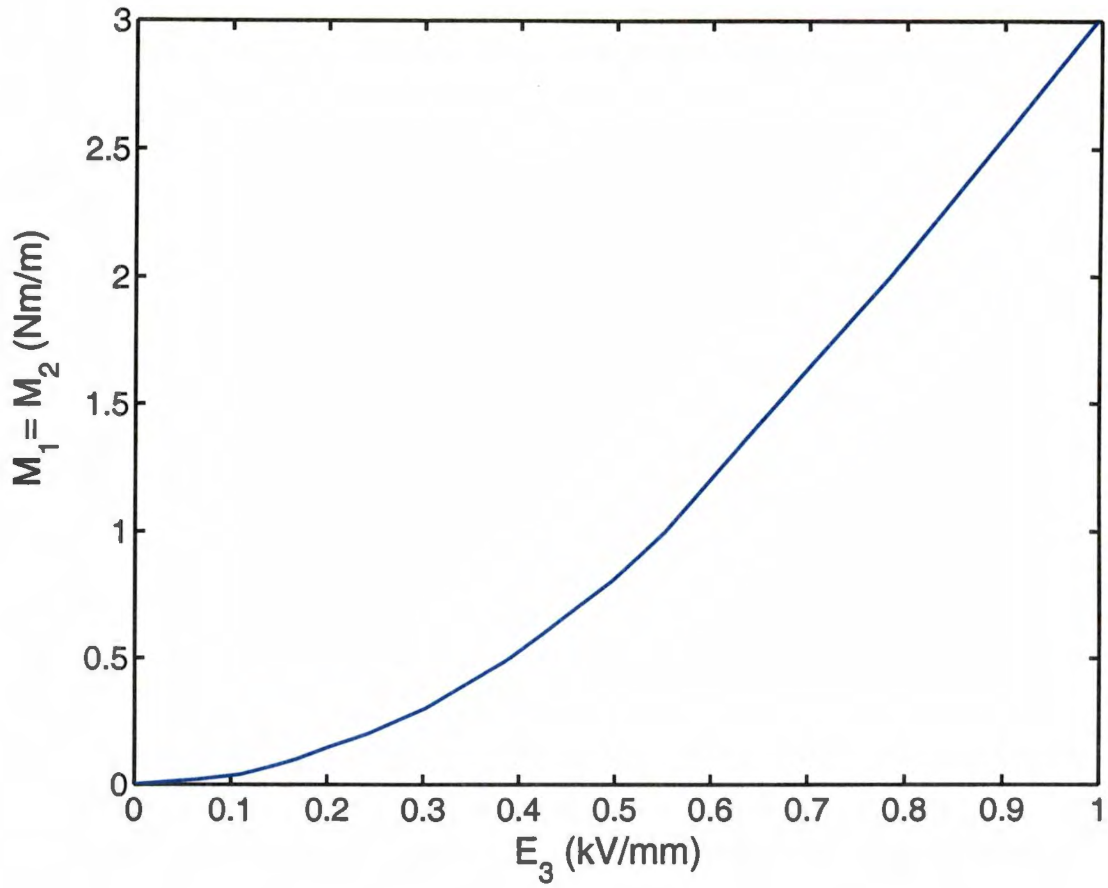

Figure 2.11: Moment M_1 ($= M_2$) as a function of electric field, E_3, for zero curvatures in brass/PMN.

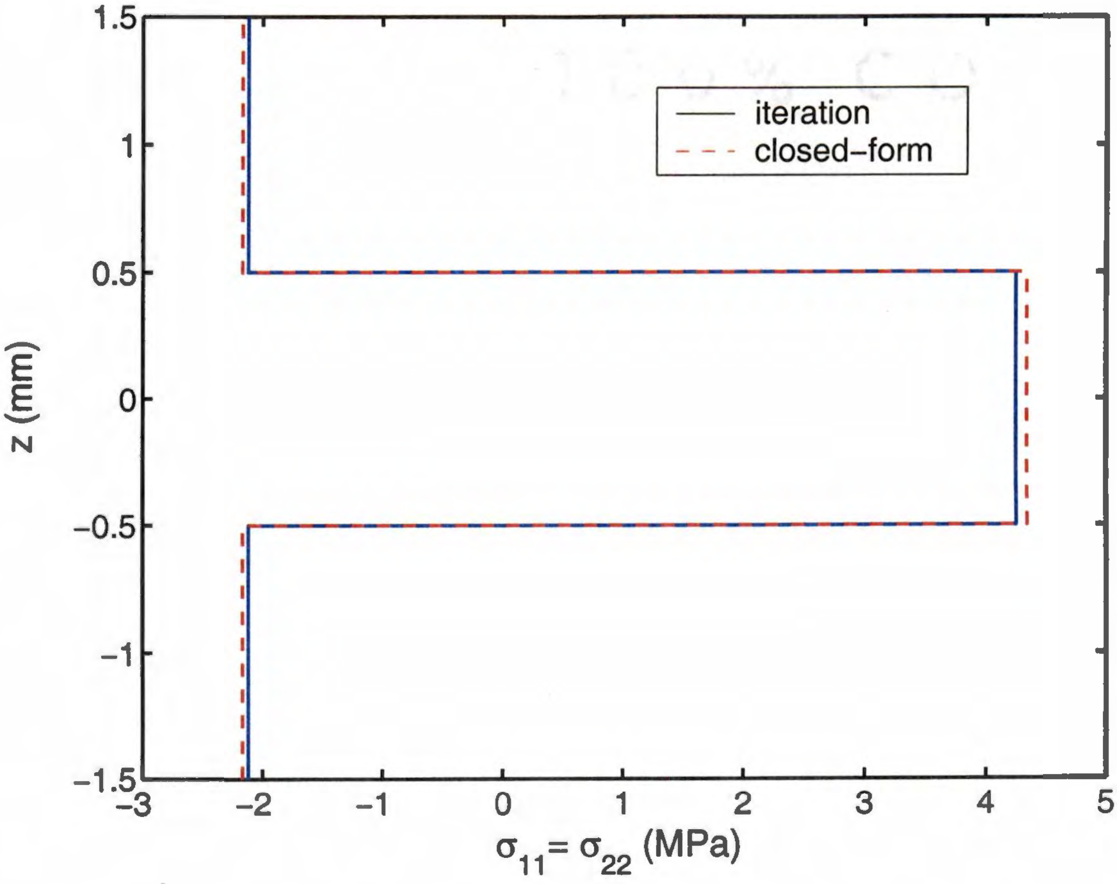

Figure 2.12: Stress σ_{11} (= σ_{22}) as a function of vertical position, z, for brass/PMN/brass subjected to $E_3 = 1$ kV/mm.

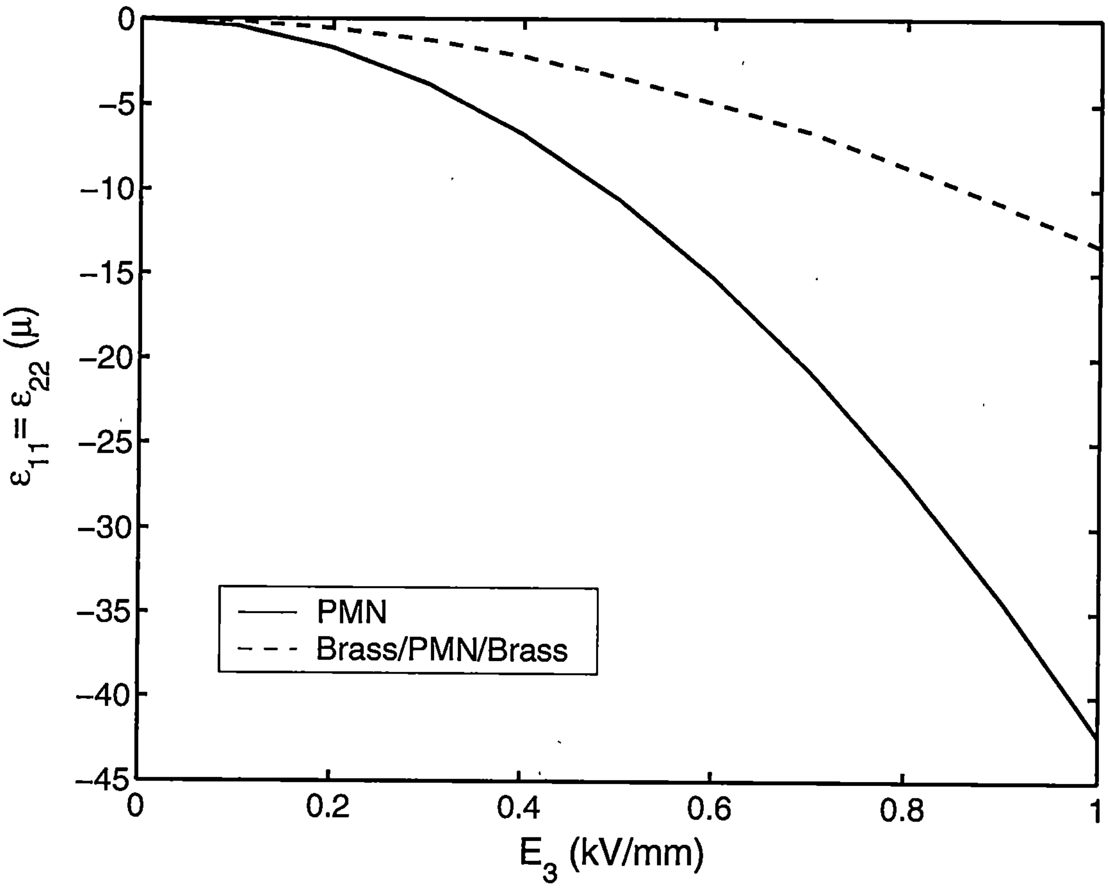

Figure 2.13: Strain ε_{11} ($= \varepsilon_{22}$) for PMN and brass/PMN/brass as a function of E_3.

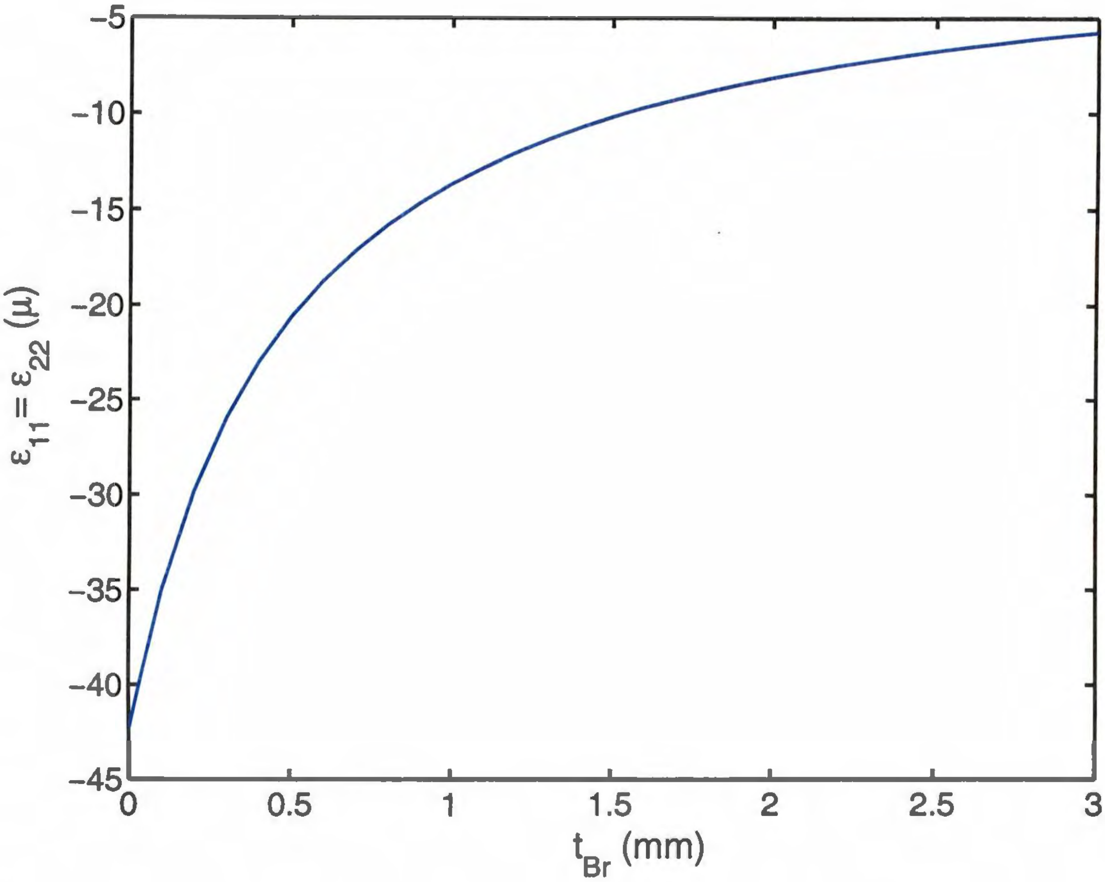

Figure 2.14: Strain ε_{11} ($= \varepsilon_{22}$) as a function of the thickness of brass for brass/PMN/brass subjected to $E_3 = 1$ kV/mm.

To study the effect of the material properties of the ductile layer, the strain, ε_{11}, of brass/PMN/brass, Al/PMN/Al, and epoxy/PMN/epoxy composites, due to the electric field $E_3 = 1$ kV/mm is shown in Table 2.2. The results show that the composite materials with compliant plies, such as epoxy, will exhibit a relatively large deformation.

Table 2.2: Strains of brass/PMN/brass, Al/PMN/Al, and epoxy/PMN/epoxy subjected to $E_3 = 1$ kV/mm.

Strain	brass/PMN/brass	Al/PMN/Al	epoxy/PMN/epoxy
$\varepsilon_{11}(=\varepsilon_{22})$	-13.4μ	-17.6μ	-40μ

Chapter 3

Electrostrictive Materials with Periodic Microstructure

3.1 Periodic Microstructure

The present micromechanics model is developed to estimate the local fields and the effective properties of electrostrictive composites. The model, based on periodic microstructure, considers an infinite electrostrictive solid containing periodically distributed electrostrictive inhomogeneities. The inhomogeneities can be laminae, long fibers, or in any shape (see Figure 3.1). In view of periodicity, the composite

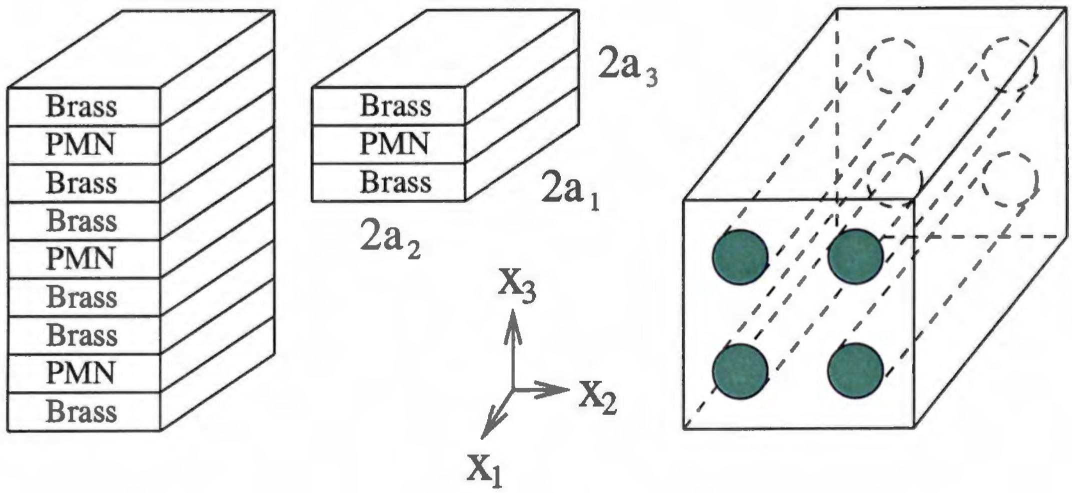

Figure 3.1: Electrostrictive solids with periodically-distributed inhomogeneities.

can be regarded as a collection of unit cells (see Figure 3.1), and the effective properties of the unit cell can represent those of the composite.

The constitutive relations of electrostrictive materials are given by (Knops, 1963)

$$\boldsymbol{\varepsilon} = \mathbf{s} : \boldsymbol{\sigma} + \mathbf{Q} : (\mathbf{P} \otimes \mathbf{P}), \tag{3.1}$$

$$\mathbf{E} = \boldsymbol{\beta} \cdot \mathbf{P}, \tag{3.2}$$

or inversely,

$$\boldsymbol{\sigma} = \mathbf{C} : \boldsymbol{\varepsilon} - \mathbf{C} : \mathbf{Q} : (\mathbf{P} \otimes \mathbf{P}) = \mathbf{C} : \boldsymbol{\varepsilon} - \mathbf{B} : (\mathbf{E} \otimes \mathbf{E}), \tag{3.3}$$

$$\mathbf{P} = \boldsymbol{\kappa} \cdot \mathbf{E}, \tag{3.4}$$

where

$$B_{ijpq} = C_{ijmn} Q_{mnkl} \kappa_{kp} \kappa_{lq} \; (i, j, p, q, m, n, k, l = 1, 2, 3); \tag{3.5}$$

$\boldsymbol{\varepsilon}$ is the strain tensor, $\boldsymbol{\sigma}$ is the stress tensor, $\mathbf{P}$ is the polarization vector, $\mathbf{E}$ is the electric field vector, $\mathbf{s}$ $(= \mathbf{C}^{-1})$ is the compliance tensor, $\mathbf{Q}$ are the electrostrictive constants, $\boldsymbol{\beta}$ $(= \boldsymbol{\kappa}^{-1})$ and $\boldsymbol{\kappa}$ $(= \boldsymbol{\beta}^{-1})$ are the permittivity tensors, and $\mathbf{C}$ $(= \mathbf{s}^{-1})$ is the stiffness tensor. Repeated indices in one term are summed over 1, 2, 3. A single dot $(\cdot)$ represents the dyadic product of a second-order tensor and a first-order tensor (i.e., a vector), whereas a double dot $(:)$ stands for the scalar product of two tensors. The notation $\otimes$ is used for the tensor product of two tensors.

The indicial form of the constitutive relations (3.3) and (3.4) are given by

$$\sigma_{ij} = C_{ijkl}\varepsilon_{kl} - C_{ijmn}Q_{mnkl}P_kP_l = C_{ijkl}\varepsilon_{kl} - B_{ijkl}E_kE_l, \tag{3.6}$$

$$P_i = \kappa_{ij}E_j. \tag{3.7}$$

3.2 The Inclusion Problem

Consider a unit cell U, consisting of a continuous electrostrictive matrix, M, and inclusions, Ω. The inclusions have the same properties as the matrix and can be the union of several subregions with an arbitrary shape. The center of the unit cell is located at the origin of a rectangular Cartesian coordinate system. The dimensions of the unit cell and the inclusion are denoted by $2a_i$ and $2b_i$ ($i = 1 \sim 3$) respectively, and are measured along the coordinate axes. Moreover, strain-free transformation stresses, $\boldsymbol{\sigma}^*(\mathbf{x})$, and electric field-free transformation polarizations, $\mathbf{P}^*(\mathbf{x})$, are prescribed in Ω, and result in perturbation fields. The constitutive relations for such a homogeneous electrostrictive unit cell are given by

$$\boldsymbol{\sigma}(\mathbf{x}) = \mathbf{C}^{\mathrm{M}} : \boldsymbol{\varepsilon}(\mathbf{x}) - \mathbf{B}^{\mathrm{M}} : [\mathbf{E}(\mathbf{x}) \otimes \mathbf{E}(\mathbf{x})] + \boldsymbol{\sigma}^*(\mathbf{x}), \tag{3.8}$$

$$\mathbf{P}(\mathbf{x}) = \boldsymbol{\kappa}^{\mathrm{M}} \cdot \mathbf{E}(\mathbf{x}) + \mathbf{P}^*(\mathbf{x}), \tag{3.9}$$

where the superscript M represents the properties of the matrix.

Because of periodicity, the transformation stresses, $\boldsymbol{\sigma}^*(\mathbf{x})$, and the transformation polarizations, $\mathbf{P}^*(\mathbf{x})$, can be expressed in terms of Fourier series,

$$\begin{aligned}
\boldsymbol{\sigma}^*(\mathbf{x}) &= \sum_{\boldsymbol{\xi}=0}^{\pm\infty} \hat{\boldsymbol{\sigma}}^*(\boldsymbol{\xi})\exp(i\boldsymbol{\xi}\cdot\mathbf{x}) \\
&= <\boldsymbol{\sigma}^*(\mathbf{x})>_U + \sum_{\boldsymbol{\xi}\neq 0}^{\pm\infty} \hat{\boldsymbol{\sigma}}^*(\boldsymbol{\xi})\exp(i\boldsymbol{\xi}\cdot\mathbf{x}) \\
&= \boldsymbol{\sigma}^{*\mathrm{o}} + \boldsymbol{\sigma}^{*\mathrm{p}}(\mathbf{x}),
\end{aligned} \tag{3.10}$$

$$\begin{aligned}
\mathbf{P}^*(\mathbf{x}) &= \sum_{\boldsymbol{\xi}=0}^{\pm\infty} \hat{\mathbf{P}}^*(\boldsymbol{\xi})\exp(i\boldsymbol{\xi}\cdot\mathbf{x}) \\
&= <\mathbf{P}^*(\mathbf{x})>_U + \sum_{\boldsymbol{\xi}\neq 0}^{\pm\infty} \hat{\mathbf{P}}^*(\boldsymbol{\xi})\exp(i\boldsymbol{\xi}\cdot\mathbf{x}), \\
&= \mathbf{P}^{*\mathrm{o}} + \mathbf{P}^{*\mathrm{p}}(\mathbf{x}),
\end{aligned} \tag{3.11}$$

where $\boldsymbol{\sigma}^{*\mathrm{o}} = <\boldsymbol{\sigma}^*(\mathbf{x})>_U$, and $\mathbf{P}^{*\mathrm{o}} = <\mathbf{P}^*(\mathbf{x})>_U$. The superscript o stands for a uniform field. The angle brackets with a subscript U represent the volume averages over U. The superscript p implies that the corresponding field is a *periodic* function of $\mathbf{x}$, $i = \sqrt{-1}$, and $\boldsymbol{\xi}$ is a vector with three components:

$$\xi_j = \frac{n_j\pi}{a_j}, \ (j = 1 \sim 3;\ \text{no sum on } \ j) \tag{3.12}$$

$$n_j = 0, \pm1, \pm2, \ldots. \tag{3.13}$$

The Fourier coefficients $\hat{\boldsymbol{\sigma}}^*(\boldsymbol{\xi})$ and $\hat{\mathbf{P}}^*(\boldsymbol{\xi})$ are defined by

$$\hat{\boldsymbol{\sigma}}^*(\boldsymbol{\xi}) = \frac{1}{V_U}\int_U \boldsymbol{\sigma}^*(\mathbf{x})\exp(-i\boldsymbol{\xi}\cdot\mathbf{x})dV_{\mathbf{x}}, \tag{3.14}$$

$$\hat{\mathbf{P}}^*(\boldsymbol{\xi}) = \frac{1}{V_U}\int_U \mathbf{P}^*(\mathbf{x})\exp(-i\boldsymbol{\xi}\cdot\mathbf{x})dV_{\mathbf{x}}, \tag{3.15}$$

with V_U being the volume of the unit cell. Similarly, the resulting periodic displacements and electric potential fields can be expressed in Fourier series by

$$\mathbf{u}^{\mathrm{p}}(\mathbf{x}) = \sum_{\boldsymbol{\xi}\neq 0}^{\pm\infty} \hat{\mathbf{u}}^{\mathrm{p}}(\boldsymbol{\xi})\exp(i\boldsymbol{\xi}\cdot\mathbf{x}), \tag{3.16}$$

$$\phi^{\mathrm{p}}(\mathbf{x}) = \sum_{\boldsymbol{\xi}\neq 0}^{\pm\infty} \hat{\phi}^{\mathrm{p}}(\boldsymbol{\xi})\exp(i\boldsymbol{\xi}\cdot\mathbf{x}), \tag{3.17}$$

where

$$\hat{\mathbf{u}}^{\mathrm{p}}(\boldsymbol{\xi}) = \frac{1}{V_U}\int_U \mathbf{u}^{\mathrm{p}}(\mathbf{x})\exp(-i\boldsymbol{\xi}\cdot\mathbf{x})dV_{\mathbf{x}}, \tag{3.18}$$

$$\hat{\phi}^{\mathrm{p}}(\boldsymbol{\xi}) = \frac{1}{V_U}\int_U \phi^{\mathrm{p}}(\mathbf{x})\exp(-i\boldsymbol{\xi}\cdot\mathbf{x})dV_{\mathbf{x}}. \tag{3.19}$$

The average terms $\mathbf{u}^{\circ}(\mathbf{x})$ and $\phi^{\circ}(\mathbf{x})$, which are the rigid body translations and uniform electric potential fields respectively, are excluded. The strain and electric fields are thus given by

$$\begin{aligned}\boldsymbol{\varepsilon}^{\mathrm{p}}(\mathbf{x}) &= \frac{1}{2}\{\nabla\otimes\mathbf{u}^{\mathrm{p}}(\mathbf{x}) + [\nabla\otimes\mathbf{u}^{\mathrm{p}}(\mathbf{x})]^T\} \\ &= \frac{1}{2}\sum_{\boldsymbol{\xi}\neq 0}^{\pm\infty}\{i\boldsymbol{\xi}\otimes\hat{\mathbf{u}}^{\mathrm{p}}(\boldsymbol{\xi}) + i\hat{\mathbf{u}}^{\mathrm{p}}(\boldsymbol{\xi})\otimes\boldsymbol{\xi}\}\exp(i\boldsymbol{\xi}\cdot\mathbf{x}),\end{aligned} \tag{3.20}$$

$$\begin{aligned}\mathbf{E}^{\mathrm{p}}(\mathbf{x}) &= -\nabla\cdot\phi^{\mathrm{p}}(\mathbf{x}) \\ &= -i\sum_{\boldsymbol{\xi}\neq 0}^{\pm\infty}\boldsymbol{\xi}\hat{\phi}^{\mathrm{p}}(\boldsymbol{\xi})\exp(i\boldsymbol{\xi}\cdot\mathbf{x}).\end{aligned} \tag{3.21}$$

Since all the variable fields can be divided into uniform and periodic perturbation parts, it is convenient to rewrite the constitutive relations (3.8) and (3.9) as follows

$$\begin{aligned}\boldsymbol{\sigma}^{\circ}+\boldsymbol{\sigma}^{\mathrm{p}}(\mathrm{x}) &= \mathrm{C}^{\mathrm{M}}:(\boldsymbol{\varepsilon}^{\circ}+\boldsymbol{\varepsilon}^{\mathrm{p}}(\mathrm{x})) \\ &\quad -\mathrm{B}^{\mathrm{M}}:[(\mathrm{E}^{\circ}+\mathrm{E}^{\mathrm{p}}(\mathrm{x}))\otimes(\mathrm{E}^{\circ}+\mathrm{E}^{\mathrm{p}}(\mathrm{x}))] \\ &\quad +\boldsymbol{\sigma}^{*\circ}+\boldsymbol{\sigma}^{*\mathrm{p}}(\mathrm{x}), \end{aligned} \tag{3.22}$$

$$\mathrm{P}^{\circ}+\mathrm{P}^{\mathrm{p}}(\mathrm{x})=\boldsymbol{\kappa}^{\mathrm{M}}\cdot(\mathrm{E}^{\circ}+\mathrm{E}^{\mathrm{p}}(\mathrm{x}))+\mathrm{P}^{*\circ}+\mathrm{P}^{*\mathrm{p}}(\mathrm{x}). \tag{3.23}$$

The equilibrium and Gauss's law require that

$$\nabla\cdot\boldsymbol{\sigma}(\mathrm{x})=0, \tag{3.24}$$

$$\nabla\cdot\mathrm{P}(\mathrm{x})=0, \tag{3.25}$$

where ∇ denotes partial differentiation with respect to the space coordinates. To find the relation between arbitrary transformation fields and their resulting periodic perturbation fields, substituting Eq. (3.22) and (3.23), expressed in Fourier series, into Eq. (3.24) and (3.25), gives

$$\begin{aligned}&\sum_{\boldsymbol{\xi}\neq 0}^{\pm\infty}\{-(\boldsymbol{\xi}\cdot\mathrm{C}^{\mathrm{M}}\cdot\boldsymbol{\xi})^{-1}\cdot\hat{\mathrm{u}}^{\mathrm{p}}(\boldsymbol{\xi})-\boldsymbol{\xi}\cdot\mathrm{B}^{\mathrm{M}}:(\mathrm{E}^{\circ}\otimes\boldsymbol{\xi}+\boldsymbol{\xi}\otimes\mathrm{E}^{\circ})\hat{\phi}^{\mathrm{P}}(\boldsymbol{\xi}) \\ &+i\boldsymbol{\xi}\cdot\mathrm{B}^{\mathrm{M}}:\sum_{\boldsymbol{\eta}\neq 0,\boldsymbol{\eta}\neq\boldsymbol{\xi}}^{\pm\infty}\boldsymbol{\eta}\otimes(\boldsymbol{\xi}-\boldsymbol{\eta})\hat{\phi}^{\mathrm{P}}(\boldsymbol{\eta})\hat{\phi}^{\mathrm{P}}(\boldsymbol{\xi}-\boldsymbol{\eta})+i\boldsymbol{\xi}\cdot\hat{\boldsymbol{\sigma}}^{*}(\boldsymbol{\xi})\}\exp(i\boldsymbol{\xi}\cdot\mathrm{x})=0,\end{aligned} \tag{3.26}$$

$$\sum_{\boldsymbol{\xi}\neq 0}^{\pm\infty}\{(\boldsymbol{\xi}\cdot\boldsymbol{\kappa}^{\mathrm{M}}\cdot\boldsymbol{\xi})\hat{\phi}^{\mathrm{P}}(\boldsymbol{\xi})+i\boldsymbol{\xi}\cdot\hat{\mathrm{P}}^{*}(\boldsymbol{\xi})\}\exp(i\boldsymbol{\xi}\cdot\mathrm{x})=0, \tag{3.27}$$

or in indicial notation,

$$\sum_{\xi\neq 0}^{\pm\infty}\{-i\xi_i C^M_{ijkl}\xi_l\hat{u}^p_k(\xi)-\xi_i B^M_{ijkl}(E^\circ_k\xi_l+\xi_k E^\circ_l)\hat{\phi}^p(\xi)$$

$$+i\xi_i B^M_{ijkl}\sum_{\eta\neq 0,\eta\neq\xi}^{\pm\infty}\eta_k(\xi-\eta)_l\hat{\phi}^p(\eta)\hat{\phi}^p(\xi-\eta)+i\xi_i\hat{\sigma}^*_{ij}(\xi)\}\exp(i\xi\cdot x)=0, \tag{3.28}$$

$$\sum_{\xi\neq 0}^{\pm\infty}\{\xi_i\kappa^M_{ij}\xi_j\hat{\phi}^p(\xi)+i\xi_i\hat{P}^*_i(\xi))\}\exp(i\xi\cdot x)=0. \tag{3.29}$$

where the product of two Fourier series is given by (Bary, 1964)

$$\begin{aligned}\mathbf{E}^\mathrm{p}(\mathbf{x})\otimes\mathbf{E}^\mathrm{p}(\mathbf{x}) &= [-i\sum_{\boldsymbol{\xi}\neq 0}^{\pm\infty}\boldsymbol{\xi}\hat{\boldsymbol{\phi}}^\mathrm{P}(\boldsymbol{\xi})\exp(i\boldsymbol{\xi}\cdot\mathbf{x})]\otimes[-i\sum_{\boldsymbol{\eta}\neq 0}^{\pm\infty}\boldsymbol{\eta}\hat{\boldsymbol{\phi}}^\mathrm{P}(\boldsymbol{\eta})\exp(i\boldsymbol{\eta}\cdot\mathbf{x})]\\ &= -\sum_{\boldsymbol{\xi}\neq 0}^{\pm\infty}\sum_{\boldsymbol{\eta}\neq 0,\boldsymbol{\eta}\neq\boldsymbol{\xi}}^{\pm\infty}[\boldsymbol{\eta}\hat{\boldsymbol{\phi}}^\mathrm{P}(\boldsymbol{\eta})]\otimes[(\boldsymbol{\xi}-\boldsymbol{\eta})\hat{\boldsymbol{\phi}}^\mathrm{P}(\boldsymbol{\xi}-\boldsymbol{\eta})]\exp(i\boldsymbol{\xi}\cdot\mathbf{x}),\end{aligned} \tag{3.30}$$

where

$$\hat{\boldsymbol{\phi}}^\mathrm{P}(\boldsymbol{\eta})=\frac{1}{V_U}\int_U\boldsymbol{\phi}^\mathrm{P}(\mathbf{x})\exp(-i\boldsymbol{\eta}\cdot\mathbf{x})dV_\mathbf{x}, \tag{3.31}$$

$$\hat{\boldsymbol{\phi}}^\mathrm{P}(\boldsymbol{\xi}-\boldsymbol{\eta})=\frac{1}{V_U}\int_U\boldsymbol{\phi}^\mathrm{P}(\mathbf{x})\exp(-i(\boldsymbol{\xi}-\boldsymbol{\eta})\cdot\mathbf{x})dV_\mathbf{x}. \tag{3.32}$$

Then, the *exact* solutions of perturbation displacements and electric potential fields can be obtained from solving Eq. (3.26) and (3.27):

$$\begin{aligned}\hat{\mathbf{u}}^\mathrm{P}(\boldsymbol{\xi}) &= -(\boldsymbol{\xi}\cdot\mathbf{C}^\mathrm{M}\cdot\boldsymbol{\xi})^{-1}\otimes\boldsymbol{\xi}:[-i\hat{\boldsymbol{\sigma}}^*(\boldsymbol{\xi})+2\mathbf{B}^\mathrm{M}:(\boldsymbol{\xi}\otimes\mathbf{E}^\circ)\hat{\boldsymbol{\phi}}^\mathrm{P}(\boldsymbol{\xi})\\ &\quad -i\mathbf{B}^\mathrm{M}:\sum_{\boldsymbol{\eta}\neq 0,\boldsymbol{\eta}\neq\boldsymbol{\xi}}^{\pm\infty}\boldsymbol{\eta}\otimes(\boldsymbol{\xi}-\boldsymbol{\eta})\hat{\boldsymbol{\phi}}^\mathrm{P}(\boldsymbol{\eta})\hat{\boldsymbol{\phi}}^\mathrm{P}(\boldsymbol{\xi}-\boldsymbol{\eta})],\end{aligned} \tag{3.33}$$

$$\hat{\phi}^{\mathrm{p}}(\boldsymbol{\xi}) = -i\boldsymbol{\xi}\cdot\hat{\mathrm{P}}^{*}(\boldsymbol{\xi})/(\boldsymbol{\xi}\cdot\boldsymbol{\kappa}^{\mathrm{M}}\cdot\boldsymbol{\xi}), \tag{3.34}$$

or in indicial notation,

$$\begin{aligned}\hat{u}_i^p(\xi) &= -(\xi\cdot C^M\cdot\xi)_{ij}^{-1}\xi_p[-i\hat{\sigma}_{jp}^{*}(\xi) + 2B_{jpqr}^{M}\xi_q E_r^{\circ}\hat{\phi}^p(\xi)\\ &\quad -iB_{jpqr}^{M}\sum_{\eta\neq 0,\eta\neq\xi}^{\pm\infty}\eta_q(\xi-\eta)_r\hat{\phi}^p(\eta)\hat{\phi}^p(\xi-\eta)],\end{aligned} \tag{3.35}$$

$$\hat{\phi}^{\mathrm{p}}(\xi) = -i\xi_i\hat{P}_i^{*}(\xi)/(\xi_m\kappa_{mn}^{M}\xi_n). \tag{3.36}$$

The *exact* periodic perturbation strains and electrical fields can thus be determined from Eq. (3.20), (3.21), (3.33), and (3.34):

$$\begin{aligned}\boldsymbol{\varepsilon}^{\mathrm{p}}(\mathrm{x}) &= \sum_{\boldsymbol{\xi}\neq 0}^{\pm\infty} -\boldsymbol{\Gamma}' : \{\hat{\boldsymbol{\sigma}}^{*}(\boldsymbol{\xi}) + 2\mathrm{B}^{\mathrm{M}} : (\boldsymbol{\xi}\otimes\mathrm{E}^{\circ})[\boldsymbol{\xi}\cdot\hat{\mathrm{P}}^{*}(\boldsymbol{\xi})]/(\boldsymbol{\xi}\cdot\boldsymbol{\kappa}^{\mathrm{M}}\cdot\boldsymbol{\xi}) - \mathrm{B}^{\mathrm{M}} :\\ &\quad \sum_{\boldsymbol{\eta}\neq 0,\boldsymbol{\eta}\neq\boldsymbol{\xi}}^{\pm\infty}\frac{\boldsymbol{\eta}\otimes(\boldsymbol{\xi}-\boldsymbol{\eta})[\boldsymbol{\eta}\cdot\hat{\mathrm{P}}^{*}(\boldsymbol{\eta})][(\boldsymbol{\xi}-\boldsymbol{\eta})\cdot\hat{\mathrm{P}}^{*}(\boldsymbol{\xi}-\boldsymbol{\eta})]}{(\boldsymbol{\eta}\cdot\boldsymbol{\kappa}^{\mathrm{M}}\cdot\boldsymbol{\eta})((\boldsymbol{\xi}-\boldsymbol{\eta})\cdot\boldsymbol{\kappa}^{\mathrm{M}}\cdot(\boldsymbol{\xi}-\boldsymbol{\eta}))}\}\exp(i\boldsymbol{\xi}\cdot\mathrm{x}),\end{aligned} \tag{3.37}$$

$$\mathrm{E}^{\mathrm{p}}(\mathrm{x}) = -\sum_{\boldsymbol{\xi}\neq 0}^{\pm\infty}\{\boldsymbol{\xi}\otimes[\hat{\mathrm{P}}^{*}(\boldsymbol{\xi})\cdot\boldsymbol{\xi}]/(\boldsymbol{\xi}\cdot\boldsymbol{\kappa}^{\mathrm{M}}\cdot\boldsymbol{\xi})\}\exp(i\boldsymbol{\xi}\cdot\mathrm{x}), \tag{3.38}$$

or in indicial notation,

$$\begin{aligned}\varepsilon_{ij}^{p}(x) &= \sum_{\xi\neq 0}^{\pm\infty}\boldsymbol{\Gamma}'_{ijlp}\{\hat{\sigma}_{lp}^{*}(\xi) + 2B_{lpqr}^{M}\xi_q E_r^{\circ}\xi_k\hat{P}_k^{*}(\xi)/(\xi_m\kappa_{mn}^{M}\xi_n)\\ &\quad -B_{lpqr}^{M}\sum_{\eta\neq 0,\eta\neq\xi}^{\pm\infty}\frac{\eta_q(\xi-\eta)_r\eta_k\hat{P}_k^{*}(\eta)(\xi-\eta)_s\hat{P}_s^{*}(\xi-\eta)}{(\eta_m\kappa_{mn}^{M}\eta_n)((\xi-\eta)_e\kappa_{ef}^{M}(\xi-\eta)_f)}\}\exp(i\xi\cdot x).\end{aligned} \tag{3.39}$$

$$E_j^p(x) = -\sum_{\xi\neq 0}^{\pm\infty}\xi_j\hat{P}_i^{*}(\xi)\xi_i/(\xi_m\kappa_{mn}^{M}\xi_n)\exp(i\xi\cdot x). \tag{3.40}$$

where

$$\Gamma' = sym\{\bar{\boldsymbol{\xi}} \otimes (\bar{\boldsymbol{\xi}} \cdot \mathbf{C}^{\mathrm{M}} \cdot \bar{\boldsymbol{\xi}})^{-1} \otimes \bar{\boldsymbol{\xi}}\}, \tag{3.41}$$

$$\bar{\boldsymbol{\xi}} = \frac{\boldsymbol{\xi}}{\sqrt{\boldsymbol{\xi} \cdot \boldsymbol{\xi}}}, \tag{3.42}$$

with sym being the symmetric part of the corresponding fouth-order tensor. For exemple,

$$\Gamma'_{ijkl} = \frac{1}{4}\{\Gamma'_{ijkl} + \Gamma'_{jikl} + \Gamma'_{ijlk} + \Gamma'_{jilk}\}. \tag{3.43}$$

It is noted that Eq. (3.33), (3.34), (3.37), and (3.38) are in essence integral equations and thus are difficult to deal with. If the transformation stresses and transformation polarization fields are uniform in Ω, i.e.,

$$\boldsymbol{\sigma}^*(\mathbf{x}) = \bar{\boldsymbol{\sigma}}^* \text{ and } \mathbf{P}^*(\mathbf{x}) = \bar{\mathbf{P}}^*, \tag{3.44}$$

where $\bar{\boldsymbol{\sigma}}^*$ and $\bar{\mathbf{P}}^*$ are constant, Eq. (3.14) and (3.15) can be rewritten by

$$\hat{\boldsymbol{\sigma}}^*(\boldsymbol{\xi}) = fg(-\boldsymbol{\xi})\bar{\boldsymbol{\sigma}}^*, \tag{3.45}$$

$$\hat{\mathbf{P}}^*(\boldsymbol{\xi}) = fg(-\boldsymbol{\xi})\bar{\mathbf{P}}^*, \tag{3.46}$$

where

$$g(-\boldsymbol{\xi}) = \frac{1}{V_\Omega} \int_\Omega \exp(-i\boldsymbol{\xi} \cdot \mathbf{x}) dV_{\mathbf{x}}. \tag{3.47}$$

Similarly,

$$\hat{\mathbf{P}}^*(\boldsymbol{\eta}) = fg(-\boldsymbol{\eta})\bar{\mathbf{P}}^*, \tag{3.48}$$

$$\hat{\mathbf{P}}^*(\boldsymbol{\xi} - \boldsymbol{\eta}) = fg(\boldsymbol{\eta} - \boldsymbol{\xi})\bar{\mathbf{P}}^*, \tag{3.49}$$

where

$$g(-\boldsymbol{\eta}) = \frac{1}{V_\Omega}\int_\Omega \exp(-i\boldsymbol{\eta}\cdot\mathrm{x})dV_{\mathrm{x}}, \tag{3.50}$$

$$g(\boldsymbol{\eta}-\boldsymbol{\xi}) = \frac{1}{V_\Omega}\int_\Omega \exp(i(\boldsymbol{\eta}-\boldsymbol{\xi})\cdot\mathrm{x})dV_{\mathrm{x}}; \tag{3.51}$$

$f = V_\Omega/V_U$ is the inclusion volume fraction.

The effects of the inclusion geometry are fully addressed by $g(-\boldsymbol{\xi})$. The expressions of a class of inclusion geometry are listed as follows (Nemat-Nasser *et al.*, 1993):

(1) The geometrical parameter, $g(\boldsymbol{\xi})$, of an elliptical particulate with principal radii b_i is given by

$$g = 3(\sin\zeta - \zeta\cos\zeta)/\zeta^3, \tag{3.52}$$

where

$$\zeta = \pi\sqrt{(\frac{n_1 b_1}{a_1})^2 + (\frac{n_2 b_2}{a_2})^2 + (\frac{n_3 b_3}{a_3})^2}. \tag{3.53}$$

Eq. (3.52) and (3.53) include the g-parameters for cases of spherical, oblate spheroidal, and prolate speroidal particles when $b_1 = b_2 = b_3$, $b_1 = b_2 > b_3$, and $b_1 = b_2 < b_3$, respectively.

(2) The geometrical parameter, $g(\boldsymbol{\xi})$, of a parallelepiped whisker with dimensions $2b_i$ is giving by

$$g = \frac{\sin(\frac{\pi n_1 b_1}{a_1})\sin(\frac{\pi n_2 b_2}{a_2})\sin(\frac{\pi n_3 b_3}{a_3})}{(\frac{\pi n_1 b_1}{a_1})(\frac{\pi n_2 b_2}{a_2})(\frac{\pi n_3 b_3}{a_3})}, \tag{3.54}$$

When $a_1 \neq b_1$, $a_2 = b_2$, and $a_3 \neq b_3$, Eq. (3.54) represents the g-parameter for a continuous fiber with a rectangular cross section. When $a_1 = b_1$, $a_2 = b_2$, and $a_3 \neq b_3$, Eq. (3.54) represents the g-parameter for a lamina.

(3) The geometrical parameter, $g(\boldsymbol{\xi})$, of an elliptical-cylindrical fiber with principal radii b_1 and b_3 and length $2b_2$ is given by

$$g = \frac{sin(\frac{n_3\pi b_3}{a_3})2J_1(\sqrt{(\frac{n_1\pi b_1}{a_1})^2 + (\frac{n_2\pi b_2}{a_2})^2})}{\frac{n_3\pi b_3}{a_3}(\sqrt{(\frac{n_1\pi b_1}{a_1})^2 + (\frac{n_2\pi b_2}{a_2})^2})}, \tag{3.55}$$

where J_1 is the Bessel function of the first kind. The special cases of a continuous fiber ($a_2 = b_2$) and a circular-cylindrical continuous fiber ($b_1 = b_3$ and $a_2 = b_2$) are included in Eq. (3.55).

To determine the *average* perturbation fields of the inclusion, substituting Eq. (3.45), (3.46), (3.48), and (3.49) into Eq. (3.38) and (3.37), the *average* perturbation strains and electric fields are given by

$$\begin{aligned} < \boldsymbol{\varepsilon}^{\mathrm{P}}(\mathbf{x}) >_{\Omega} \;=\; & -\sum_{\boldsymbol{\xi}\neq 0}^{\pm\infty} f g(\boldsymbol{\xi}) g(-\boldsymbol{\xi}) \boldsymbol{\Gamma}' : \bar{\boldsymbol{\sigma}}^* \\ & -2\sum_{\boldsymbol{\xi}\neq 0}^{\pm\infty} f g(\boldsymbol{\xi}) g(-\boldsymbol{\xi}) \boldsymbol{\Gamma}' : \mathbf{B}^{\mathrm{M}} : (\bar{\boldsymbol{\xi}} \otimes \mathbf{E}^{\circ})(\bar{\boldsymbol{\xi}} \cdot \bar{\mathbf{P}}^*)/(\bar{\boldsymbol{\xi}} \cdot \boldsymbol{\kappa}^{\mathrm{M}} \cdot \bar{\boldsymbol{\xi}}) \\ & +\sum_{\boldsymbol{\xi}\neq 0}^{\pm\infty} f g(\boldsymbol{\xi}) \boldsymbol{\Gamma}' : \mathbf{B}^{\mathrm{M}} : \mathbf{A}(\boldsymbol{\xi}) : (\bar{\mathbf{P}}^* \otimes \bar{\mathbf{P}}^*), \end{aligned} \tag{3.56}$$

$$< \mathbf{E}^{\mathrm{P}}(\mathbf{x}) >_{\Omega} = -\sum_{\boldsymbol{\xi}\neq 0}^{\pm\infty} f g(\boldsymbol{\xi}) g(-\boldsymbol{\xi}) \bar{\boldsymbol{\xi}} (\bar{\mathbf{P}}^* \cdot \bar{\boldsymbol{\xi}})/(\bar{\boldsymbol{\xi}} \cdot \boldsymbol{\kappa}^{\mathrm{M}} \cdot \bar{\boldsymbol{\xi}}), \tag{3.57}$$

where

$$g(\boldsymbol{\xi}) = \frac{1}{V_\Omega} \int_\Omega \exp(i\boldsymbol{\xi} \cdot \mathbf{x}) dV_{\mathbf{x}}, \tag{3.58}$$

$$\mathbf{A}(\boldsymbol{\xi}) = \sum_{\boldsymbol{\eta} \neq 0, \boldsymbol{\eta} \neq \boldsymbol{\xi}}^{\pm\infty} \frac{f g(-\boldsymbol{\eta}) g(\boldsymbol{\eta} - \boldsymbol{\xi}) \bar{\boldsymbol{\eta}} \otimes (\bar{\boldsymbol{\xi}} - \bar{\boldsymbol{\eta}}) \otimes \bar{\boldsymbol{\eta}} \otimes (\bar{\boldsymbol{\xi}} - \bar{\boldsymbol{\eta}})}{(\bar{\boldsymbol{\eta}} \cdot \boldsymbol{\kappa}^{\mathrm{M}} \cdot \bar{\boldsymbol{\eta}})[(\bar{\boldsymbol{\xi}} - \bar{\boldsymbol{\eta}}) \cdot \boldsymbol{\kappa}^{\mathrm{M}} \cdot (\bar{\boldsymbol{\xi}} - \bar{\boldsymbol{\eta}})]}, \tag{3.59}$$

$$\bar{\boldsymbol{\eta}} = \frac{\boldsymbol{\eta}}{\sqrt{\boldsymbol{\eta} \cdot \boldsymbol{\eta}}}. \tag{3.60}$$

3.3 The Inhomogeneity Problem

Consider a parallelepiped unit cell, which is subjected to the uniform strains and electric fields, $\boldsymbol{\varepsilon}^\circ$ and $\mathbf{E}^\circ$. The unit cell may consist of one or more inhomogeneities with properties being different from those of the matrix. Due to the existence of periodically-distributed inhomogeneities, the local strains and electric fields can be expressed by

$$\boldsymbol{\varepsilon}(\mathbf{x}) = \boldsymbol{\varepsilon}^\circ + \boldsymbol{\varepsilon}^{\mathrm{p}}(\mathbf{x}), \tag{3.61}$$

$$\mathbf{E}(\mathbf{x}) = \mathbf{E}^\circ + \mathbf{E}^{\mathrm{p}}(\mathbf{x}), \tag{3.62}$$

where $\boldsymbol{\varepsilon}^{\mathrm{p}}$ and $\mathbf{E}^{\mathrm{p}}$ are the *periodic perturbation* strains and electric fields. In order to solve the inhomogeneity problem, one can replace the inhomogeneity by the matrix, and to compensate for the materials' mismatch after homogenization, prescribes strain-free transformation stresses, $\boldsymbol{\sigma}^*(\mathbf{x})$, and electric field-free transformation polarizations, $\mathbf{P}^*(\mathbf{x})$, within the Ω.

Before and after the homogenization, the stresses and polarizations in Ω must be conserved. Therefore, the following constraint conditions must hold:

$$\mathbf{C}^{\Omega} :< \boldsymbol{\varepsilon}(\mathbf{x}) >_{\Omega} - \mathbf{B}^{\Omega} : (< \mathbf{E}(\mathbf{x}) >_{\Omega} \otimes < \mathbf{E}(\mathbf{x}) >_{\Omega}) =$$

$$\mathbf{C}^{\mathrm{M}} :< \boldsymbol{\varepsilon}(\mathbf{x}) >_{\Omega} - \mathbf{B}^{\mathrm{M}} : (< \mathbf{E}(\mathbf{x}) >_{\Omega} \otimes < \mathbf{E}(\mathbf{x}) >_{\Omega}) + < \boldsymbol{\sigma}^*(\mathbf{x}) >_{\Omega}, \tag{3.63}$$

$$\boldsymbol{\kappa}^{\Omega} \cdot < \mathbf{E}(\mathbf{x}) >_{\Omega} = \boldsymbol{\kappa}^{\mathrm{M}} \cdot < \mathbf{E}(\mathbf{x}) >_{\Omega} + < \mathbf{P}^*(\mathbf{x}) >_{\Omega} . \tag{3.64}$$

where the properties with a superscript, Ω and M, represent the inhomogeneity properties and matrix properties, respectively, and the angle brackets with a subscript Ω represent the averages over the inhomogeneity Ω.

To determine the suitable transformation fields, $\boldsymbol{\sigma}^*(\mathbf{x})$ and $\mathbf{P}^*(\mathbf{x})$, which satisfy Eq. (3.63) and (3.64), one needs to determine the relationship between the periodic perturbation fields, $\boldsymbol{\varepsilon}^{\mathrm{p}}(\mathbf{x})$ and $\mathbf{E}^{\mathrm{p}}(\mathbf{x})$, and the transformation fields, $\boldsymbol{\sigma}^*(\mathbf{x})$ and $\mathbf{P}^*(\mathbf{x})$, which is the so-called inclusion problem and has been solved in the previous section.

Substituting Eq. (3.56), (3.57), Eq. (3.61), and (3.62) into the constraint conditions Eq. (3.63) and (3.64), one finds that

$$\begin{aligned}\bar{\boldsymbol{\sigma}}^* &= (\mathbf{I} + \triangle\mathbf{C} : \boldsymbol{\Gamma})^{-1} : \triangle\mathbf{C} : \boldsymbol{\varepsilon}^{\circ} - (\mathbf{I} + \triangle\mathbf{C} : \boldsymbol{\Gamma})^{-1} : \{2\triangle\mathbf{C} : \mathbf{N} \\ &\quad -\triangle\mathbf{C} : \mathbf{R} : \mathbf{V} + \triangle\mathbf{B} - 2\triangle\mathbf{B} \cdot \mathbf{Y} \cdot (\mathbf{1}^{(2)} + \triangle\boldsymbol{\kappa} \cdot \mathbf{Y})^{-1} \cdot \triangle\boldsymbol{\kappa}\end{aligned}$$

$$+\triangle\mathbf{B}:\mathbf{J}\}:(\mathbf{E}^{\circ}\otimes\mathbf{E}^{\circ}), \tag{3.65}$$

$$\bar{\mathbf{P}}^{*}=(\mathbf{1}^{(2)}+\triangle\boldsymbol{\kappa}\cdot\mathbf{Y})^{-1}\cdot\triangle\boldsymbol{\kappa}\cdot\mathbf{E}^{\circ}, \tag{3.66}$$

where

$$V_{mnqt}=(1^{(2)}+\triangle\kappa\cdot Y)^{-1}_{mp}\triangle\kappa_{pq}(1^{(2)}+\triangle\kappa\cdot Y)^{-1}_{ns}\triangle\kappa_{st}, \tag{3.67}$$

$$J_{klqt}=Y_{kp}(1^{(2)}+\triangle\kappa\cdot Y)^{-1}_{pr}\triangle\kappa_{rq}Y_{ln}(1^{(2)}+\triangle\kappa\cdot Y)^{-1}_{ns}\triangle\kappa_{st}, \tag{3.68}$$

$$\triangle\boldsymbol{\kappa}=\boldsymbol{\kappa}^{\Omega}-\boldsymbol{\kappa}^{\mathrm{M}},\ \triangle\mathbf{C}=\mathbf{C}^{\Omega}-\mathbf{C}^{\mathrm{M}},\ \triangle\mathbf{B}=\mathbf{B}^{\Omega}-\mathbf{B}^{\mathrm{M}}, \tag{3.69}$$

$\mathbf{1}^{(2)}$ is the second-order identity tensor, and $\mathbf{I}$ is the fourth-order identity tensor. The fourth-order tensor $\mathbf{\Gamma}$, $\mathbf{Y}$, $\mathbf{R}$, and $\mathbf{N}$ include infinite series and are given by

$$\mathbf{\Gamma}=\sum_{\boldsymbol{\xi}\neq0}^{\pm\infty}fg(\boldsymbol{\xi})g(-\boldsymbol{\xi})\mathbf{\Gamma}', \tag{3.70}$$

$$\mathbf{R}=\sum_{\boldsymbol{\xi}\neq0}^{\pm\infty}fg(\boldsymbol{\xi})\mathbf{\Gamma}':\mathbf{B}^{\mathrm{M}}:\mathbf{A}(\boldsymbol{\xi}), \tag{3.71}$$

$$\mathbf{Y}=\sum_{\boldsymbol{\xi}\neq0}^{\pm\infty}fg(\boldsymbol{\xi})g(-\boldsymbol{\xi})(\bar{\boldsymbol{\xi}}\otimes\bar{\boldsymbol{\xi}})/(\bar{\boldsymbol{\xi}}\cdot\boldsymbol{\kappa}^{\mathrm{M}}\cdot\bar{\boldsymbol{\xi}}), \tag{3.72}$$

$$\mathbf{N}=\sum_{\boldsymbol{\xi}\neq0}^{\pm\infty}fg(\boldsymbol{\xi})g(-\boldsymbol{\xi})\mathbf{\Gamma}':\mathbf{B}^{\mathrm{M}}\cdot(\bar{\boldsymbol{\xi}}\otimes\bar{\boldsymbol{\xi}})\cdot(\mathbf{1}^{(2)}+\triangle\boldsymbol{\kappa}\cdot\mathbf{Y})^{-1}\cdot\triangle\boldsymbol{\kappa}/(\bar{\boldsymbol{\xi}}\cdot\boldsymbol{\kappa}^{\mathrm{M}}\cdot\bar{\boldsymbol{\xi}}). \tag{3.73}$$

3.4 Effective Properties

The average strains and electric fields over the unit cell, U, are equal to the applied loads $\boldsymbol{\varepsilon}^{\circ}$ and $\mathbf{E}^{\circ}$, since the averages of the *periodic* perturbation strains and electric fields over U vanish. The effective dielectric, stiffness, and electrostrictive properties of electrostrictive composites, $\bar{\boldsymbol{\kappa}}$, $\bar{\mathbf{C}}$, $\bar{\mathbf{B}}$, and $\bar{\mathbf{Q}}$, respectively, are defined by

$$<\mathbf{P}(\mathbf{x})>_U = \bar{\boldsymbol{\kappa}} \cdot <\mathbf{E}(\mathbf{x})>_U = \bar{\boldsymbol{\kappa}} \cdot \mathbf{E}^\circ, \tag{3.74}$$

$$<\boldsymbol{\sigma}(\mathbf{x})>_U = \bar{\mathbf{C}} : \boldsymbol{\varepsilon}^\circ - \bar{\mathbf{B}} : (\mathbf{E}^\circ \otimes \mathbf{E}^\circ), \tag{3.75}$$

$$\bar{B}_{ijpq} = \bar{C}_{ijmn} \bar{Q}_{mnkl} \bar{\kappa}_{kp} \bar{\kappa}_{lq}. \tag{3.76}$$

After the homogenization, Eq. (3.74) and (3.75) become

$$<\mathbf{P}(\mathbf{x})>_U = \bar{\boldsymbol{\kappa}} \cdot \mathbf{E}^\circ = \boldsymbol{\kappa}^{\mathbf{M}} \cdot \mathbf{E}^\circ + f <\mathbf{P}^*(\mathbf{x})>_\Omega, \tag{3.77}$$

$$\begin{aligned} <\boldsymbol{\sigma}(\mathbf{x})>_U &= \bar{\mathbf{C}} : \boldsymbol{\varepsilon}^\circ - \bar{\mathbf{B}} : (\mathbf{E}^\circ \otimes \mathbf{E}^\circ) \\ &= \mathbf{C}^{\mathbf{M}} : \boldsymbol{\varepsilon}^\circ - \mathbf{B}^{\mathbf{M}} : (\mathbf{E}^\circ \otimes \mathbf{E}^\circ) + f <\boldsymbol{\sigma}^*(\mathbf{x})>_\Omega . \end{aligned} \tag{3.78}$$

where f is the inhomogeneity volume fraction.

To estimate the effective properties of electrostrictive composite materials, one substitutes Eq. (3.65) and (3.66) into Eq. (3.77) and (3.78) and compares both sides of Eq. (3.77) and (3.78). The effective properties of the electrostrictive composite materials are thus given by

$$\bar{\boldsymbol{\kappa}} = \boldsymbol{\kappa}^{\mathbf{M}} + f(\mathbf{1}^{(2)} + \triangle\boldsymbol{\kappa} \cdot \mathbf{Y})^{-1} \cdot \triangle\boldsymbol{\kappa}, \tag{3.79}$$

$$\bar{\mathbf{C}} = \mathbf{C}^{\mathbf{M}} + f(\mathbf{I} + \triangle\mathbf{C} : \boldsymbol{\Gamma})^{-1} : \triangle\mathbf{C}, \tag{3.80}$$

$$\begin{aligned}\bar{\mathbf{B}} &= \mathbf{B}^{\mathbf{M}} + f(\mathbf{I} + \triangle\mathbf{C} : \mathbf{\Gamma})^{-1} : \{2\triangle\mathbf{C} : \mathbf{N} - \triangle\mathbf{C} : \mathbf{R} : \mathbf{V} + \triangle\mathbf{B} \\ &\quad -2\triangle\mathbf{B} \cdot \mathbf{Y} \cdot (\mathbf{1}^{(2)} + \triangle\boldsymbol{\kappa} \cdot \mathbf{Y})^{-1} \cdot \triangle\boldsymbol{\kappa} + \triangle\mathbf{B} : \mathbf{J}\}. \qquad (3.81)\end{aligned}$$

It is noted that $\bar{\mathbf{Q}}$ can be computed from Eq. (3.76).

3.5 Results and Discussions

Consider a laminate with layers of PMN sandwiched between layers of brass; see Figure 3.1. The dimensions of the brass layer are $2b_i$ ($i = 1 \sim 3$). Let $a_1 = a_2$, $b_1 = b_2$, and $r = b_3/(a_3 - b_3)$, the ratio of the thickness of brass to that of PMN. The Young modulus, E, and Poisson's ratio, ν, of brass are 69 GPa and 0.37, respectively. The material properties of isotropic PMN are given by: $E = 112$ GPa, $\nu = 0.26$, $\kappa_{11} = \kappa_{22} = \kappa_{33} = 6.6375\text{x}10^{-8}\,\text{F/m}$, $Q_{11} = 0.026\,\text{m}^4/\text{C}^2$, and $Q_{12} = -0.0096\,\text{m}^4/\text{C}^2$ (Sundar and Newhnam, 1992). Let the composite be subjected to E_3 only. The linear relationship between the polarization, P_3, and the electric field, E_3, is shown in Figure 3.2. An increase in the thickness of brass results in an increase in the polarization, P_{33}. The strain ε_{33} as a function of electric field E_3 is shown in Figure 3.3. The relationship between the strain, ε_{33} , and the electric field, E_3, is nonlinear. The results show that an increase in the thickness of brass results in a decrease in the composite strains, ε_{33}. Furthermore, the strain ε_{11} as a function of electric field E_3 in brass/PMN/brass ($r = 0.5$),

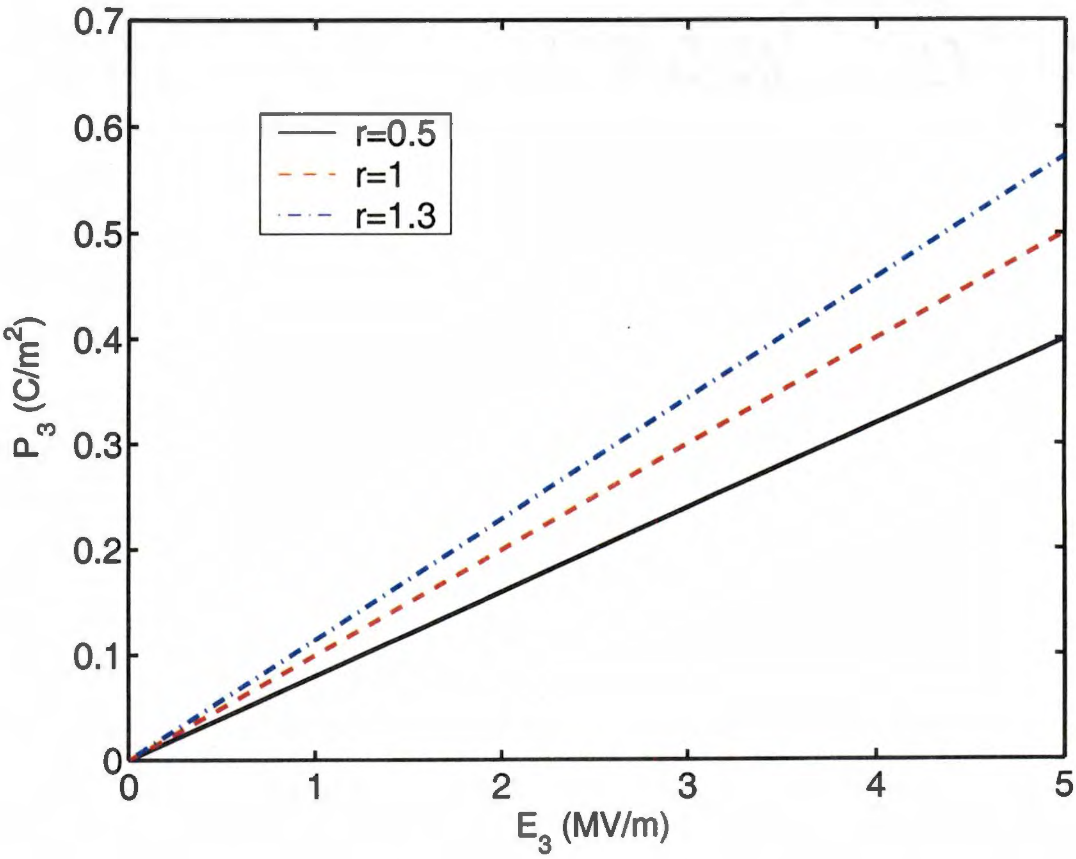

Figure 3.2: Polarization P_3 as a function of electric field E_3 in brass/PMN/brass.

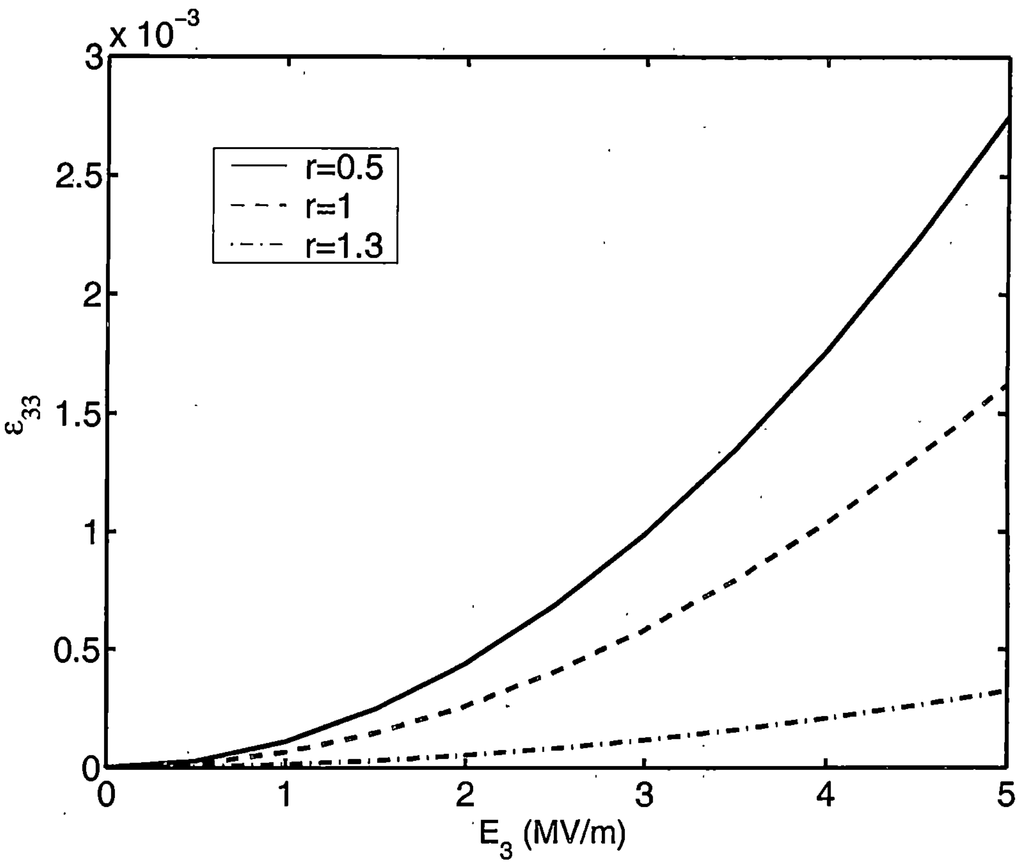

Figure 3.3: Strain ε_{33} as a function of electric field E_3 in brass/PMN/brass.

obtained by the periodic microstructure model in comparison with that obtained by the laminated plate theory model is shown Figure 3.4. The strain predicted by the periodic microstructure model is lower than that by the laminated plated theory. The predicted trends are, however similar to each other. The strain ε_{11} as a function of thickness of brass in brass/PMN/brass obtained by the periodic microstructure model in comparison with that obtained by the laminated plate theory model also is shown Figure 3.5. When the thickness of brass increases, the strain predicted by the periodic microstructure model decreases faster than that of the laminated plated theory. However, when the thickness of brass is less 0.2mm, the result predicted by the periodic microstructure model agrees quite well with that predicted by the laminated plate theory model. To check the convergence of Fourier series, the tensors, Y_{33}, Γ_{33}, N_{33}, and R_{33}, as a function of the number terms used in Fouries series for the case of brass/PMN/brass ($r = 0.5$) are shown in Figure 3.6 - Figure 3.9, respectively.

Consider a PMN/epoxy composite, in which the electrostrictive PMN ceramics are long square rods embedded in epoxy. The unit cell is a cube with a square electrostrictive ceramics rod being located in the center of the matrix; see Figure 3.10. The dimensions of the unit cell are given by: $2a_1 = 2a_2 = 2a_3$ (i.e., a cube), and the dimensions of the square electrostrictive ceramics are given by: $2b_1 = 2a_1$

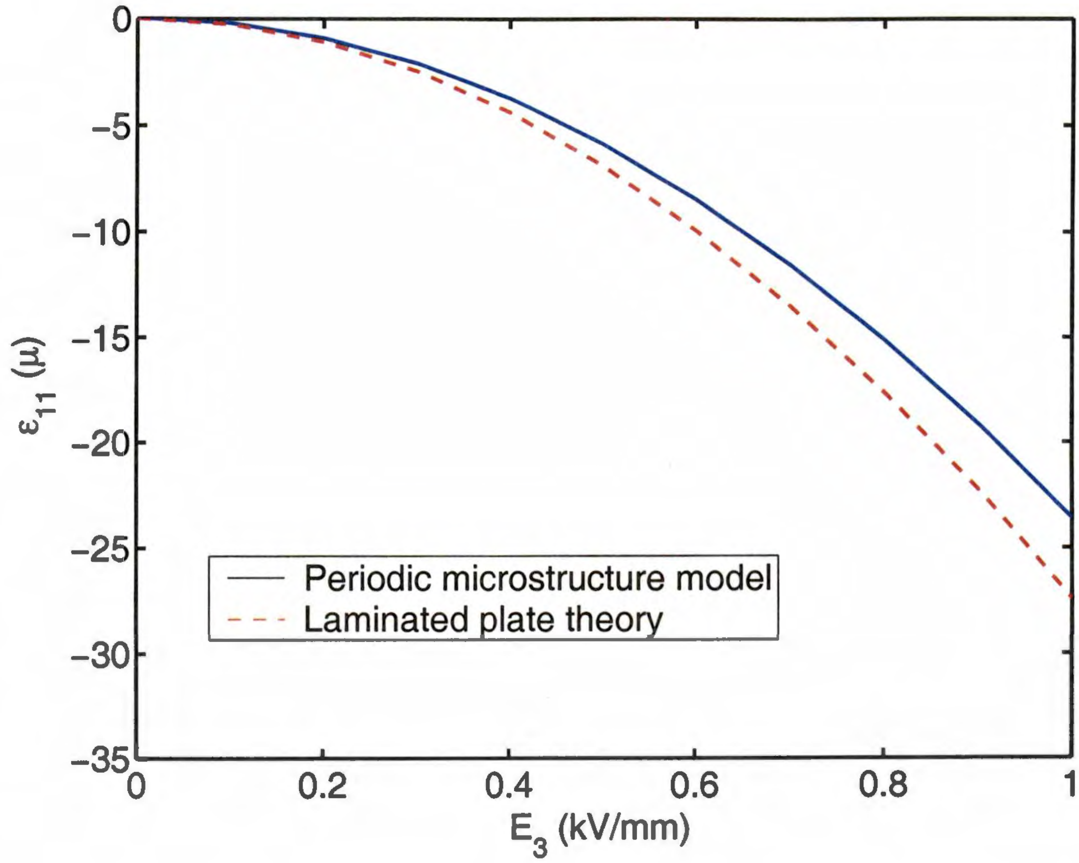

Figure 3.4: Comparison of strain ε_{11} as a function of electric field E_3 in brass/PMN/brass between the laminated plate theory and the periodic model.

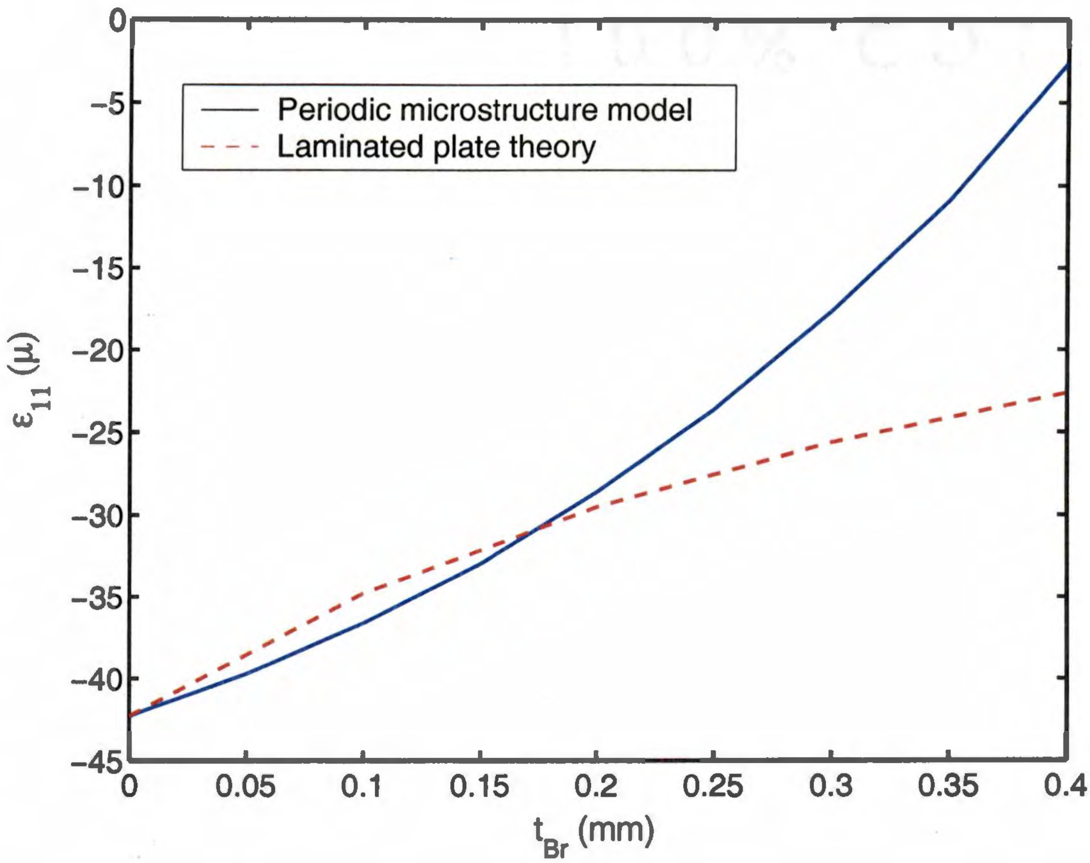

Figure 3.5: Comparison of strain ε_{11} as a function of thickness of brass t_{Br} in brass/PMN/brass between the laminated plate theory and the periodic model.

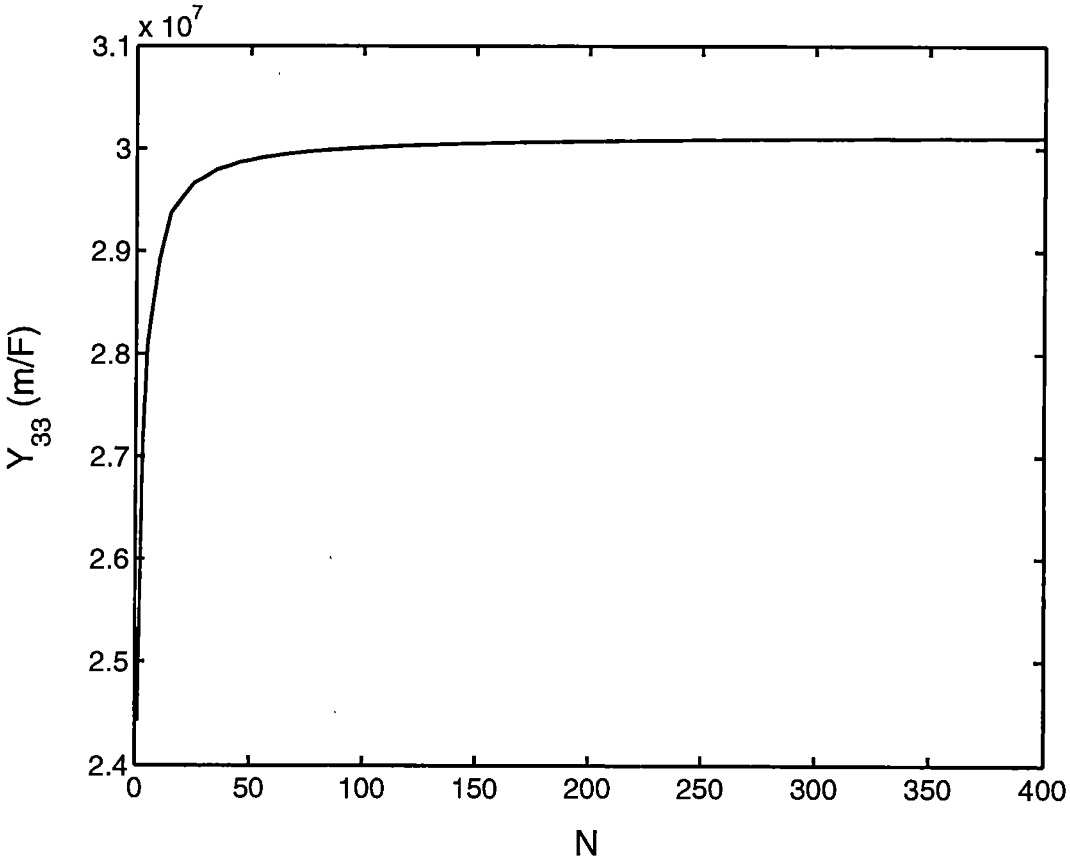

Figure 3.6: Tensor Y_{33} of brass/PMN/brass as a function of the number of Fourier series term, N.

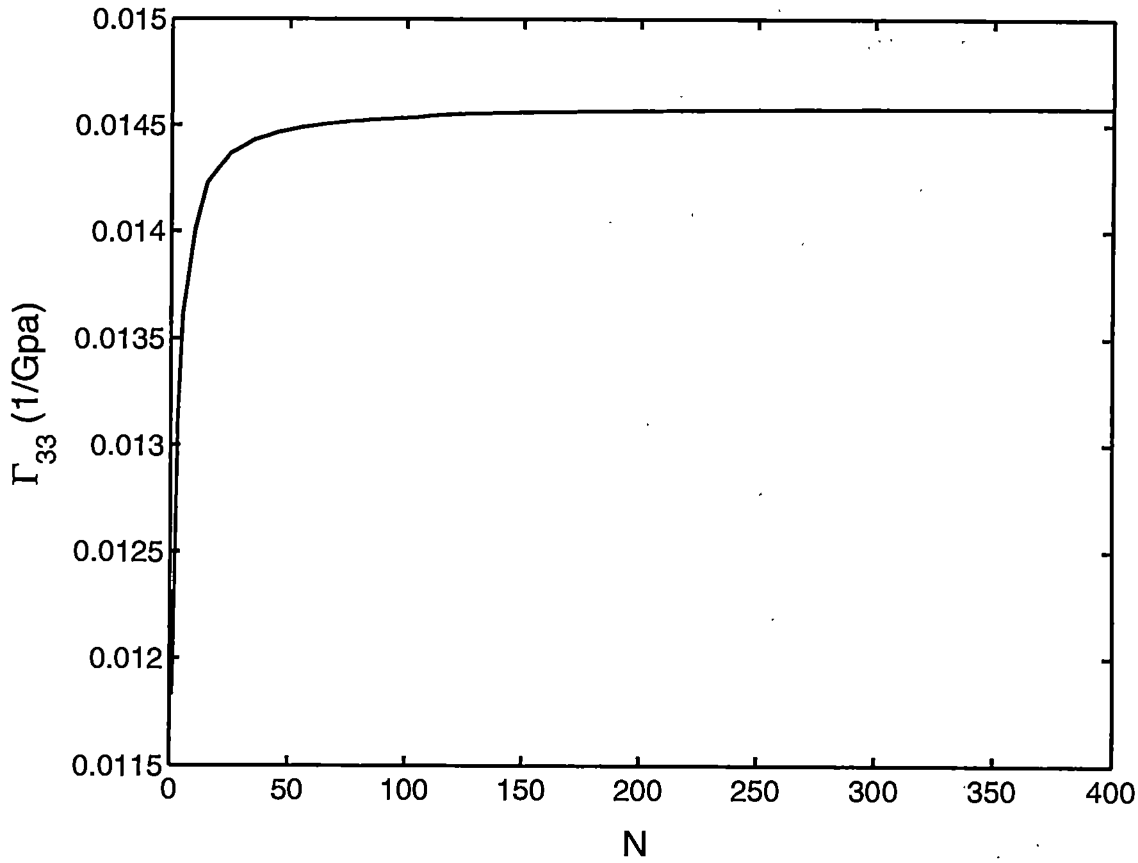

Figure 3.7: Tensor Γ_{33} of brass/PMN/brass as a function of the number of Fourier series term, N.

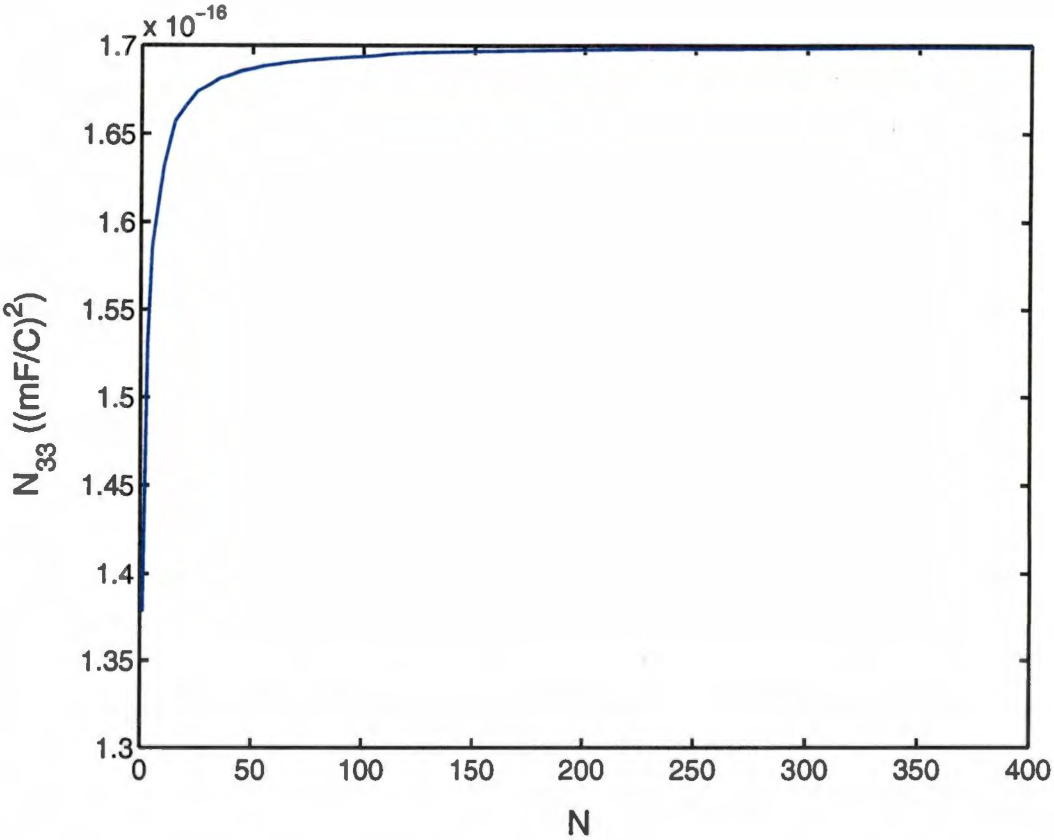

Figure 3.8: Tensor N_{33} of brass/PMN/brass as a function of the number of Fourier series term, N.

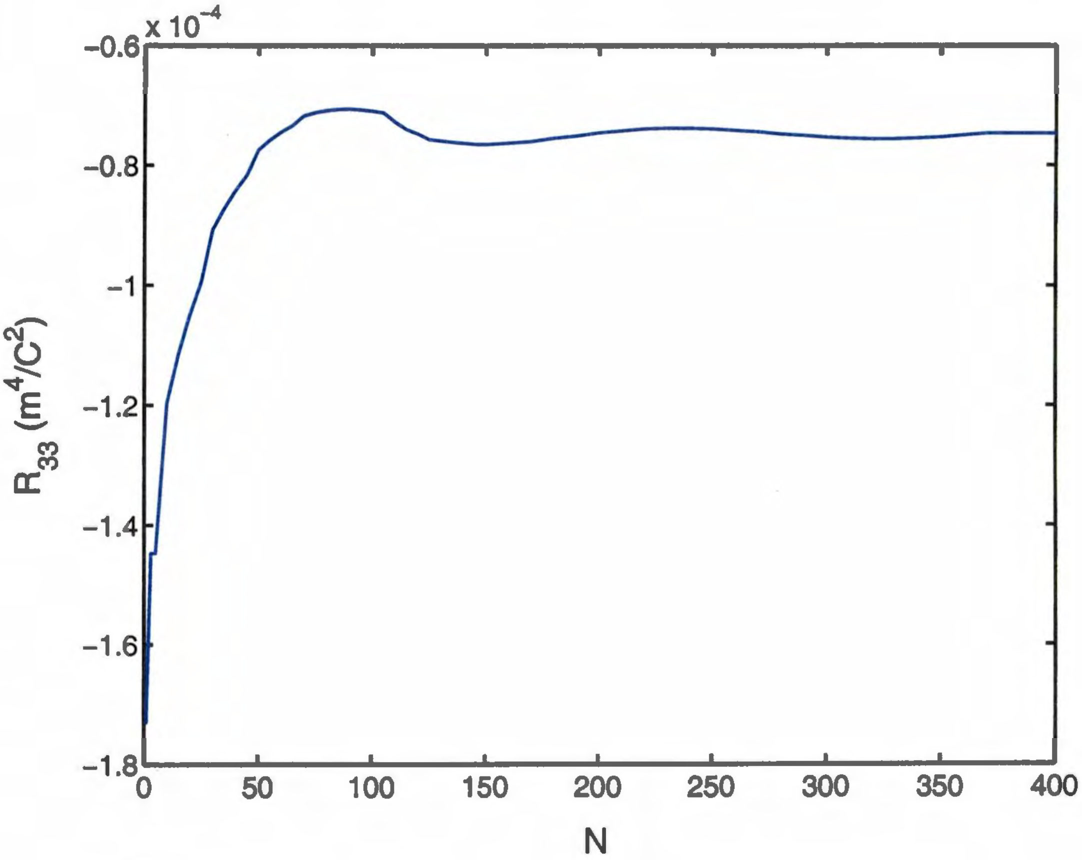

Figure 3.9: Tensor R_{33} of brass/PMN/brass as a function of the number of Fourier series term, N.

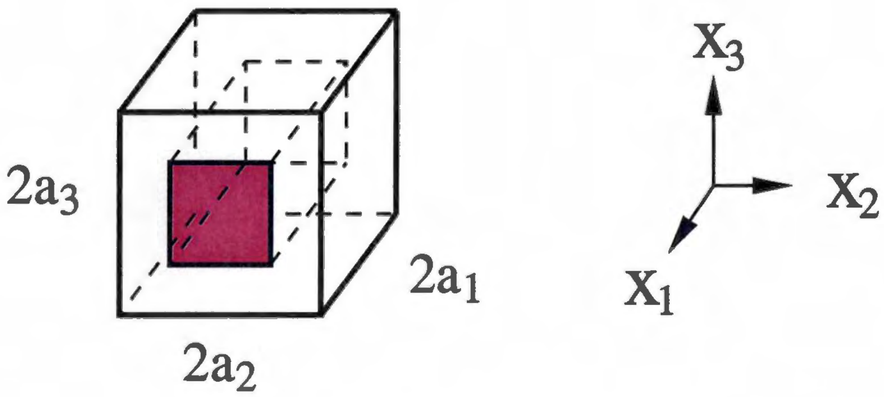

Figure 3.10: PMN-fiber/epoxy composite.

(i.e., continuous fibers) and $2b_2 = 2b_3$. The material properties of the epoxy are given by: $E = 2.5$ GPa, $\nu = 0.33$, and $\kappa_{11} = \kappa_{22} = \kappa_{33} = 0.0037\text{x}10^{-8}\,\text{F/m}$. The effective properties of the electrostrictive composites as a function of fiber volume fraction, f, is shown in Figure 3.11 - 3.13. An increase in the volume fraction of PMN, results in an increase in the stiffness, C_{33}, the dielectric constant, κ_{33}, and the electrostrictive constant, Q_{33}, of the composite. The strain ε_{33} as a function of electric field E_3 is shown in Figure 3.14. The relationship between the strain, ε_{33} , and the electric field, E_3, is nonlinear. The composite strain, ε_{33}, increases with an increase the volume fraction of PMN due to the electric field, E_3.

It is pointed out by Suo (1991) and Hom and Shankar (1994) that the polarization approaches to an asymptotic value due to saturation when the electric field increases. To account for the saturation of polarization, higher order terms may need to be included in the constitutive relation Eq. (3.4). If the electric field is not very high, the present formulation based on the constitutive relation Eq. (3.4) is valid.

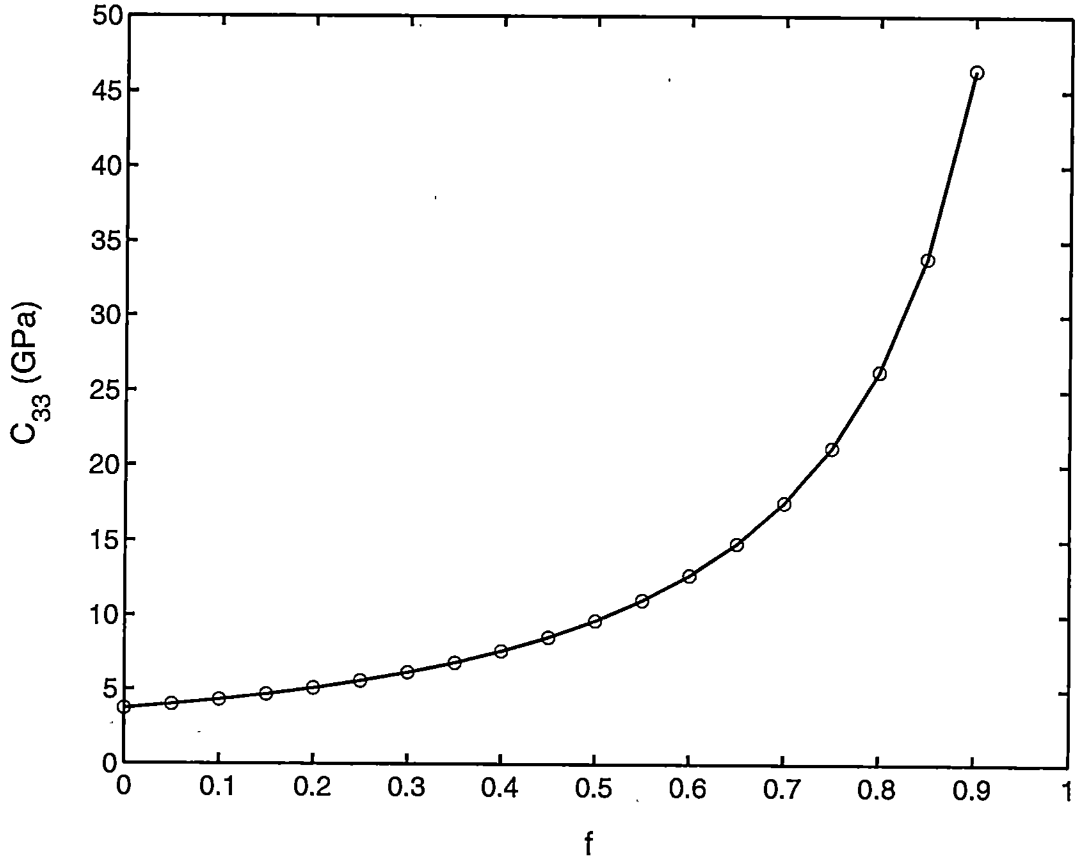

Figure 3.11: Effective stiffness, $\bar{C}_{33}$, as a function of fiber volume fraction, f, of PMN_f/epoxy.

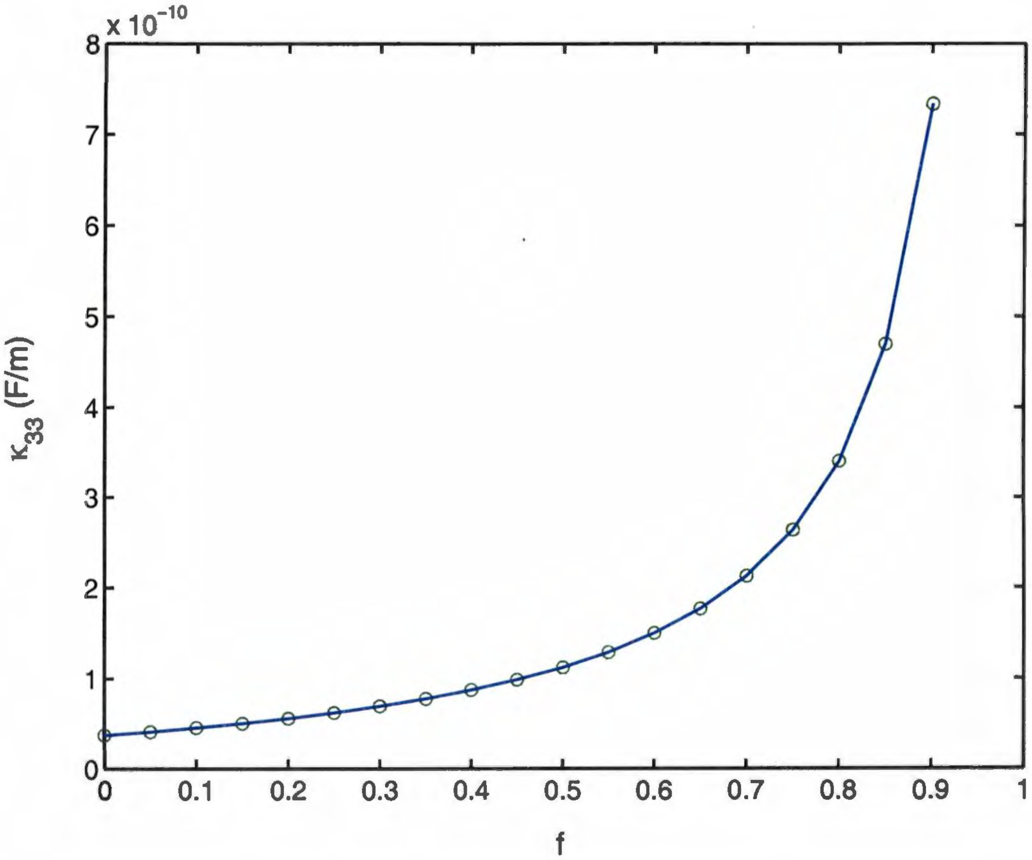

Figure 3.12: Effective permittivity, $\bar{\kappa}_{33}$, as a function of fiber volume fraction, f, of PMN_f/epoxy.

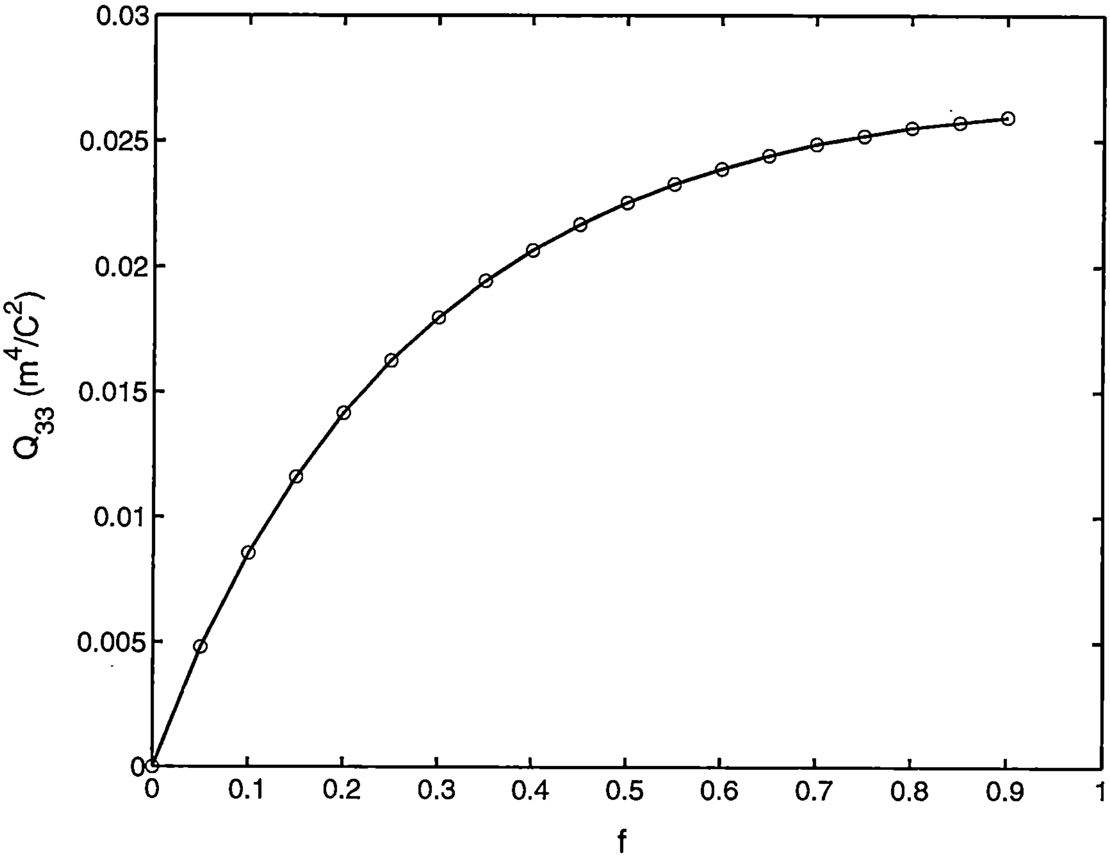

Figure 3.13: Effective electrostrictive constant, $\bar{Q}_{33}$, as a function of fiber volume fraction, f, of PMN$_f$/epoxy.

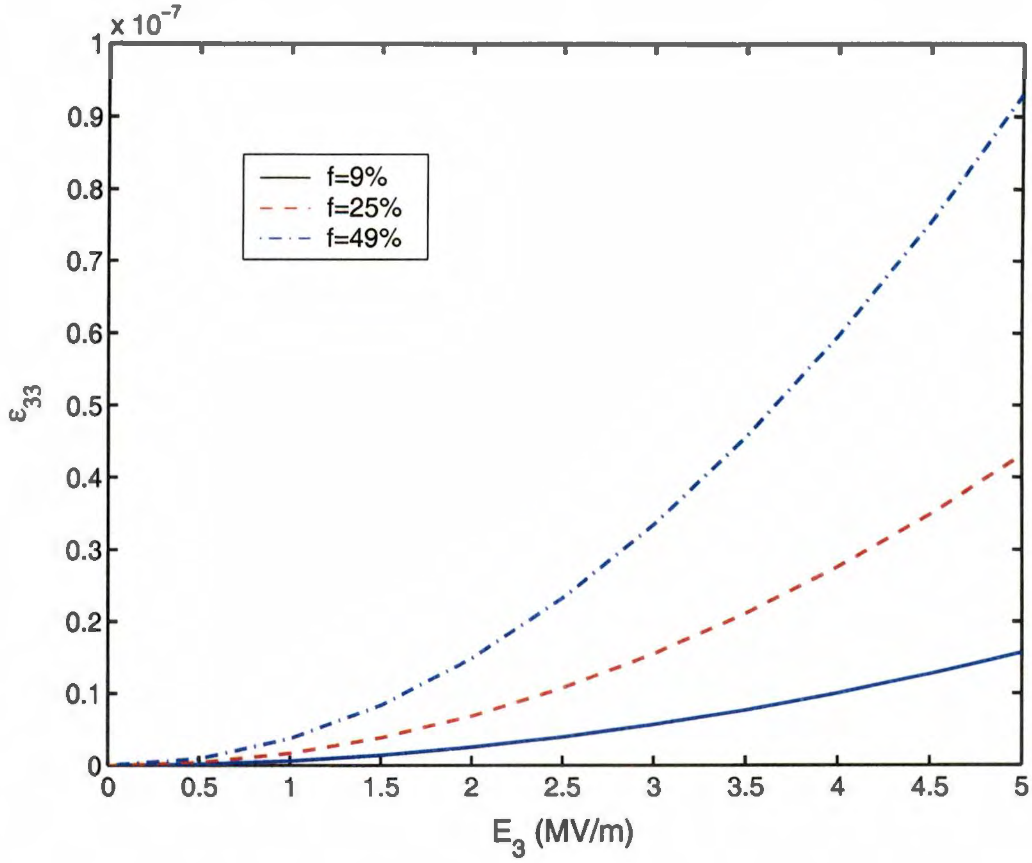

Figure 3.14: Strain ε_{33} as a function of electric field E_3 in PMN$_f$/epoxy.

Chapter 4

Electrostrictive Materials with Periodically Distributed Cracks

4.1 Electrostrictive Materials with Voids

Electrostrictive ceramics are brittle and susceptible to micro-flaws. The property degradation due to microcracking in electrostrictive materials is thus technologically important. In this chapter, the formulations for the effective properties of electrostrictive materials with periodically distributed voids are derived, and one extended to the case of an electrostrictive solid containing periodically distributed, aligned 2-D line cracks.

The effective properties of electrostrictive materials with periodically distributed voids can be estimated by the method presented in Chapter 3.

Since the inhomogeneities are now voids, the stiffness and the electrostrictive constants of the voids vanish ($\mathbf{C}^{\Omega} = 0$; $\mathbf{Q}^{\Omega} = 0$), which also implies that $\mathbf{B}^{\Omega}$ ($B^{\Omega}_{ijpq} = C^{\Omega}_{ijmn} Q^{\Omega}_{mnkl} \kappa^{\Omega}_{kp} \kappa^{\Omega}_{lq}$) is equal to zero. However, the permittivity, $\boldsymbol{\kappa}^{\Omega}$, within the voids is not equal to zero ($\boldsymbol{\kappa}^{\Omega} = \boldsymbol{\kappa}^{\text{air}} = 8.85\text{x}10^{-12}\text{F/m}$). Therefore, Eq. (3.65) and (3.66) become

$$\begin{aligned}
\bar{\boldsymbol{\sigma}}^{*} &= -(\mathbf{I} - \mathbf{C}^{\mathrm{M}} : \boldsymbol{\Gamma})^{-1} : \mathbf{C}^{\mathrm{M}} : \boldsymbol{\varepsilon}^{\circ} - (\mathbf{I} - \mathbf{C}^{\mathrm{M}} : \boldsymbol{\Gamma})^{-1} : \{2\mathbf{C}^{\mathrm{M}} : \mathbf{N} \\
&\quad -\mathbf{C}^{\mathrm{M}} : \mathbf{R} : \mathbf{V} + \mathbf{B}^{\mathrm{M}} - 2\mathbf{B}^{\mathrm{M}} \cdot \mathbf{Y} \cdot (\mathbf{1}^{(2)} + \triangle\boldsymbol{\kappa} \cdot \mathbf{Y})^{-1} \cdot \triangle\boldsymbol{\kappa} \\
&\quad +\mathbf{B}^{\mathrm{M}} : \mathbf{J}\} : (\mathbf{E}^{\circ} \otimes \mathbf{E}^{\circ}),
\end{aligned} \tag{4.1}$$

$$\bar{\mathbf{P}}^{*} = (\mathbf{1}^{(2)} + \triangle\boldsymbol{\kappa} \cdot \mathbf{Y})^{-1} \cdot \triangle\boldsymbol{\kappa} \cdot \mathbf{E}^{\circ}. \tag{4.2}$$

or, in indicial notation,

$$\begin{aligned}
\bar{\sigma}^{*}_{ij} &= -(1^{4} - C^{M} : \Gamma)^{-1}_{ijef} C^{M}_{efkl} \varepsilon^{\circ}_{kl} - (1^{4} - C^{M} : \Gamma)^{-1}_{ijef} \{2C^{M}_{efkl} N_{klqt} \\
&\quad -C^{M}_{efkl} R_{klmn} V_{mnqt} + B^{M}_{efqt} - 2B^{M}_{efql} Y_{ln} (1^{2} + \triangle\kappa \cdot Y)^{-1}_{ns} \triangle\kappa_{st} \\
&\quad +B^{M}_{efkl} J_{klqt}\} E^{\circ}_{q} E^{\circ}_{t},
\end{aligned} \tag{4.3}$$

$$\bar{P}^{*}_{i} = (1^{2} + \triangle\kappa \cdot Y)^{-1}_{ij} \triangle\kappa_{jk} E^{\circ}_{k}, \tag{4.4}$$

where $\mathbf{V}$ and $\mathbf{J}$ are given by

$$V_{mnqt} = (1^{(2)} + \triangle\kappa \cdot Y)^{-1}_{mp} \triangle\kappa_{pq} (1^{(2)} + \triangle\kappa \cdot Y)^{-1}_{ns} \triangle\kappa_{st}, \tag{4.5}$$

$$J_{klqt} = Y_{kp} (1^{(2)} + \triangle\kappa \cdot Y)^{-1}_{pr} \triangle\kappa_{rq} Y_{ln} (1^{(2)} + \triangle\kappa \cdot Y)^{-1}_{ns} \triangle\kappa_{st}, \tag{4.6}$$

$$\triangle\boldsymbol{\kappa} = \boldsymbol{\kappa}^{\Omega} - \boldsymbol{\kappa}^{\mathrm{M}}. \tag{4.7}$$

The fourth-order tensors $\boldsymbol{\Gamma}$, $\mathbf{Y}$, $\mathbf{R}$, and $\mathbf{N}$ include infinite series and are expressed by

$$\boldsymbol{\Gamma} = \sum_{\boldsymbol{\xi}\neq 0}^{\pm\infty} f g(\boldsymbol{\xi}) g(-\boldsymbol{\xi}) \boldsymbol{\Gamma}', \tag{4.8}$$

$$\mathbf{R} = \sum_{\boldsymbol{\xi}\neq 0}^{\pm\infty} f g(\boldsymbol{\xi}) \boldsymbol{\Gamma}' : \mathbf{B}^{\mathrm{M}} : \mathbf{A}(\boldsymbol{\xi}), \tag{4.9}$$

$$\mathbf{Y} = \sum_{\boldsymbol{\xi}\neq 0}^{\pm\infty} f g(\boldsymbol{\xi}) g(-\boldsymbol{\xi}) (\bar{\boldsymbol{\xi}} \otimes \bar{\boldsymbol{\xi}})/(\bar{\boldsymbol{\xi}} \cdot \boldsymbol{\kappa}^{\mathrm{M}} \cdot \bar{\boldsymbol{\xi}}), \tag{4.10}$$

$$\mathrm{N} = \sum_{\boldsymbol{\xi}\neq 0}^{\pm\infty} f g(\boldsymbol{\xi}) g(-\boldsymbol{\xi}) \boldsymbol{\Gamma}' : \mathbf{B}^{\mathrm{M}} \cdot (\bar{\boldsymbol{\xi}} \otimes \bar{\boldsymbol{\xi}}) \cdot (\mathbf{1}^{(2)} + \triangle\boldsymbol{\kappa} \cdot \mathbf{Y})^{-1} \cdot \triangle\boldsymbol{\kappa}/(\bar{\boldsymbol{\xi}} \cdot \boldsymbol{\kappa}^{\mathrm{M}} \cdot \bar{\boldsymbol{\xi}}). \tag{4.11}$$

The average strains and electric fields over the unit cell, U, are $\boldsymbol{\varepsilon}^{\circ}$ and E°, since the averages of the *periodic* perturbation strains and electric fields over U vanish. The effective dielectric, stiffness, and electrostrictive properties, $\bar{\boldsymbol{\kappa}}$, $\bar{\mathbf{C}}$ and $\bar{\mathbf{B}}$, of electrostrictive materials with periodically distributed cracks are given by

$$< \mathbf{P}(\mathrm{x}) >_U = \bar{\boldsymbol{\kappa}} \cdot \mathbf{E}^{\circ} = \boldsymbol{\kappa}^{\mathrm{M}} \cdot \mathbf{E}^{\circ} + f < \mathbf{P}^{*}(\mathrm{x}) >_{\Omega}, \tag{4.12}$$

$$\begin{aligned} < \boldsymbol{\sigma}(\mathrm{x}) >_U &= \bar{\mathbf{C}} : \boldsymbol{\varepsilon}^{\circ} - \bar{\mathbf{B}} : (\mathbf{E}^{\circ} \otimes \mathbf{E}^{\circ}) \\ &= \mathbf{C}^{\mathrm{M}} : \boldsymbol{\varepsilon}^{\circ} - \mathbf{B}^{\mathrm{M}} : (\mathbf{E}^{\circ} \otimes \mathbf{E}^{\circ}) + f < \boldsymbol{\sigma}^{*}(\mathrm{x}) >_{\Omega}, \end{aligned} \tag{4.13}$$

where f is the inhomogeneity volume fraction.

To estimate the properties of electrostrictive materials with periodically distributed cracks, one substitutes Eq. (4.1) and (4.2) into Eq. (4.12) and (4.13). The effective properties of the electrostrictive materials with periodically distributed cracks are obtained by comparing both sides of Eq. (4.12) and (4.13):

$$\bar{\boldsymbol{\kappa}} = \boldsymbol{\kappa}^{\mathrm{M}} + f(\mathbf{1}^{(2)} + \triangle\boldsymbol{\kappa} \cdot \mathbf{Y})^{-1} \cdot \triangle\boldsymbol{\kappa}, \tag{4.14}$$

$$\bar{\mathbf{C}} = \mathbf{C}^{\mathrm{M}} - f(\mathbf{I} - \mathbf{C}^{\mathrm{M}} : \boldsymbol{\Gamma})^{-1} : \mathbf{C}^{\mathrm{M}}, \tag{4.15}$$

$$\begin{aligned} \bar{\mathbf{B}} \;&=\; \mathbf{B}^{\mathrm{M}} - f(\mathbf{I} - \mathbf{C}^{\mathrm{M}} : \boldsymbol{\Gamma})^{-1} : \{2\mathbf{C}^{\mathrm{M}} : \mathbf{N} - \mathbf{C}^{\mathrm{M}} : \mathbf{R} : \mathbf{V} + \mathbf{B}^{\mathrm{M}} \\ &\quad -2\mathbf{B}^{\mathrm{M}} \cdot \mathbf{Y} \cdot (\mathbf{1}^{(2)} + \triangle\boldsymbol{\kappa} \cdot \mathbf{Y})^{-1} \cdot \triangle\boldsymbol{\kappa} + \mathbf{B}^{\mathrm{M}} : \mathbf{J}\}. \end{aligned} \tag{4.16}$$

4.2 2-D Line Cracks

An electrostrictive solid containing periodically distributed, aligned 2-D line cracks is shown in Figure 4.1. Basically, the 2-D line crack can be considered as a special case of a flat elliptic cylindrical void; see Figure 4.2, where $2a_i$ $(i = 1 \sim 3)$ are the dimensions of the unit cell, and $2b_i$ are the dimensions of the void. When the aspect ratio of the flat void, $\beta = b_3/b_1$, goes to zero, the flat elliptic cylindrical void becomes a 2-D line crack (Nemat-Nasser *et al.,* 1993). To study the local fields and the effective properties of cracked electrostrictive materials, a limiting process is performed on the formulation developed in Section 4.1. Namely, for the

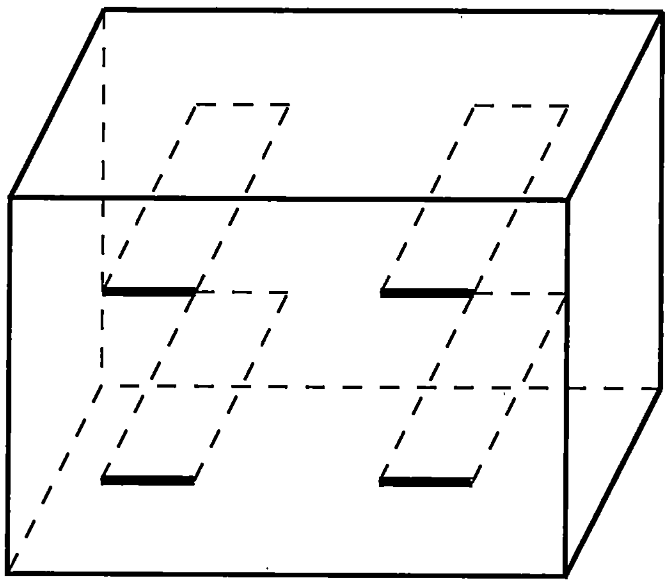

Figure 4.1: Periodically distributed 2-D line cracks.

effective properties of cracked electrostrictive materials, Eq. (4.14), (4.15), and (4.16) become

$$\bar{\boldsymbol{\kappa}} = \boldsymbol{\kappa}^{\mathbf{M}} + \lim_{\beta\to 0} f(\mathbf{1}^{(2)} + \triangle\boldsymbol{\kappa}\cdot\mathbf{Y})^{-1}\cdot\triangle\boldsymbol{\kappa}, \tag{4.17}$$

$$\bar{\mathbf{C}} = \mathbf{C}^{\mathbf{M}} - \lim_{\beta\to 0} f(\mathbf{I} - \mathbf{C}^{\mathbf{M}} : \boldsymbol{\Gamma})^{-1} : \mathbf{C}^{\mathbf{M}}, \tag{4.18}$$

$$\begin{aligned} \bar{\mathbf{B}} &= \mathbf{B}^{\mathbf{M}} - \lim_{\beta\to 0} f(\mathbf{I} - \mathbf{C}^{\mathbf{M}} : \boldsymbol{\Gamma})^{-1} : \{2\mathbf{C}^{\mathbf{M}} : \mathbf{N} - \mathbf{C}^{\mathbf{M}} : \mathbf{R} : \mathbf{V} + \mathbf{B}^{\mathbf{M}} \\ &\quad -2\mathbf{B}^{\mathbf{M}}\cdot\mathbf{Y}\cdot(\mathbf{1}^{(2)} + \triangle\boldsymbol{\kappa}\cdot\mathbf{Y})^{-1}\cdot\triangle\boldsymbol{\kappa} + \mathbf{B}^{\mathbf{M}} : \mathbf{J}\}. \end{aligned} \tag{4.19}$$

Define

$$s^{pq} \equiv \sum_{\boldsymbol{\xi}\neq 0}^{\pm\infty} g(\boldsymbol{\xi})g(-\boldsymbol{\xi})(\bar{\xi}_1^2)^p(\bar{\xi}_2^2)^q \text{ for } p,\ q = 0,\ 1,\ 2., \tag{4.20}$$

and

$$d = \frac{f}{\beta}. \tag{4.21}$$

The components of the effective permittivities can be expressed by

$$\begin{aligned} \bar{\kappa}_{11} &= \kappa_{11}^M + \frac{f\triangle\kappa_{11}}{1 + \frac{\triangle\kappa_{11}}{\kappa_{11}^M} f \sum\limits_{\boldsymbol{\xi}\neq 0}^{\pm\infty} g(\boldsymbol{\xi})g(-\boldsymbol{\xi})\bar{\xi}_1^2} \\ &= \kappa_{11}^M + \frac{d\beta\triangle\kappa_{11}}{1 + d\beta\frac{\triangle\kappa_{11}}{\kappa_{11}^M}s^{10}} \\ &= \kappa_{11}^M + \frac{O(\beta)}{1 + O(\beta)}, \end{aligned} \tag{4.22}$$

$$\bar{\kappa}_{22} = \kappa_{22}^M + \frac{f\triangle\kappa_{22}}{1 + \frac{\triangle\kappa_{22}}{\kappa_{22}^M} f \sum\limits_{\boldsymbol{\xi}\neq 0}^{\pm\infty} g(\boldsymbol{\xi})g(-\boldsymbol{\xi})\bar{\xi}_2^2}$$

$$
\begin{aligned}
&= \kappa_{22}^M + \frac{d\beta \triangle\kappa_{22}}{1 + d\beta \frac{\triangle\kappa_{22}}{\kappa_{22}^M} s^{01}} \\
&= \kappa_{22}^M + \frac{O(\beta)}{1 + O(\beta)},
\end{aligned}
\tag{4.23}
$$

$$
\begin{aligned}
\bar{\kappa}_{33} &= \kappa_{33}^M + \frac{f\triangle\kappa_{33}}{1 + \frac{\triangle\kappa_{33}}{\kappa_{33}^M} f \sum\limits_{\boldsymbol{\xi}\neq 0}^{\pm\infty} g(\boldsymbol{\xi}) g(-\boldsymbol{\xi}) \bar{\xi}_3^3} \\
&= \kappa_{33}^M + \frac{f\triangle\kappa_{33}}{1 + \frac{\triangle\kappa_{33}}{\kappa_{33}^M} - f(\frac{\triangle\kappa_{33}}{\kappa_{33}^M} - \frac{\triangle\kappa_{33}}{\kappa_{33}^M} \sum\limits_{\boldsymbol{\xi}\neq 0}^{\pm\infty} g(\boldsymbol{\xi}) g(-\boldsymbol{\xi})(\bar{\xi}_1^2 + \bar{\xi}_2^2))} \\
&= \kappa_{33}^M + \frac{d\beta\triangle\kappa_{33}}{1 + \frac{\triangle\kappa_{33}}{\kappa_{33}^M} - d\beta(\frac{\triangle\kappa_{33}}{\kappa_{33}^M} - \frac{\triangle\kappa_{33}}{\kappa_{33}^M}(s^{10} + s^{01}))} \\
&= \kappa_{33}^M + \frac{O(\beta)}{1 + \frac{\triangle\kappa_{33}}{\kappa_{33}^M} + O(\beta)}.
\end{aligned}
\tag{4.24}
$$

where

$$
\bar{\boldsymbol{\xi}}_1^2 + \bar{\boldsymbol{\xi}}_2^2 + \bar{\boldsymbol{\xi}}_3^2 = 1, \tag{4.25}
$$

$$
\sum_{\boldsymbol{\xi}\neq 0}^{\pm\infty} f g(\boldsymbol{\xi}) g(-\boldsymbol{\xi}) = 1 - f, \tag{4.26}
$$

are used.

When β approaches to 0, $\bar{\kappa}_{11} = \kappa_{11}^M$, $\bar{\kappa}_{22} = \kappa_{22}^M$, and $\bar{\kappa}_{33} = \kappa_{33}^M$. That is, the dielectric properties of electroctrictive solids are not degraded due to the existence of cracks.

For an isotropic matrix, the stiffness is given by

$$
C_{ijmn} = \frac{2\mu\nu}{1 - 2\nu} \delta_{ij}\delta_{mn} + \mu(\delta_{im}\delta_{jn} + \delta_{in}\delta_{jm}), \tag{4.27}
$$

where μ is the shear modulus and ν is the Poisson ratio. Consequently,

$$C_{ijmn}\Gamma_{mnkl} = 2\text{sym}(\bar{\xi}_i\delta_{jk}\bar{\xi}_l) - \frac{1}{1-\nu}\bar{\xi}_i\bar{\xi}_j\bar{\xi}_k\bar{\xi}_l + \frac{\nu}{1-\nu}\delta_{ij}\bar{\xi}_k\bar{\xi}_l, \tag{4.28}$$

Thus $\mathbf{I} - \mathbf{C}^{\mathbf{M}} : \mathbf{\Gamma}$ can be expressed by

$$[\mathbf{I} - \mathbf{C}^{\mathbf{M}} : \mathbf{\Gamma}] = \begin{bmatrix} U_{11} & U_{12} & U_{13} & 0 & 0 & 0 \\ U_{21} & U_{22} & U_{23} & 0 & 0 & 0 \\ U_{31} & U_{32} & U_{33} & 0 & 0 & 0 \\ 0 & 0 & 0 & U_{44} & 0 & 0 \\ 0 & 0 & 0 & 0 & U_{55} & 0 \\ 0 & 0 & 0 & 0 & 0 & U_{66} \end{bmatrix}, \tag{4.29}$$

where

$$U_{11} = 1 - d\beta(2s^{10} - \frac{1}{1-\nu}s^{20} + \frac{\nu}{1-\nu}s^{10}), \tag{4.30}$$

$$U_{12} = -d\beta(-\frac{1}{1-\nu}s^{11} + \frac{\nu}{1-\nu}s^{01}), \tag{4.31}$$

$$U_{13} = -\frac{\nu}{1-\nu} + d\beta(\frac{\nu}{1-\nu} + \frac{1}{1-\nu}(s^{10} - s^{20} - s^{11}) + \frac{\nu}{1-\nu}(s^{10} + s^{01})), \tag{4.32}$$

$$U_{21} = -d\beta(-\frac{1}{1-\nu}s^{11} + \frac{\nu}{1-\nu}s^{10}), \tag{4.33}$$

$$U_{22} = 1 - d\beta(2s^{01} - \frac{1}{1-\nu}s^{02} + \frac{\nu}{1-\nu}s^{01}), \tag{4.34}$$

$$U_{23} = -\frac{\nu}{1-\nu} + d\beta(\frac{\nu}{1-\nu} + \frac{1}{1-\nu}(s^{01} - s^{02} - s^{11}) + \frac{\nu}{1-\nu}(s^{10} + s^{01})), \tag{4.35}$$

$$U_{31} = -d\beta(-\frac{1}{1-\nu}(s^{10} - s^{20} - s^{11}) + \frac{\nu}{1-\nu}s^{10}), \tag{4.36}$$

$$U_{32} = -d\beta(-\frac{1}{1-\nu}(s^{01} - s^{02} - s^{11}) + \frac{\nu}{1-\nu}s^{01}), \tag{4.37}$$

$$U_{33} = d\beta(1+2s^{10}+2s^{01}+\frac{1}{1-\nu}(s^{20}-2s^{10}-2s^{01}+2s^{11}+s^{02})+\frac{\nu}{1-\nu}(s^{10}+s^{01})), \tag{4.38}$$

$$U_{44} = d\beta(1 + s^{10} + s^{01} + \frac{1}{1-\nu}(s^{01} - s^{11} - s^{02})), \tag{4.39}$$

$$U_{55} = d\beta(1 + s^{10} + s^{01} + \frac{1}{1-\nu}(s^{10} - s^{11} - s^{20})), \tag{4.40}$$

$$U_{66} = 1 - d\beta(1 + s^{01} + \frac{1}{1-\nu}s^{11}). \tag{4.41}$$

By inverting the $[\mathbf{I} - \mathbf{C}^{\mathbf{M}} : \mathbf{\Gamma}]$, one finds

$$f[\mathbf{I} - \mathbf{C}^{\mathbf{M}} : \mathbf{\Gamma}]^{-1} = \begin{bmatrix} O(\beta) & O(\beta) & O(\beta) & 0 & 0 & 0 \\ O(\beta) & O(\beta) & O(\beta) & 0 & 0 & 0 \\ \frac{\frac{\nu}{1-\nu}+O(\beta)}{\Delta_1+O(\beta)} & \frac{\frac{\nu}{1-\nu}+O(\beta)}{\Delta_1+O(\beta)} & \frac{1+O(\beta)}{\Delta_1+O(\beta)} & 0 & 0 & 0 \\ 0 & 0 & 0 & \frac{1}{\Delta_2} & 0 & 0 \\ 0 & 0 & 0 & 0 & \frac{1}{\Delta_3} & 0 \\ 0 & 0 & 0 & 0 & 0 & O(\beta) \end{bmatrix}, \tag{4.42}$$

where

$$\begin{aligned} \Delta_1 \quad = \quad & 1 + 2s^{10} + 2s^{01} + \frac{1}{1-\nu}(s^{20} - 2s^{10} - 2s^{01} + 2s^{11} + s^{02}) \\ & + \frac{\nu}{1-\nu}(s^{10} + s^{01}) + \frac{1}{(1-\nu)^2}(s^{10} - s^{20} - s^{11}) - (\frac{\nu}{1-\nu})^2 s^{10} \\ & + \frac{1}{(1-\nu)^2}(s^{01} - s^{02} - s^{11}) - (\frac{\nu}{1-\nu})^2 s^{01}, \end{aligned} \tag{4.43}$$

$$\Delta_2 = 1 + s^{10} + s^{01} + \frac{1}{1-\nu}(s^{01} - s^{11} - s^{02}), \tag{4.44}$$

$$\Delta_3 = 1 + s^{10} + s^{01} + \frac{1}{1-\nu}(s^{10} - s^{11} - s^{20}). \tag{4.45}$$

When β approaches to 0, Eq. (4.42) becomes

$$f[\mathbf{I} - \mathbf{C^M} : \mathbf{\Gamma}]^{-1} = \begin{bmatrix} 0 & 0 & 0 & 0 & 0 & 0 \\ 0 & 0 & 0 & 0 & 0 & 0 \\ \frac{\nu}{(1-\nu)\Delta_1} & \frac{\nu}{(1-\nu)\Delta_1} & \frac{1}{\Delta_1} & 0 & 0 & 0 \\ 0 & 0 & 0 & \frac{1}{\Delta_2} & 0 & 0 \\ 0 & 0 & 0 & 0 & \frac{1}{\Delta_3} & 0 \\ 0 & 0 & 0 & 0 & 0 & 0 \end{bmatrix}. \tag{4.46}$$

Thus, the effective stiffness of electrostrictive solids containing periodically aligned cracks is given by substituting Eq. (4.46) into Eq. (4.18):

$$\begin{bmatrix} \bar{C}_{11} & \bar{C}_{12} & \bar{C}_{13} & 0 & 0 & 0 \\ \bar{C}_{21} & \bar{C}_{22} & \bar{C}_{23} & 0 & 0 & 0 \\ \bar{C}_{31} & \bar{C}_{32} & \bar{C}_{33} & 0 & 0 & 0 \\ 0 & 0 & 0 & \bar{C}_{44} & 0 & 0 \\ 0 & 0 & 0 & 0 & \bar{C}_{55} & 0 \\ 0 & 0 & 0 & 0 & 0 & \bar{C}_{66} \end{bmatrix} = \begin{bmatrix} C_{11}^M & C_{12}^M & C_{13}^M & 0 & 0 & 0 \\ C_{12}^M & C_{22}^M & C_{23}^M & 0 & 0 & 0 \\ C_{13}^M & C_{23}^M & C_{33}^M & 0 & 0 & 0 \\ 0 & 0 & 0 & C_{44}^M & 0 & 0 \\ 0 & 0 & 0 & 0 & C_{55}^M & 0 \\ 0 & 0 & 0 & 0 & 0 & C_{66}^M \end{bmatrix}$$

$$
- \begin{bmatrix} 0 & 0 & 0 & 0 & 0 & 0 \\ 0 & 0 & 0 & 0 & 0 & 0 \\ \frac{\nu}{(1-\nu)\Delta_1} & \frac{\nu}{(1-\nu)\Delta_1} & \frac{1}{\Delta_1} & 0 & 0 & 0 \\ 0 & 0 & 0 & \frac{1}{\Delta_2} & 0 & 0 \\ 0 & 0 & 0 & 0 & \frac{1}{\Delta_3} & 0 \\ 0 & 0 & 0 & 0 & 0 & 0 \end{bmatrix} \begin{bmatrix} C_{11}^M & C_{12}^M & C_{13}^M & 0 & 0 & 0 \\ C_{12}^M & C_{22}^M & C_{23}^M & 0 & 0 & 0 \\ C_{13}^M & C_{23}^M & C_{33}^M & 0 & 0 & 0 \\ 0 & 0 & 0 & C_{44}^M & 0 & 0 \\ 0 & 0 & 0 & 0 & C_{55}^M & 0 \\ 0 & 0 & 0 & 0 & 0 & C_{66}^M \end{bmatrix} . \tag{4.47}
$$

Thus, the components of effective stiffness can be expressed by

$$
\bar{C}_{11} = C_{11}^M, \quad \bar{C}_{12} = C_{12}^M, \quad \bar{C}_{13} = C_{13}^M, \tag{4.48}
$$

$$
\bar{C}_{21} = C_{12}^M, \quad \bar{C}_{22} = C_{22}^M, \quad \bar{C}_{23} = C_{23}^M, \tag{4.49}
$$

$$
\bar{C}_{31} = C_{31}^M + \frac{1}{\Delta_1}(\frac{\nu}{1-\nu}C_{11}^M + \frac{\nu}{1-\nu}C_{12}^M + C_{13}^M), \tag{4.50}
$$

$$
\bar{C}_{32} = C_{33}^M + \frac{1}{\Delta_1}(\frac{\nu}{1-\nu}C_{12}^M + \frac{\nu}{1-\nu}C_{22}^M + C_{23}^M), \tag{4.51}
$$

$$
\bar{C}_{33} = C_{33}^M + \frac{1}{\Delta_1}(\frac{\nu}{1-\nu}C_{13}^M + \frac{\nu}{1-\nu}C_{23}^M + C_{33}^M), \tag{4.52}
$$

$$
\bar{C}_{44} = C_{44}^M + \frac{C_{44}^M}{\Delta_2}, \tag{4.53}
$$

$$
\bar{C}_{55} = C_{55}^M + \frac{C_{44}^M}{\Delta_3}, \tag{4.54}
$$

$$
\bar{C}_{66} = C_{66}^M, \tag{4.55}
$$

and the rest of components of effective stiffness are equal to zero.

In order to determine $\bar{\mathbf{B}}$ given in Eq. (4.19), one finds

$$[N] = \begin{bmatrix} O(\beta) & O(\beta) & O(\beta) & 0 & 0 & 0 \\ O(\beta) & O(\beta) & O(\beta) & 0 & 0 & 0 \\ O(\beta) & O(\beta) & N_{33} & 0 & 0 & 0 \\ 0 & 0 & 0 & N_{44} & 0 & 0 \\ 0 & 0 & 0 & 0 & N_{55} & 0 \\ 0 & 0 & 0 & 0 & 0 & O(\beta) \end{bmatrix}, \tag{4.56}$$

where

$$N_{33} = (\frac{1-2\nu^M}{2\kappa_{33}^M \mu^M (1-\nu^M)})(\frac{1}{1+\frac{\triangle\kappa_{33}}{\kappa_{33}^M}+O(\beta)})B_{33}^M \triangle\kappa_{33} + O(\beta), \tag{4.57}$$

$$N_{44} = (\frac{1}{2\kappa_{33}^M \mu^M})(\frac{1}{1+\frac{\triangle\kappa_{33}}{\kappa_{33}^M}+O(\beta)})B_{44}^M \triangle\kappa_{33} + O(\beta), \tag{4.58}$$

$$N_{55} = (\frac{1}{2\kappa_{33}^M \mu^M})(\frac{1}{1+\frac{\triangle\kappa_{33}}{\kappa_{33}^M}+O(\beta)})B_{55}^M \triangle\kappa_{33} + O(\beta), \tag{4.59}$$

Similarly,

$$[\mathbf{B^M}\cdot\mathbf{Y}\cdot(\mathbf{1}^{(2)}+\triangle\boldsymbol{\kappa}\cdot\mathbf{Y})^{-1}\cdot\triangle\boldsymbol{\kappa}] = \begin{bmatrix} O(\beta) & O(\beta) & L_{13} & 0 & 0 & 0 \\ O(\beta) & O(\beta) & L_{23} & 0 & 0 & 0 \\ O(\beta) & O(\beta) & L_{33} & 0 & 0 & 0 \\ 0 & 0 & 0 & L_{44} & 0 & 0 \\ 0 & 0 & 0 & 0 & L_{55} & 0 \\ 0 & 0 & 0 & 0 & 0 & O(\beta) \end{bmatrix}, \tag{4.60}$$

where

$$L_{13} = \frac{B_{13}^M \triangle\kappa_{33}}{\kappa_{33}^M}\left(\frac{1}{1 + \frac{\triangle\kappa_{33}}{\kappa_{33}^M} + O(\beta)}\right) + O(\beta), \tag{4.61}$$

$$L_{23} = \frac{B_{23}^M \triangle\kappa_{33}}{\kappa_{33}^M}\left(\frac{1}{1 + \frac{\triangle\kappa_{33}}{\kappa_{33}^M} + O(\beta)}\right) + O(\beta), \tag{4.62}$$

$$L_{33} = \frac{B_{33}^M \triangle\kappa_{33}}{\kappa_{33}^M}\left(\frac{1}{1 + \frac{\triangle\kappa_{33}}{\kappa_{33}^M} + O(\beta)}\right) + O(\beta), \tag{4.63}$$

$$L_{44} = \frac{B_{44}^M \triangle\kappa_{33}}{2\kappa_{33}^M}\left(\frac{1}{1 + \frac{\triangle\kappa_{33}}{\kappa_{33}^M} + O(\beta)}\right) + O(\beta), \tag{4.64}$$

$$L_{55} = \frac{B_{55}^M \triangle\kappa_{33}}{2\kappa_{33}^M}\left(\frac{1}{1 + \frac{\triangle\kappa_{33}}{\kappa_{33}^M} + O(\beta)}\right) + O(\beta). \tag{4.65}$$

The fourth-order tensors R and J can be expressed by

$$[R] = \begin{bmatrix} O(\beta) & O(\beta) & O(\beta) & 0 & 0 & 0 \\ O(\beta) & O(\beta) & O(\beta) & 0 & 0 & 0 \\ O(\beta) & O(\beta) & O(\beta) & 0 & 0 & 0 \\ 0 & 0 & 0 & O(\beta) & 0 & 0 \\ 0 & 0 & 0 & 0 & O(\beta) & 0 \\ 0 & 0 & 0 & 0 & 0 & O(\beta) \end{bmatrix}, \tag{4.66}$$

$$
[J] = \begin{bmatrix} O(\beta) & 0 & 0 & 0 & 0 & 0 \\ 0 & O(\beta) & 0 & 0 & 0 & 0 \\ 0 & 0 & J_{33} & 0 & 0 & 0 \\ 0 & 0 & 0 & O(\beta) & 0 & 0 \\ 0 & 0 & 0 & 0 & O(\beta) & 0 \\ 0 & 0 & 0 & 0 & 0 & O(\beta) \end{bmatrix}, \tag{4.67}
$$

where

$$
J_{33} = \left(\frac{\triangle\kappa_{33}}{\kappa_{33}^M(1 + \frac{\triangle\kappa_{33}}{\kappa_{33}^M} + O(\beta))}\right)^2 + O(\beta). \tag{4.68}
$$

When β approaches zero after the multiplication of matrixes, the effective electrostrictive constants, $\bar{B}$, is given by

$$
\begin{bmatrix} \bar{B}_{11} & \bar{B}_{12} & \bar{B}_{13} \\ \bar{B}_{21} & \bar{B}_{22} & \bar{B}_{23} \\ \bar{B}_{31} & \bar{B}_{32} & \bar{B}_{33} \end{bmatrix} = \begin{bmatrix} B_{11}^M & B_{12}^M & B_{13}^M \\ B_{21}^M & B_{22}^M & B_{23}^M \\ B_{31}^M & B_{32}^M & B_{33}^M \end{bmatrix} - \begin{bmatrix} O(\beta) & O(\beta) & O(\beta) \\ O(\beta) & O(\beta) & O(\beta) \\ \frac{\frac{\nu}{1-\nu}+O(\beta)}{\Delta_1+O(\beta)} & \frac{\frac{\nu}{1-\nu}+O(\beta)}{\Delta_1+O(\beta)} & \frac{1+O(\beta)}{\Delta_1+O(\beta)} \end{bmatrix}
$$

$$
* \left\{ 2 \begin{bmatrix} C_{11}^M & C_{12}^M & C_{13}^M \\ C_{12}^M & C_{22}^M & C_{23}^M \\ C_{13}^M & C_{23}^M & C_{33}^M \end{bmatrix} \begin{bmatrix} O(\beta) & O(\beta) & O(\beta) \\ O(\beta) & O(\beta) & O(\beta) \\ O(\beta) & O(\beta) & N_{33} \end{bmatrix} + \begin{bmatrix} B_{11}^M & B_{12}^M & B_{13}^M \\ B_{21}^M & B_{22}^M & B_{23}^M \\ B_{31}^M & B_{32}^M & B_{33}^M \end{bmatrix} \right.
$$

$$
\left. -2 \begin{bmatrix} O(\beta) & O(\beta) & L_{13}^M \\ O(\beta) & O(\beta) & L_{23}^M \\ O(\beta) & O(\beta) & L_{33}^M \end{bmatrix} + \begin{bmatrix} B_{11}^M & B_{12}^M & B_{13}^M \\ B_{21}^M & B_{22}^M & B_{23}^M \\ B_{31}^M & B_{32}^M & B_{33}^M \end{bmatrix} \begin{bmatrix} O(\beta) & 0 & 0 \\ 0 & O(\beta) & 0 \\ 0 & 0 & J_{33} \end{bmatrix} \right\}, \tag{4.69}
$$

$$
\begin{bmatrix} \bar{B}_{44} & 0 & 0 \\ 0 & \bar{B}_{55} & 0 \\ 0 & 0 & \bar{B}_{66} \end{bmatrix} = \begin{bmatrix} B_{44}^M & 0 & 0 \\ 0 & B_{55}^M & 0 \\ 0 & 0 & B_{66}^M \end{bmatrix} - \begin{bmatrix} \frac{1}{\Delta_2} & O & O \\ O & \frac{1}{\Delta_3} & O \\ O & 0 & O(\beta) \end{bmatrix}
$$

$$
* \left\{ 2 \begin{bmatrix} C_{44}^M & 0 & 0 \\ 0 & C_{55}^M & 0 \\ 0 & 0 & C_{66}^M \end{bmatrix} \begin{bmatrix} N_{44} & O & O \\ O & N_{55} & O \\ O & O & O(\beta) \end{bmatrix} + \begin{bmatrix} B_{44}^M & 0 & 0 \\ 0 & B_{55}^M & 0 \\ 0 & 0 & B_{66}^M \end{bmatrix} \right.
$$

$$
\left. -2 \begin{bmatrix} L_{44} & O & O \\ O & L_{55} & O \\ O & O & O(\beta) \end{bmatrix} + \begin{bmatrix} B_{44}^M & 0 & 0 \\ 0 & B_{55}^M & 0 \\ 0 & 0 & B_{66}^M \end{bmatrix} \begin{bmatrix} O(\beta) & 0 & 0 \\ 0 & O(\beta) & 0 \\ 0 & 0 & O(\beta) \end{bmatrix} \right\}. \tag{4.70}
$$

Thus, the components of electrostrictive constant can be expressed by

$$
\bar{B}_{11} = B_{11}^M, \quad \bar{B}_{12} = B_{12}^M, \quad \bar{B}_{13} = B_{13}^M, \tag{4.71}
$$

$$
\bar{B}_{21} = B_{21}^M, \quad \bar{B}_{22} = B_{22}^M, \quad \bar{B}_{23} = B_{23}^M, \tag{4.72}
$$

$$
\bar{B}_{31} = B_{31}^M + \frac{1}{\Delta_1}\left(\frac{\nu}{1-\nu}B_{11}^M + \frac{\nu}{1-\nu}B_{21}^M + B_{31}^M\right), \tag{4.73}
$$

$$
\bar{B}_{32} = B_{32}^M + \frac{1}{\Delta_1}\left(\frac{\nu}{1-\nu}B_{12}^M + \frac{\nu}{1-\nu}B_{22}^M + B_{32}^M\right), \tag{4.74}
$$

$$
\begin{aligned}
\bar{B}_{33} \;\; = \;\; & B_{33}^M - \frac{1}{\Delta_1}[2N_{33}(\frac{\nu}{1-\nu}C_{13}^M + \frac{\nu}{1-\nu}C_{32}^M + C_{33}^M) \\
& +(J_{33}+1)(\frac{\nu}{1-\nu}B_{13}^M + \frac{\nu}{1-\nu}B_{32}^M + B_{33}^M) \\
& -2(\frac{\nu}{1-\nu}L_{13}^M + \frac{\nu}{1-\nu}L_{32}^M + L_{33}^M)],
\end{aligned} \tag{4.75}
$$

$$\bar{B}_{44} = B_{44}^M - \frac{1}{\Delta_2}(2N_{44}C_{44}^M + B_{44}^M - 2L_{44}), \quad (4.76)$$

$$\bar{B}_{55} = B_{55}^M - \frac{1}{\Delta_3}(2N_{55}C_{55}^M + B_{55}^M - 2L_{55}), \quad (4.77)$$

$$\bar{B}_{66} = B_{66}^M, \quad (4.78)$$

where

$$N_{33} = \frac{1 - 2\mu^M}{2\mu^M(1-\mu^M)}(\frac{B_{33}^M \triangle\kappa_{33}}{\kappa_{33}^M + \triangle\kappa_{33}}), \quad (4.79)$$

$$N_{44} = (\frac{1}{2\mu^M})(\frac{B_{44}^M \triangle\kappa_{33}}{\kappa_M^{33} + \triangle\kappa_{33}}), \quad (4.80)$$

$$N_{55} = (\frac{1}{2\mu^M})(\frac{B_{55}^M \triangle\kappa_{33}}{\kappa_M^{33} + \triangle\kappa_{33}}), \quad (4.81)$$

$$J_{33} = (\frac{\kappa_{33}^M \triangle\kappa_{33}}{\kappa_{33}^M + \triangle\kappa_{33}})^2, \quad (4.82)$$

$$L_{13} = \frac{B_{13}^M \triangle\kappa_{33}}{\kappa_{33}^M + \triangle\kappa_{33}}, \quad (4.83)$$

$$L_{23} = \frac{B_{23}^M \triangle\kappa_{33}}{\kappa_{33}^M + \triangle\kappa_{33}}, \quad (4.84)$$

$$L_{33} = \frac{B_{33}^M \triangle\kappa_{33}}{\kappa_{33}^M + \triangle\kappa_{33}}, \quad (4.85)$$

$$L_{44} = \frac{B_{44}^M \triangle\kappa_{33}}{\kappa_{33}^M + \triangle\kappa_{33}}, \quad (4.86)$$

$$L_{55} = \frac{B_{55}^M \triangle\kappa_{33}}{\kappa_{33}^M + \triangle\kappa_{33}}. \quad (4.87)$$

The geometrical parameter, $g(\boldsymbol{\xi})$, of an elliptical-cylindrical void as shown in Figure 4.2 is given by (Nemat-Nasser *et al.*, 1993)

$$g(\boldsymbol{\xi}) = \frac{\sin(\frac{n_2\pi b_2}{a_2})2J_1(\sqrt{(\frac{n_1\pi}{a_1})^2 + (\frac{n_3\pi}{a_3})^2(\beta)^2})}{\frac{n_2\pi b_2}{a_2}(\sqrt{(\frac{n_1\pi}{a_1})^2 + (\frac{n_3\pi}{a_3})^2(\beta)^2}}, \quad (4.88)$$

where J_1 is the Bessel function of the first kind.

When the aspect ratio of the flat void, $\beta\,(= b_3/b_1)$, approaches zero, and the crack length, b_2, is assumed to be the same as the length of the unit cell, a_2; the flat void becomes a 2-D line crack. Thus, Eq. (4.88) can be reduced as

$$g^*(\boldsymbol{\xi}) \equiv \lim_{\beta\to 0} g(\boldsymbol{\xi}) = \frac{\sin(n_2\pi) 2J_1(\frac{n_1 b_1 \pi}{a_1})}{n_2\pi(\frac{n_1 b_1 \pi}{a_1})}. \tag{4.89}$$

Since

$$\frac{\sin(n_2\pi)}{n_2\pi} = \begin{cases} 1 & \text{when } n_2 = 0, \\ 0 & \text{when } n_2 \neq 0\,, \end{cases} \tag{4.90}$$

the three-dimensional Fourier series expansion becomes a two-dimensional one. Furthermore, one can reduce a two-dimensional series problem into a one-dimensional one by using the following identities:

$$\sum_{n}^{\pm\infty} \frac{m^2}{m^2+n^2} = (\pi m)\coth(\pi m), \tag{4.91}$$

$$\sum_{n}^{\pm\infty} (\frac{m^2}{m^2+n^2})^2 = \frac{1}{2}[(\pi m)\coth(\pi m) + (\pi m)^2 \operatorname{csch}^2(\pi m)], \tag{4.92}$$

where m is a constant. Consequently, one finds

$$\begin{aligned} s^{10} &= \sum_{\boldsymbol{\xi}\neq 0}^{\pm\infty} g^*(\boldsymbol{\xi}) g^*(-\boldsymbol{\xi}) (\frac{\xi_1}{\sqrt{\xi_1^2+\xi_3^2}})^2 \\ &= \frac{4J_1^2(\frac{n_1 b_1 \pi}{a_1})}{(\frac{n_1 b_1 \pi}{a_1})^2} (\pi n_1 \gamma_3)\coth(\pi n_1 \gamma_3), \end{aligned} \tag{4.93}$$

where $\gamma_i = a_i/a_1$. Similarly,

$$s^{20} = \frac{2J_1^2(\frac{n_1 b_1 \pi}{a_1})}{(\frac{n_1 b_1 \pi}{a_1})^2} [(\pi n_1 \gamma_3)\coth(\pi n_1 \gamma_3) + (\pi n_1 \gamma_3)^2 \operatorname{csch}^2(\pi n_1 \gamma_3)]. \tag{4.94}$$

It can be shown that other series, s^{01}, s^{02}, and s^{11}, are equal to zero for 2-D line cracks. Therefore, Eq. (4.43), (4.44), and (4.45) become

$$\Delta_1 = 1 + 2s^{10} + \frac{1}{1-\nu}(s^{20} - 2s^{10}) + \frac{\nu}{1-\nu}s^{10} + \frac{1}{(1-\nu)^2}s^{10} - (\frac{\nu}{1-\nu})^2 s^{10}, \quad (4.95)$$

$$\Delta_2 = 1 + s^{10}, \quad (4.96)$$

$$\Delta_3 = 1 + s^{10} + \frac{1}{1-\nu}s^{10}. \quad (4.97)$$

The crack density parameter f^* of the 2-D line crack is defined by

$$f^* \equiv \lim_{\substack{f\to 0\\ \beta\to 0}} \frac{f}{\pi\beta} = \frac{(\frac{b_1}{a_1})^2}{4\gamma_3}. \quad (4.98)$$

4.3 Results and Discussions

Consider a PMN containing periodic 2-D line cracks; see Figure 4.1. The dimensions of the unit cell are given as follows: $2a_1 = 2a_2 = 2a_3$ and $2b_2 = 2a_2$. The Young modulus, E, Poisson's ratio, ν, the permittivity, κ, and the electrostrictive constants, Q, of isotropic PMN are used: $E = 112$ GPa, $\nu = 0.26$, $\kappa_{11} = \kappa_{22} = \kappa_{33} = 6.6375\text{x}10^{-8}\,\text{F/m}$, $Q_{11} = 0.026\,\text{m}^4/\text{C}^2$, and $Q_{12} = -0.0096\,\text{m}^4/\text{C}^2$ (Sundar and Newhnam, 1992). The Young modulus and the electrostrictive constants are equal to zero within the crack. The permittivity within the crack is assumed to be the permittivity of air: $\kappa_{11} = \kappa_{22} = \kappa_{33} = 8.85\text{x}10^{-12}\,\text{F/m}$. The permittivity within the crack has been discussed by Dunn (1994), who states that if the crack is very sharp, the permittivity within the crack is equal to the permittivity of air. But if the crack is fairly blunt, the assumption that the permittivity within the crack is equal to zero is valid. The normalized properties, $\bar{C}_{33}/C_{33}^M$ and $\bar{B}_{33}/B_{33}^M$, of PMN containing 2-D line cracks as a function of the crack density parameter are shown in Figure 4.3 and Figure 4.4, respectively. The stiffness, C_{33}, and the electrostrictive constant, B_{33}, of electrostrictive ceramics decreases with an increase in the crack density parameter. The results also show that the effective permittivity, $\bar{\kappa}_{33}$, is equal to the permittivity of the matrix, κ_{33}^M; see Eq. (4.22) $\sim$ (4.24). The existence of the 2-D line crack does not influence the effective permittivity $\bar{\kappa}_{33}$. The effective electrostrictive constants $\bar{Q}_{33}$ are also not affected by the existence of microcracking; see Figure 4.5 Finally, the convergence of the infinite series, s^{10} and s^{20}, of PMN with periodically distributed 2-D line cracks ($f^* = 0.0025$) are shown in Figure 4.6. The results show that the infinite series converge rapidly. Therefore, the truncation errors can be negligible.

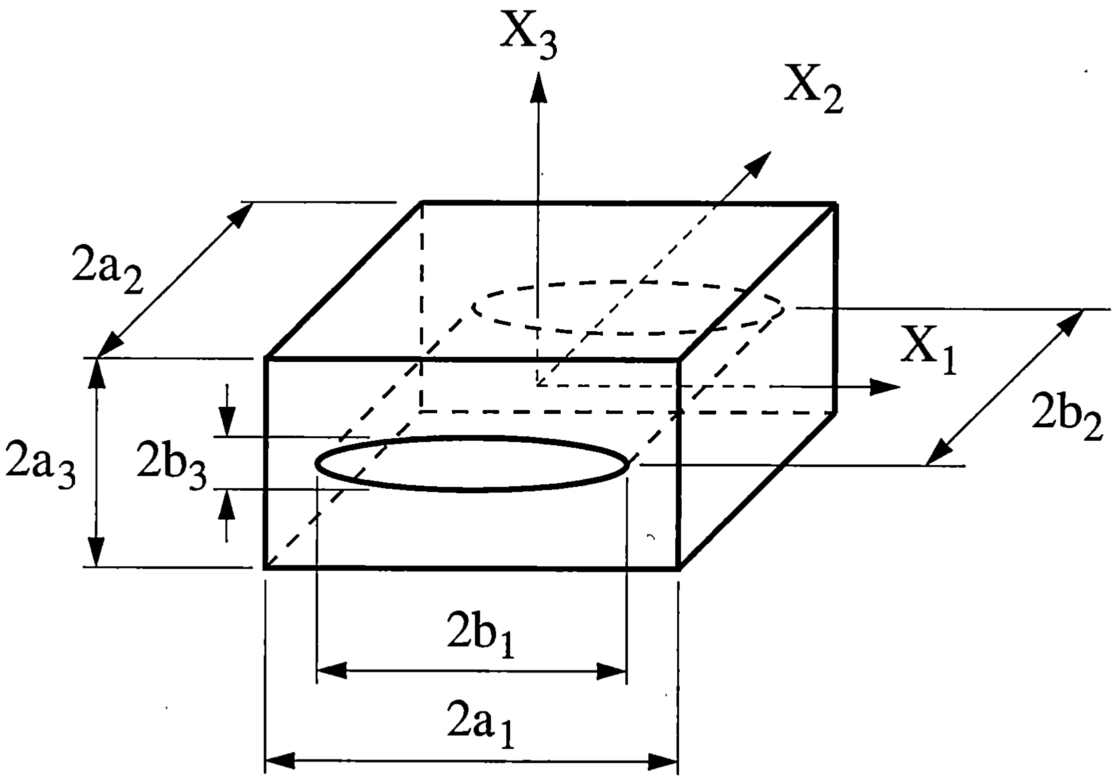

Figure 4.2: Flat elliptical cylindrical void.

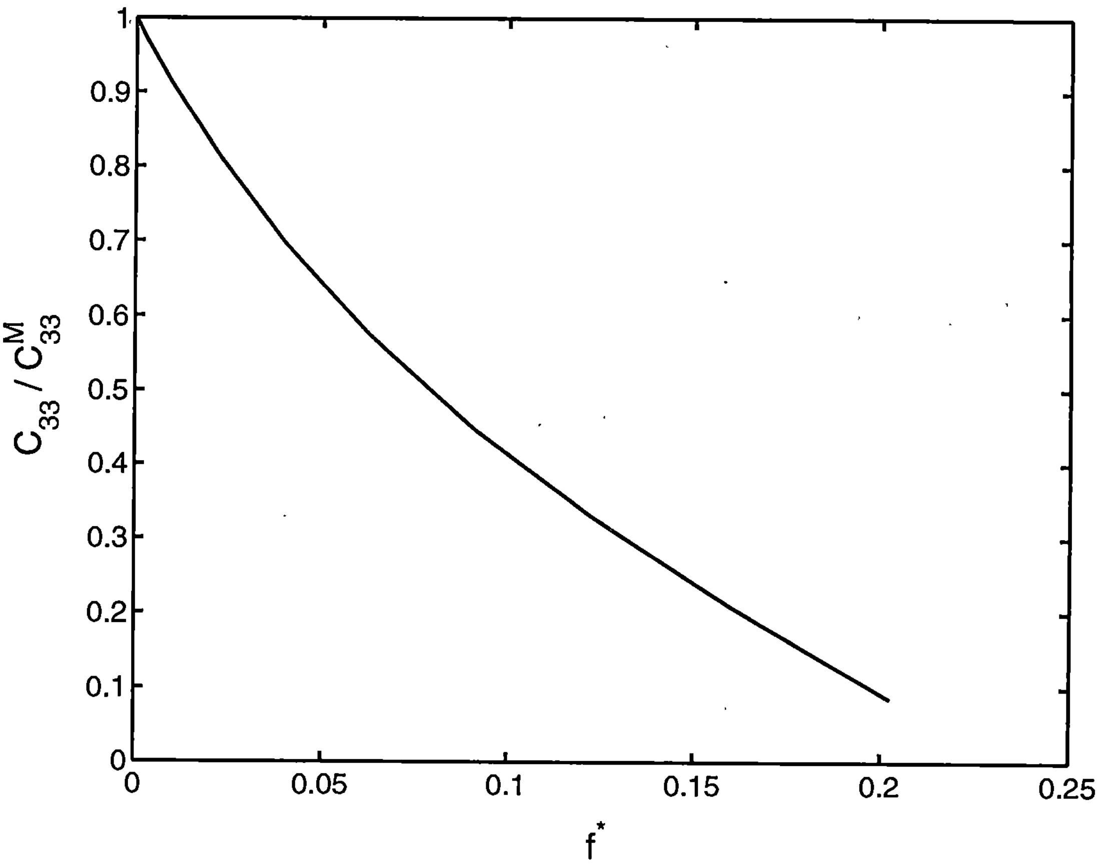

Figure 4.3: Normalized stiffness $\bar{C}_{33}/C_{33}^M$ of PMN with periodically distributed 2-D line cracks as a function of crack density parameter f^*.

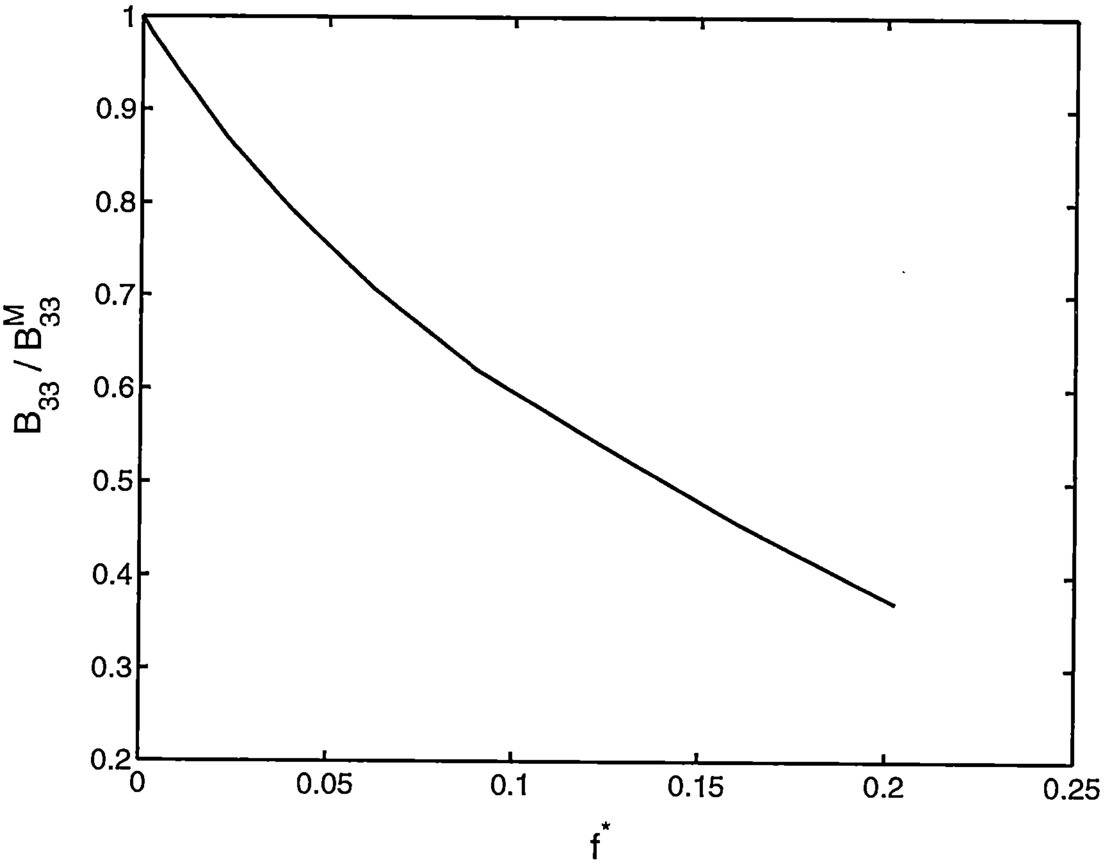

Figure 4.4: Normalized electrostrictive constant $\bar{B}_{33}/B_{33}^M$ of PMN with periodically distributed 2-D line cracks as a function of crack density parameter f^*.

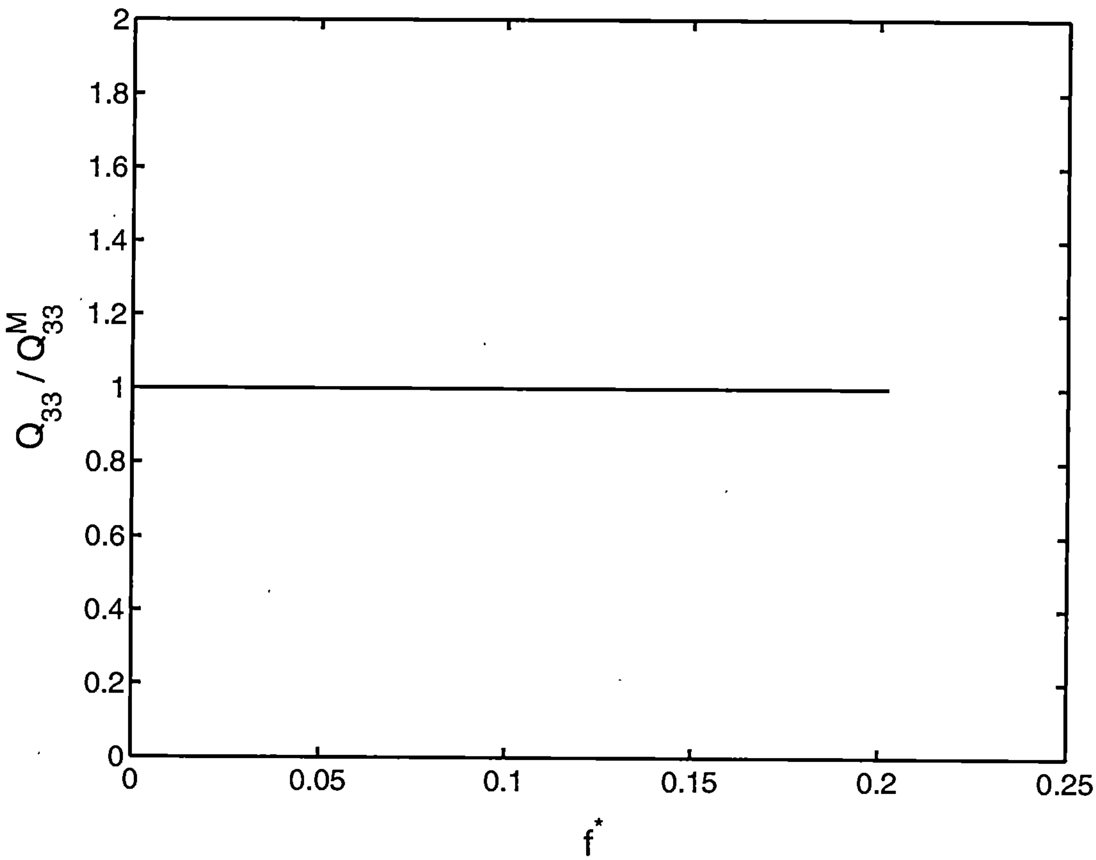

Figure 4.5: Normalized electrostrictive constant, $\bar{Q}^*_{33}/Q^M_{33}$, of PMN with periodically distributed 2-D line crack as a function of crack density parameter f^*.

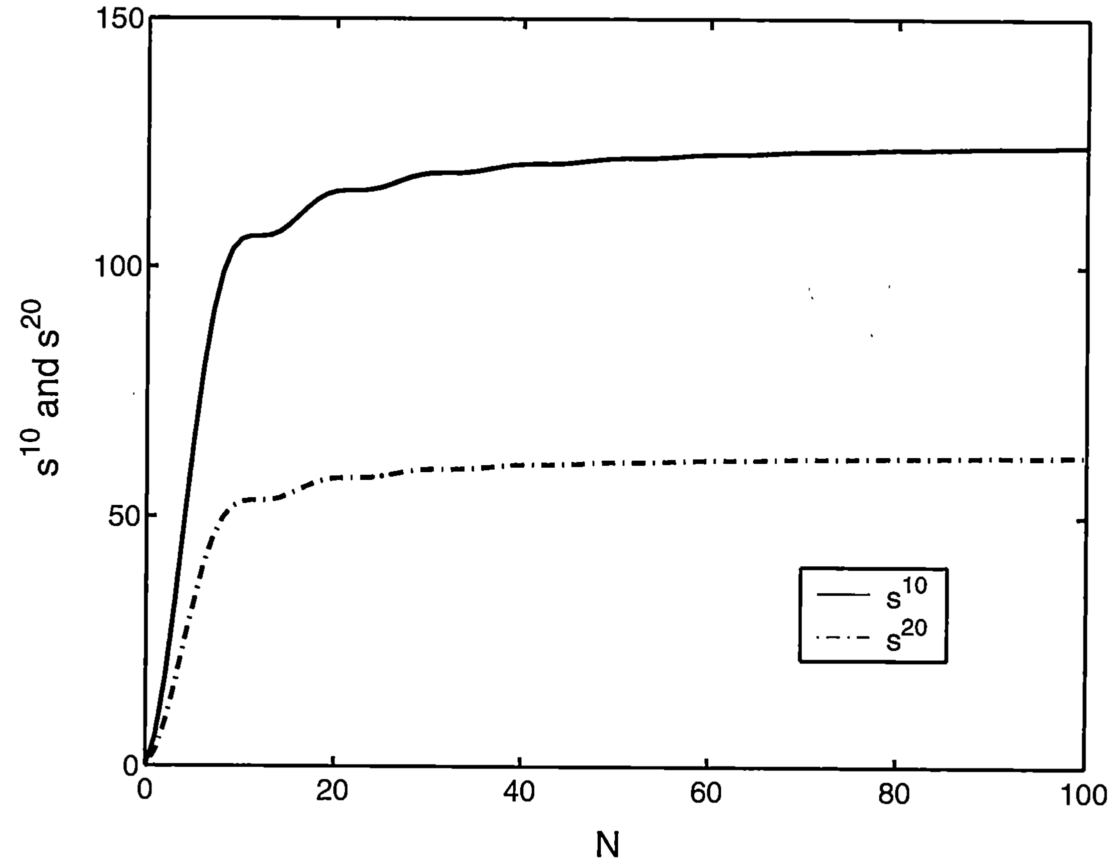

Figure 4.6: Truncated infinite series s^{10} and s^{20} for PMN with periodically distributed 2-D line cracks.

Chapter 5

Conclusions and Discussions

5.1 Conclusions

Two micromechanics models have been developed to estimate the local fields and the effective properties of smart electrostrictive materials. One is based on the laminated plate theory, and the other is based on periodic microstructure. The latter can be used for a broad class of three-dimensional electrostrictive composites and involves very few assumptions. Electrostrictive materials containing periodically distributed 2-D line cracks are special cases included in the periodic microstructure model.

For the modified laminated plate theory, both the linear and nonlinear relations between the polarization and the electric field are considered. As a result, iterative and closed-form solutions have been developed. The effects of material properties, the thickness of brass, and the number of plies on the mechanical and electrical response of electrostrictive laminated composites are studied. One finds

(1) The closed-form solutions agree well with the iterative solutions.

(2) The relationship between the electric field, E_3, and the strains, ε_{11} $(= \varepsilon_{22})$, in electrostrictive laminated composite is nonlinear.

(3) For a two-layered composite, brass/PMN, subjected to E_3 only, the compressive strains, ε_{11} $(= \varepsilon_{22})$, of the top PMN increase, but the compressive strains, ε_{11} $(= \varepsilon_{22})$, of the bottom of the brass decrease if the thickness of brass is increased but remains less than 0.5 mm. On the other hand, when the thickness of brass is greater than 0.5 mm, the compressive strains, ε_{11} $(= \varepsilon_{22})$, of the top PMN decrease, but the tensile strains, ε_{11} $(= \varepsilon_{22})$, of the bottom brass increase as the thickness of brass increases. For a three-layered composite, brass/PMN/brass, subjected to E_3 only, an increase in the thickness of brass will result in a decrease in the compressive composite strains, ε_{11} $(= \varepsilon_{22})$, in the x_1 and x_2 directions.

(4) For two-layered composite, brass/PMN, subjected to E_3 only, the top PMN ply will contract in the x_1 and x_2 directions, whereas the bottom brass ply will extend in the x_1 and x_2 directions. For epoxy/PMN composite subjected to E_3 only, both plies contract in the x_1 and x_2 directions. A three-layered composite, brass/PMN/brass, subjected to E_3, exhibits less compressive strain, ε_{11} ($= \varepsilon_{22}$), in the x_1 and x_2 directions than an epoxy/PMN/epoxy composite.

(5) For a four-layered composite, brass/PMN/brass/PMN, subjected to E_3 only, the composite undergoes contraction in the x_1 and x_2 directions. For two-layered composite, brass/PMN, subjected to E_3 only, the top PMN contracts in the x_1 and x_2 directions while the bottom brass undergoes an elongation in the x_1 and x_2 directions.

For the model based on periodic microstructure, a linear relation between the polarization and the electric field is used since the nonlinear term is found in the laminated plate theory to be insignificant. The periodic microstructure model regards the electrostrictive composite as a collection of unit cells. The local fields and effective properties of electrostrictive composites are predicted using the equivalent inclusion technique (Esheby, 1957) and the Fourier series (Nemat-Nasser *et al.*, 1993).

To determine the effective properties of heterogeneous electrostrictive materials, the inhomogeneities are replaced by the matrix, and transformation fields are prescribed within the inhomogeneities to compensate the materials' mismatch. Thus, the inhomogeneities become inclusions. For simplicity, the transformation fields are assumed to be uniform in inclusions to yield closed-form estimates of effective properties of electrostrictive composites. The present approach can be applied to electrostrictive composites with inhomogeneities in any arbitrary shape, such as laminae, long fibers, etc. In addition, the solution to the inclusion problem of electrostrictive materials, Eq. (3.37) and (3.38), is exact.

Two examples are considered by the periodic microstructural model. One is a laminate with layers of PMN sandwiched between layers of brass; the other is a square PMN continuos fiber-reinforced epoxy-matrix composite. For laminate with layers of PMN sandwiched between layers of brass, the polarization, P_3, is a linear function of the electric field, E_3, whereas the relationship between the strain, ε_{33}, and the electric field, E_3, is nonlinear. An increase in the thickness of brass will result in a decrease in the composite strain, ε_{33}, due to the electric field, E_3.

For a PMN fiber-reinforced epoxy-matrix composite, an increase in the fiber volume fraction results in an increase in the stiffness, C_{33}, the dielectric constant, κ_{33}, and the electrostrictive constant, Q_{33}, of the composite. The composite strain, ε_{33}, due to the electric field, E_3, increases with an increase in the volume fraction of PMN.

The effective properties of the electrostrictive materials containing periodically distributed 2-D line cracks are studied in the present work. A 2-D line crack can be considered as a limiting case of a flat elliptic-cylindrical void with its aspect ratio approaching zero. A limiting process is developed to derive the effective properties of an electrostrictive solid with periodically distributed 2-D line cracks from those of porous electrostrictive materials. An increase in the crack density parameter, f^*, results in a decrease in the stiffness, C_{33}, and the electrostrictive constant, B_{33} of cracked electrostrictive materials. However, the existence of the 2-D line crack does not influence the permittivity, κ_{33} and the electrostrictive constant, Q_{33},

5.2 Discussions

Based on the laminated plate theory, the line perpendicular to the middle surface is presumed to have a constant length after deformation so that the strain perpendicular to the middle surface can be ignored, i.e., $\varepsilon_{33} = 0$. The laminated plate theory is not able to predict the deformation in the thickness direction of composites. The periodic microstructure model is developed to estimate the local fields and effective properties of *three-dimensional* electrostrictive composites. The model involves very few assumptions and can be used for a broad class of three-dimensional electrostrictive materials, such as fibrous, particulate, and laminated composites, porous, and cracked materials.

The constitutive relations between the polarization and the electric field are given by (Suo, 1991; Hom and Shankar, 1994)

$$E_n = \beta_{nm} P_m - 2Q_{klmn} \sigma_{kl} P_m + \text{higher order terms} \tag{5.1}$$

Both the linear term, $\beta_{nm}P_m$, and the nonlinear term, $2Q_{klmn}\sigma_{kl}P_m$, in Eq. (5.1) are considered in laminated plate theory and an iterative formulation has been developed. Closed-form solutions are also obtained by ignoring the nonlinear term, $2Q_{klmn}\sigma_{kl}P_m$, in Eq. (5.1). The studies show that the closed-form solutions agree well with the iterative solutions and the nonlinear term, $2Q_{klmn}\sigma_{kl}P_m$, in Eq. (5.1) is found to be insignificant in comparison with the first term, $\beta_{nm}P_m$. Therefore, only the linear term, $\beta_{nm}P_m$, is considered in the periodic microstructure model.

When the aspect ratio of a flat elliptic cylindrical void approaches zero, the flat void collapses into a 2-D line crack. The periodic microstructure model is used to study cracked electrostrictive materials. The results show that an increase in crack density parameter results in a decrease in the stiffness C_{33} and the electrostrictive constant B_{33}, but has no effect on the permittivity κ_{33}. These results may be due to the fact that the nonlinear term in Eq. (5.1) is ignored. Although the nonlinear term, $2Q_{klmn}\sigma_{kl}P_m$, in Eq. (5.1) is negligible in comparison with the first term, $\beta_{nm}P_m$, in computing the electro-mechanical coupling in laminated composites, it may need to be considered in modeling cracked electrostrictive materials.

Suo (1991) and Hom and Shankar (1994) point out that the polarization decreases and approaches to asymptotic values due to saturation when the electric field is high. To fully account for the saturation of polarization, higher order terms may need to be included in the constitutive relation Eq. (5.1). If the electric field is not very high, the present formulations are valid.

REFERENCES

References

Bary, N. K. (1964), *A Treatise on Trigonometric Series*, The Macmillan Company, New York.

Bernstein, J., Spicer, J. B., Wagner, J. W., and Ritter, A. P. (1996), "Ultrasonic Characterization of Degradation in Lead Magnesium Niobate (PMN) Smart Materials," *Materials Science Forum*, **210-213**, pp. 775-782.

Brown, L. F., Carlson, R. L., Sempsrott, J. M., Stranford, G. T., and Fitzgerald, J. J. (1998), "Investigation of the Dielectric and Piezoelectric Properties of PMN and PMN-PT Materials for Ultrasonic Transducer Application," *1997 IEEE Ultrasonics Symposium*, pp. 561-564.

Chen, J., Shurland, A., Perry, J., Ossmann, B., and Gururaja, T. R. (1996), "Electrostrictive Transducers for Medical Ultrasonic Applications" *Proceedings of the IEEE International Symposium on Applications of Ferroelectric*, **1**, 10, pp. 27-30.

Chopra, I. (1996), *Smart Structures and Integrated Systems*, The International Society for Optical Engineering.

Coutte, J., Debus, J. C., Dubus, B., Bossut, R., Granger, C., and Haw, G. (1998), "Finite Element Modeling of PMN Electrostrictive Materials and Application to the Design of Transducers," *Proceedings of the Annual IEEE International Frequency Control Symposium*, pp. 703-708.

Crowe, C. R. (1996), *Industrial and Commercial Applications of Smart Structures Technologies*, The International Society for Optical Engineering.

Damjanovic, D. and Newnham, R. E. (1992), "Electrostrictive and Piezoelectric Materials for Actuator Application," *Journal of Intelligent Material Systems and Structures*, **3**, pp. 190-208.

Debus, J. C. and Dubus, B. (1996), "Finite Element of PMN Electrostrictive Materials," *Proceedings of SPIE the International Society for Optical Engineering*, **2779**, pp. 913-918.

Dunn, M. L. (1994), "The Effects of Crack Face Boundary Conditions on the Fracture Mechanics of Piezoelectric Solid," *Engineering Fracture Mechanics*, **48**, 1, pp. 25-39.

Eshelby, J. D. (1957), "The Determination of the Elastic Field of an Ellipsoidal

Inclusion, and Related Problem," *Proceedings of the Royal Society of London*, **A241**, pp. 376-396.

Fanson, J. L. (1995), "On the Use of Electrostrictive Actuators in Recovering the Optical Performance of the Hubble Space Telescope," *Materials Research Society Symposium Proceedings*, **360**, pp. 109-120.

Gaucher, P. (1996), "Piezoelectric and Electrostrictive Bimorph Actuators and Sensors for Smart Microsystems, " *Proceedings of SPIE The International Society for Optical Engineering*, **210-213**, pp. 610-615.

Hom, C. L. and Shankar, N. (1994), "A Fully Coupled Constitutive Model for Electrostrictive Ceramic Materials," *Journal of Intelligent Material Systems and Structures*, **5**, pp. 795-801.

Hom, C. L. and Shankar, N. (1995), "Finite Element Modeling of Multilayered Electrostrictive Actuators," *Proceedings of SPIE The International Society for Optical Engineering.* Society of Photo-Optical Instrumentation Engineers, **2442**, pp. 376-384.

Hom, C. L., Pilgrim, M., Shankar, N., Bridger, K., Massuda, M., and Winzer S. R. (1994), "Calculation of Quasi-Static Electromechanical Coupling Coefficients for Electrostrictive Ceramic Materials," *IEEE Transactions on Ultrasonics, Ferroelectrics, and Frequency Control*, **41**, 4, pp. 542-551.

Ikeda, T. (1990), *Fundamentals of Piezoelectricity*, Oxford Science Publications.

Isopov, V. A., Yushin, N. K., Smirnova, E. P., Sotnikov, A. V., Tarakanov, E. A., and Maksimov, A. Y. (1994), "Electrostrictive Actuators on Base of PMN-PSN Solid Solution Ceramics," *Ferroelectrics*, **160**, pp. 239-242.

Jang, S. J., Uchino, K., Nomura, S., and Cross, L. E. (1980), "Electrostrictive Behavior of Lead Magnesium Niobate Based Ceramic Dielectrics," *Ferroelectrics*, **27**, pp. 31-34.

Knops, R. J. (1963), "Two-Dimensional Electrostriction," *Quarterly Journal of Mechanics and Applied Mathematics*, **16**, pp. 377-388.

Kornbluh, R., Pelrine, R., Eckerle, J., and Joseph, J. (1998), "Electrostrictive Polymer Artificial Muscle Actuators," *Proceedings of the 1998 IEEE International Conference on Robotics and Automations*, pp. 2174-2154.

Mangin, S. T., Leary, S. P., and Pilgrim, S. M. (1996), "Coupling and Dielectric Properties of Lead Magnesium Niobate-Based Electrostrictor," *Proceedings of the IEEE International Symposium on Applications of Ferroelectric*, pp. 715-717.

Mark, A. E. and Paul, A. D. (1990), "Standard SELECT Electrostrictive Lead Magnesium Niobate Actuators for Active and Dative Optical Components," *Optical Engineering*, **29**, 11, pp. 610-615.

Nemat-Nasser, S., Yu, N., and Hori, M. (1993), "Bounds and Estimates of Overall Moduli of Composites with Periodic Microstructure," *Mechanics of Materials*, **15**, 163-181.

Newnham, R. E. (1991), "Tunable Transducers: Nonlinear Phenomena in Electroceramics," *National Institute of Standards and Technology Special Publication*, **804**, pp. 39-52.

Newnham, R. E., Xu, Q. C., and Yoshikawa, S. (1994), *Metal-Electroactive Ceramic Composite Actuators*, U. S. Patent No. 5,276,657.

Ohuchi, H., Nakano, K., Uchino, K., Endoh, H., and Fukumoto, K. (1986), "High-Speed Electro-Hydraulic Servovalves Using Electrostrictive Ceramic PMN Actuators," *Fluid Control and Measurement*, **1**, pp. 415-420.

Ru, C. Q., Mao, X., and Epstein, M. (1998), "Electric-Field Induced Interfacial Cracking in Multilayer Electrostrictive Actuator," *Journal of the Mechanics and Physics of Solids*, **46**, 8, pp. 1313-1318.

Rittenmyer, K. M. (1994), "Electrostrictive Ceramics for Underwater Transducer Applications," *Journal of the Acoustical Society of America*, **95**, 2, pp. 849-856.

Smith, W. A. (1986), "Composite Piezoelectric Materials for Medical Ultrasonic Imaging Transducers–A review," *Proceedings of the IEEE International Symposium on Applications of Ferroelectric*, pp. 249-256.

Smolenskii, G. A., Isupov, V. A., and Yushin, N. K. (1987), "Applications of Electrostrictive Ferroelectric Ceramics," *Bulletin. Academy of Sciences of the USSR. Physical Series*, **51**, 10, pp. 72-76.

Sugawara, Y., Onisuka, K., Yoshikawa, S., Xu, Q., Newnham, R. E., and Uchino, K. (1992), "Metal-Ceramic Composite Actuators," *Journal of the American Ceramic Society*, **75**, 4, pp. 996-998.

Sundar, V. and Newnham, R. V. (1992), "Electrostriction and Polarization," *Ferroelectrics*, **135**, pp. 431-446.

Suo, Z. (1991), "Mechanics Concepts for Failure in Ferroelectric Ceramics," *Smart Structures and Materials*, AD-Vol. **24**/AMD-Vol. **123**, Haritos, G. K. and Srinivasan, A. V. (eds.), *American Society of Mechanical Engineers*, pp. 1-6.

Suyama, R., Tanemoto K., Kobayashi Y., and Yajima, M. (1990), "Autofocusing System of Optical Microscope Utilizing Electrostrictive Actuators," *Japanese Journal of Applied Physics*, **30**, 6, pp. 1290-1294.

Takeuchi, H., Masuzawa, H., Nakaya, C., and Ito, Y. (1989), "Medical Ultrasonic Probe Using Electrostrictive-Ceramics/Polymer Composite," *IEEE Ultrasonics Symposium Proceedings*, **2**, pp. 705-708.

Uchino, K. (1986), "Electrostrictive Actuators: Materials and Applications," *Ceramic Bulletin*, **65**, 4, pp. 647-652.

Uchino, K. (1997), "Piezoelectric Actuators and Ultrasonic Motors," Kluwer Academic Publishers.

Yang, W. and Suo, Z. (1994), "Cracking in Ceramic Actuators Caused by Electrostriction," *Journal of the Mechanics and Physics of Solids*, **42**, 4, pp. 649-663.

Yamamoto, K., Nomote, A., and Ueda, Y. (1982), *Proceedings. Standard Interface Control Electronics*, **1408**, pp. 121.

Wang, H. and Singh, R. N. (1995), "Electric Field Effects on the Crack Propagation in an Electrostrictive PMN-PT Ceramic," *Ferroelectrics*, **168**, pp. 281-291.

Wang, Y., Straw, A., Chan, Y. C., Gui, Z. L., and Li, L. T. (1996), "Effect of Annealing on the Ageing Properties of PMN-0.1PT Ceramics by Transition-Metallic Ions," *IEEE International Symposium on Applications of Ferro-*

electrics, **2**, pp. 647-650.

Winzer, S. R., Shankar, N., and Ritter, A. P. (1989), "Designing Cofired Multilayer Electrostrictive Actuators for Reliability," *Journal of the American Ceramic Society*, **72**, 12, pp. 2246-2257.

Zhao, J. and Zhang, Q. M. (1996), "Effect of Mechanical Stress on the Electromechchanical Performance of PZT and PMN-PT Ceramics," *Proceedings of the IEEE International Symposium on Applications of Ferroelectric*, **2**, 10, pp. 971-974.

Zhenyi, M., Scheinbeim, J. I., Lee, J. W., and Newman, B. A. (1994), "High Field Electrostrictive Response of Polymers," *Journal of Polymer Science: Part B: Polymer Physics*, **32**, pp. 2721-2731.

Yoon, K. H., Hwang, Y. H., Kim, E. S., and Hang, D. H. (1996), "Dielectric and Electrostrictive Properties of 0.9PMN-0.1PT Multilayer Ceramics with ZnO Additive," *Intergated Ferroelectrics*, **13**, pp. 17-24.

APPENDICES

Appendix A

Classical Laminated Plate Theory

The stress-strain relations for an elastic material can be expressed by Hooke's Law:

$$\sigma_{ij} = C_{ijkl}\varepsilon_{kl}, \tag{A.1}$$

where i, j, k and $l = 1, 2, 3$, σ is the stress tensor, ε is the strain tensor, and C $(= D^{-1})$ is the stiffness tensor. For orthotropic materials, Eq. (A.1) can be written in matrix form by

$$\begin{Bmatrix} \sigma_{11} \\ \sigma_{22} \\ \sigma_{33} \\ \sigma_{23} \\ \sigma_{31} \\ \sigma_{12} \end{Bmatrix} = \begin{bmatrix} C_{1111} & C_{1122} & C_{1133} & 0 & 0 & 0 \\ C_{1122} & C_{2222} & C_{2233} & 0 & 0 & 0 \\ C_{1133} & C_{2233} & C_{3333} & 0 & 0 & 0 \\ 0 & 0 & 0 & C_{2323} & 0 & 0 \\ 0 & 0 & 0 & 0 & C_{3131} & 0 \\ 0 & 0 & 0 & 0 & 0 & C_{1212} \end{bmatrix} \begin{Bmatrix} \varepsilon_{11} \\ \varepsilon_{22} \\ \varepsilon_{33} \\ 2\varepsilon_{23} \\ 2\varepsilon_{31} \\ 2\varepsilon_{12} \end{Bmatrix}. \tag{A.2}$$

A plane stress state is assumed in a thin lamina; that is,

$$\sigma_{33} = \sigma_{23} = \sigma_{31} = 0, \tag{A.3}$$

Eq. (A.2) thus reduces to

$$\begin{Bmatrix} \sigma_{11} \\ \sigma_{22} \\ \sigma_{12} \end{Bmatrix} = \begin{bmatrix} C^*_{1111} & C^*_{1122} & 0 \\ C^*_{1122} & C^*_{2222} & 0 \\ 0 & 0 & C^*_{1212} \end{bmatrix} \begin{Bmatrix} \varepsilon_{11} \\ \varepsilon_{22} \\ 2\varepsilon_{12} \end{Bmatrix}, \tag{A.4}$$

where

$$C^*_{1111} = C_{1111} - \frac{C^2_{1133}}{C_{3333}}, \tag{A.5}$$

$$C^*_{2222} = C_{2222} - \frac{C^2_{2233}}{C_{3333}}, \tag{A.6}$$

$$C^*_{1122} = C_{1122} - \frac{C_{1133}C_{2233}}{C_{3333}}, \tag{A.7}$$

$$C^*_{1212} = C_{1212}. \tag{A.8}$$

A laminate consists two or more laminae,which are presumed to be perfectly bonded together. The displacements are continuous across interfaces. That is, there is no slip between each lamina. Moreover, a line originally straight and perpendicular to the middle surface of the laminate is assumed to remain straight and perpendicular to the middle surface after deformation, which implies that the out-of-plane shear strains, ε_{13} and ε_{23}, are equal to zeros; see Figure A.1. Also the line perpendicular to the middle surface is presumed to have a constant length after deformation so that the strain perpendicular to the middle surface can be ignored, i.e., $\varepsilon_{33} = 0$.

Figure A.1 shows that the undeformed and deformed cross sections of a laminate, where u_0 and w_0 are the x- and z-component of displacement of midpoint C, respectively, z is the z-coordinate of a typical point D, and α is the slope of the middle surface and is given by

$$\alpha = \frac{\partial w_O}{\partial x}. \tag{A.9}$$

Since line AB remains straight after deformation, the displacement of point D in the x-direction can be expressed by

$$u = u_0 - z\frac{\partial w_0}{\partial x}. \tag{A.10}$$

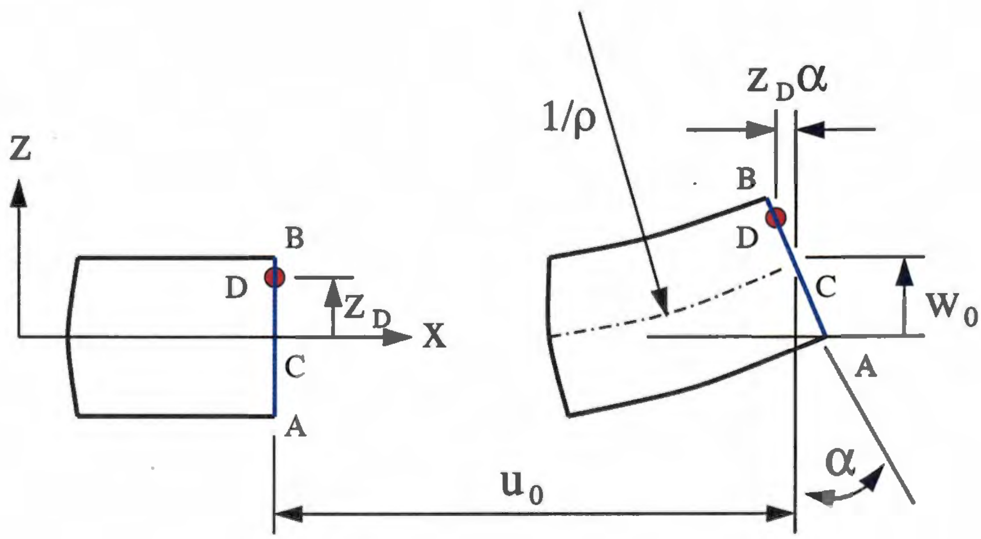

Figure A.1: Deformation of plate in the x-z plane.

Silimarly, the displacement, v, in the y-direction is given by

$$v = v_0 - z\frac{\partial w_0}{\partial y}. \tag{A.11}$$

The infinitesimal strains are defined by

$$\varepsilon_{11} = \frac{\partial u}{\partial x}, \tag{A.12}$$

$$\varepsilon_{22} = \frac{\partial v}{\partial y}, \tag{A.13}$$

$$\varepsilon_{12} = \frac{1}{2}(\frac{\partial u}{\partial y} + \frac{\partial v}{\partial x}). \tag{A.14}$$

Substituting Eqs. (A.10) and (A.11) into Eqs. (A.12) $\sim$ (A.14), one finds

$$\varepsilon_{11} = \frac{\partial u_0}{\partial x} - z\frac{\partial^2 w_0}{\partial x^2}, \tag{A.15}$$

$$\varepsilon_{22} = \frac{\partial v}{\partial y} - z\frac{\partial^2 w_0}{\partial y^2}, \tag{A.16}$$

$$\varepsilon_{12} = \frac{1}{2}(\frac{\partial u}{\partial y} + \frac{\partial v}{\partial x} - 2z\frac{\partial^2 w_0}{\partial x \partial y}); \tag{A.17}$$

or

$$\left\{ \begin{array}{c} \varepsilon_{11} \\ \\ \varepsilon_{22} \\ \\ 2\varepsilon_{12} \end{array} \right\} = \left\{ \begin{array}{c} \varepsilon_{11}^0 \\ \\ \varepsilon_{22}^0 \\ \\ 2\varepsilon_{12}^0 \end{array} \right\} + z \left\{ \begin{array}{c} \rho_{11} \\ \\ \rho_{22} \\ \\ 2\rho_{12} \end{array} \right\}, \tag{A.18}$$

where the middle surface strains are given by

$$\left\{ \begin{array}{c} \varepsilon_{11}^0 \\ \\ \varepsilon_{22}^0 \\ \\ 2\varepsilon_{12}^0 \end{array} \right\} = \left\{ \begin{array}{c} \frac{\partial u_0}{\partial x} \\ \\ \frac{\partial v_0}{\partial y} \\ \\ 2(\frac{\partial u_0}{\partial y} + \frac{\partial v_0}{\partial x}) \end{array} \right\}, \tag{A.19}$$

and the curvatures are defined by

$$\begin{Bmatrix} \rho_{11} \\ \rho_{22} \\ 2\rho_{12} \end{Bmatrix} = -\begin{Bmatrix} \frac{\partial^2 w_0}{\partial x^2} \\ \frac{\partial^2 w_0}{\partial y^2} \\ 4\frac{\partial^2 w_0}{\partial y \partial x} \end{Bmatrix}. \tag{A.20}$$

Substituting Eq. (A.18) into Eq. (A.4), gives the stresses in the k^{th} ply

$$\begin{Bmatrix} \sigma_{11} \\ \sigma_{22} \\ \sigma_{12} \end{Bmatrix}_k = \begin{bmatrix} C^*_{1111} & C^*_{1122} & 0 \\ C^*_{1122} & C^*_{2222} & 0 \\ 0 & 0 & C^*_{1212} \end{bmatrix}_k \left\{ \begin{Bmatrix} \varepsilon^0_{11} \\ \varepsilon^0_{22} \\ 2\varepsilon^0_{12} \end{Bmatrix} + z \begin{Bmatrix} \rho_{11} \\ \rho_{22} \\ 2\rho_{12} \end{Bmatrix} \right\}, \tag{A.21}$$

where the subscript k designates the ply number. Because the elastic properties can be different from ply to ply, the stress variation through the laminate thickness is piece-wise linear.

The resultant forces per unit length, $\{N_{11}, N_{22}, N_{12}\}^T$, and moments per unit length, $\{M_{11}, M_{22}, M_{12}\}^T$, acting on a laminate are given by

$$\begin{Bmatrix} N_{11} \\ N_{22} \\ N_{12} \end{Bmatrix} = \int_{-t/2}^{t/2} \begin{Bmatrix} \sigma_{11} \\ \sigma_{22} \\ \sigma_{12} \end{Bmatrix} dz = \sum_{k=1}^{n} \int_{z_{k-1}}^{z_k} \begin{Bmatrix} \sigma_{11} \\ \sigma_{22} \\ \sigma_{12} \end{Bmatrix}_k dz, \tag{A.22}$$

$$\begin{Bmatrix} M_{11} \\ M_{22} \\ M_{12} \end{Bmatrix} = \int_{-t/2}^{t/2} \begin{Bmatrix} \sigma_{11} \\ \sigma_{22} \\ \sigma_{12} \end{Bmatrix} zdz = \sum_{k=1}^{n} \int_{z_{k-1}}^{z_k} \begin{Bmatrix} \sigma_{11} \\ \sigma_{22} \\ \sigma_{12} \end{Bmatrix}_k zdz, \tag{A.23}$$

respectively, where t is the laminate thickness, n is the total number of laminae, z_k and z_{k-1} are the z-coordinates of the top and bottom surfaces of the k^{th} lamina, and the subscript k specifies the ply number; see Figure 2.1(b). Substituting Eq. (A.21) into Eqs. (A.22) and (A.23), yields

$$\left\{\begin{matrix} N_{11} \\ N_{22} \\ N_{12} \end{matrix}\right\} = \sum_{k=1}^{n} \begin{bmatrix} C^*_{1111} & C^*_{1122} & 0 \\ C^*_{1122} & C^*_{2222} & 0 \\ 0 & 0 & C^*_{1212} \end{bmatrix}_k \left\{ \int_{z_{k-1}}^{z_k} \left\{\begin{matrix} \varepsilon^0_{11} \\ \varepsilon^0_{22} \\ 2\varepsilon^0_{12} \end{matrix}\right\} dz + \int_{z_{k-1}}^{z_k} \left\{\begin{matrix} \rho_{11} \\ \rho_{22} \\ 2\rho_{12} \end{matrix}\right\} zdz \right\}, \tag{A.24}$$

$$\left\{\begin{matrix} M_{11} \\ M_{22} \\ M_{12} \end{matrix}\right\} = \sum_{k=1}^{n} \begin{bmatrix} C^*_{1111} & C^*_{1122} & 0 \\ C^*_{1122} & C^*_{2222} & 0 \\ 0 & 0 & C^*_{1212} \end{bmatrix}_k \left\{ \int_{z_{k-1}}^{z_k} \left\{\begin{matrix} \varepsilon^0_{11} \\ \varepsilon^0_{22} \\ 2\varepsilon^0_{12} \end{matrix}\right\} zdz + \int_{z_{k-1}}^{z_k} \left\{\begin{matrix} \rho_{11} \\ \rho_{22} \\ 2\rho_{12} \end{matrix}\right\} z^2dz \right\}. \tag{A.25}$$

Since ε^0_{11}, ε^0_{22}, ε^0_{12} ρ_{11}, ρ_{22}, and ρ_{12} are middle surface values and are not functions of z, Eqs. (A.24) and (A.25) give

$$\begin{Bmatrix} N_{11} \\ N_{22} \\ N_{12} \end{Bmatrix} = \begin{bmatrix} A_{1111} & A_{1122} & 0 \\ A_{1122} & A_{2222} & 0 \\ 0 & 0 & A_{1212} \end{bmatrix} \begin{Bmatrix} \varepsilon_{11}^{0} \\ \varepsilon_{22}^{0} \\ 2\varepsilon_{12}^{0} \end{Bmatrix} dz + \begin{bmatrix} B_{1111} & B_{1122} & 0 \\ B_{1122} & B_{2222} & 0 \\ 0 & 0 & B_{1212} \end{bmatrix} \begin{Bmatrix} \rho_{11} \\ \rho_{22} \\ 2\rho_{12} \end{Bmatrix} zdz, \tag{A.26}$$

$$\begin{Bmatrix} M_{11} \\ M_{22} \\ M_{12} \end{Bmatrix} = \begin{bmatrix} B_{1111} & B_{1122} & 0 \\ B_{1122} & B_{2222} & 0 \\ 0 & 0 & B_{1212} \end{bmatrix} \begin{Bmatrix} \varepsilon_{11}^{0} \\ \varepsilon_{22}^{0} \\ 2\varepsilon_{12}^{0} \end{Bmatrix} dz + \begin{bmatrix} D_{1111} & D_{1122} & 0 \\ D_{1122} & D_{2222} & 0 \\ 0 & 0 & D_{1212} \end{bmatrix} \begin{Bmatrix} \rho_{11} \\ \rho_{22} \\ 2\rho_{12} \end{Bmatrix} zdz, \tag{A.27}$$

where the three-by-three extensional stiffness, coupling stiffness, and bending stiffness are given by

$$[A] = \sum_{k=1}^{n} [C^*]_k (z_k - z_{k-1}), \tag{A.28}$$

$$[B] = \frac{1}{2} \sum_{k=1}^{n} [C^*]_k (z_k^2 - z_{k-1}^2), \tag{A.29}$$

$$[D] = \frac{1}{3} \sum_{k=1}^{n} [C^*]_k (z_k^3 - z_{k-1}^3). \tag{A.30}$$

VITA

Thada Somphone was born and attended elementary school at Chung Ching School in Luang Prabang, Laos. In August 1974, he went to Taiwan, Republic of China, and earned his high school degree from Taichung 1st High School, Taichung. He was then admitted to the National Taiwan University in August, 1977, and eventually received a Bachelor of Science degree in Mechanical Engineering in July, 1982 .

After receiving the B.S. degree, he worked at the Mechanical Industry Research Laboratories (MIRL), which is a division of the Industrial Technology Research Institute (ITRI), a government-sponsored research organization responsible for elevating the research and development capabilities of industry in Taiwan. During his six years at MIRL, he acquired experience in manufacturing and assembly technologies and took a training program in Production Automation in Sweden. He participated in the design of CNC machining center and the matrix drill machine. Subsequently, he was promoted from Assistant engineer to Associate engineer. Later, he was chosen as a project leader and led two groups of engineers at MIRL to develop a high precision plane grinder and a prepreg machine. The technologies developed by the projects elevated the industry's high-precision machining capabilities and were successfully transferred to several private companies in Taiwan. Before the prepreg machine was developed, industrial firms in Taiwan could do nothing but import composite materials and components. Afterwards, they are able to export high-quality composite materials and structures. The high precision plane grinder won the Good Product Design Award in Taiwan, and Somphone was awarded the Excellent Engineer Award at MIRL in 1988.

In 1990, he entered the Graduate School of the University of Tennessee at Chattanooga and received a Master of Science degree in Mechanical Engineering in August, 1992. After graduation, he worked as a design engineer for Sherman & Reilly, Inc., a manufacturer of utility equipment in Chattanooga, TN.

In 1996, he was admitted to the Engineering Science Program in the Mechanical and Aerospace Engineering and Engineering Science Department at the University of Tennessee, Knoxville. He was a graduate teaching assistant from 1996 to 1997 and a graduate research assistant from 1997 to 2000. His research was supported by the Historically Black Engineering Colleges (HBEC) Future Faculty Fellowship from the Office of Naval Research. His paper "Mechanics of Electrostrictive Materials with Periodic Microstructure," co-authored with his advisor, Dr. Yu, was published in *Adaptive Structures and Materials Systems*, G. Washington and J. Redmond (eds.), AD-Vol. 59/MD-Vol 87, ASME, pp.93-98. In 1998, he was awarded Graduate School Fellowship from the University of Tennessee at Knoxville. In 1999, he received another Master of Science degree in Mechanical Engineering from the University of Tennessee at Knoxville. In August, 2000, he received a Ph.D. degree in Engineering Science from the University of Tennessee at Knoxville.

HONORS AND AWARDS:

The HBEC Future Faculty Fellowship, Office of Naval Research. 1997-2000

Graduate School Fellowship, The University of Tennessee at Knoxville. 1998

The Excellent Engineer Award, Mechanical Industry Research Laboratories, Taiwan, R.O.C. 1988

Excellent Product Design Award, China External Trade Development Council, Taiwan, R.O.C. 1987

PUBLICATIONS:

Ph.D. Dissertation : *Micromechanics of Smart Electrostrictive Materials.* Advisor: Dr. N. Yu.

M.S. Thesis: *The Modeling of Hydrostatic Bearing.* Advisor: Dr. Gary H. McDonald.

T. Somphone and N. Yu, "Property Degradation due to Microcracking in Smart Electrostrictive Ceramics," to be presented at the Symposium on "Smart Materials and Adaptive Structures," *Third International Conference on Mechanics and Materials in Design*, FL, May 29-31, 2000.

T. Somphone and N. Yu, (1999), "Mechanics of Electrostrictive Materials with Periodic Microstructure," *in Adaptive Structures and Material Systems*, G. Washington and J. Redmond (eds.), AD-Vol. 59 / MD-Vol. 87, ASME, pp. 93-98.

T. Somphone, H. Li, and N. Yu, "Nonlinear Electro-Mechanical Coupling in Smart Electrostrictive Composites," presented at the Symposium on "New Advances in Smart Material Structures Control and Damage Detection," 1999 *ASME Mechanics and Materials Conference*, Virginia Tech, VA, June 27-30, 1999.

N. Yu and T. Somphone, "Micromechanics of Smart Electrostrictive Materials," presented at the Symposium on "Piezoelectric Materials," *Thirteenth U.S. National Congress of Applied Mechanics*, University of Florida, FL, June 21-26, 1998.

N. Yu and T. Somphone, "The Inclusion and Inhomogeneity Problems of Electrostrictive Materials," presented at the Symposium on "Functional Composite Systems," *1997 ASME International Mechanical Engineering Congress & Exposition*, Dallas, TX, November 16-21, 1997.